HUMBOLDT-UNIVERSITÄT ZU BERLIN

Impact of MACC1 in Cargo Specific Clathrin-Mediated Endocytosis

DISSERTATION

zur Erlangung des akademischen Grades

Doctor of Philosophy

(Ph.D.)

eingereicht an der

Lebenswissenschaftlichen Fakultät der Humboldt-Universität zu Berlin

Von

M.Sc. Francesca Imbastari

Präsidentin der Humboldt-Universität zu Berlin

Prof. Dr.-Ing. Dr. Sabine Kunst

Dekan der Lebenswissenschaftlichen Fakultät der Humboldt-Universität zu Berlin

Prof. Dr. Bernhard Grimm

Gutachter/innen

1. Prof. Dr. Ulrike Stein
2. Prof. Dr. Adam Lange
3. Prof. Dr. Andreas Herrmann

Tag der mündlichen Prüfung: 22.11.2019

Erklärung

Hiermit erkläre ich, die Dissertation selbstständig und nur unter Verwendung der angegebenen Hilfen und Hilfsmittel angefertigt zu haben. Ich habe mich anderwärts nicht um einen Doktorgrad beworben und besitze keinen entsprechenden Doktorgrad. Ich erkläre, dass ich die Dissertation oder Teile davon nicht bereits bei einer anderen wissenschaftlichen Einrichtung eingereicht habe und dass sie dort weder angenommen noch abgelehnt wurde. Ich erkläre die Kenntnisnahme der dem Verfahren zugrunde liegenden Promotionsordnung der Lebenswissenschaftlichen Fakultät der Humboldt-Universität zu Berlin vom 5. März 2015. Weiterhin erkläre ich, dass keine Zusammenarbeit mit gewerblichen Promotionsberaterinnen/Promotionsberatern stattgefunden hat und dass die Grundsätze der Humboldt-Universität zu Berlin zur Sicherung guter wissenschaftlicher Praxis eingehalten wurden.

Berlin, den

Francesca Imbastari

Table of Contents

Index of Figures

Abstract

Metastasis Associated in Colon Cancer 1 (MACC1) is a newly discovered prognostic and predictive biomarker associated with tumor progression and metastasis development. Since our first report concerning MACC1 in 2009, MACC1-related research has been exponentially increasing. At present, MACC1 involvement in the progression of many cancer types has become increasingly clear. MACC1 does not only promote invasion and metastasis formation, but it also induces angiogenesis, stemness and prevents apoptosis. Although in the last years our research concerning MACC1 gained new insights into cancer progression, little is known about its structural role and functions in physiological processes.

In this thesis, I will address for the first time the role of MACC1 during CME (clathrin-mediated endocytosis). Importantly, MACC1's role in CME was first suggested by interactome analysis. Thus, MACC1's CME interactors (CLTC, DNM2, AP2α and TfR), were first identified and validated. In addition, MACC1's impact on TfR endocytic traffic was addressed by studying its effect on surface distribution, uptake, recycling and degradation of the receptor with pioneering and newly established methods. As a result of this research, MACC1 shows a clear impact on TfR internalization and recycling. Thus, the present work dissects the MACC1 protein structure containing predicted CME domains such as clathrin box, NPFs and DPF. By deleting these domains, first the impact on the binding between MACC1 and CLTC, DNM2 and TfR were analyzed. Also, we characterized the distribution of MACC1 in the cell depending on the presence of its CME domains, and then I addressed their specific impact during TfR endocytic traffic.

After we elucidated the MACC1-dependent increase in TfR recycling, we compared its newly discovered function during EGFR endocytic traffic. By analyzing TfR -EGFR coupled early endocytic traffic during EGF-stimulated internalization in MACC1 overexpressing cell lines, we discovered that MACC1 promotes faster recycling of EGFR to PM, in two different cell lines. In order to understand the MACC1 CME domains impact on EGFR endocytic traffic, we dissected not only EGFR endocytic fate in MACC1 CME mutant cell lines but also the impact on EGFR trans-activation after EGF-stimulated internalization and downstream signaling, in particular, AKT and ERK1/2. To conclude with functional analysis, we also addressed MACC1 CME domains impact on cell proliferation revealing that CME domains integrity is important for efficient cell proliferation.

The present work sheds new light on MACC1's role during endocytosis, opening a possibility of intervention on metastasis development in CRC to improve the survival of patients.

Zusammenfassung

Metastasis Associated in Colon Cancer 1 (MACC1) ist ein prognostischer und prädiktiver Biomarker für Tumorprogression und Fernmetastasierung von Darmkrebs. Der exponentielle Anstieg der MACC1-verbundenen Publikationen seit dessen Entdeckung im Jahr 2009 verdeutlicht Mitwirkung von MACC1 am Krankheitsfortschritt vieler solider Tumore. Dies umfasst sich nicht nur die erhöhte Tumorinvasion und Metastasierung, sondern ebenso erhöhte Tumorangiogenese, dessen Stammzellfähigkeit und die Vermeidung von Apoptose. Obwohl unsere Forschungsarbeiten in den letzten Jahren neue Erkenntnisse über die Auswirkung von MACC1 in der Tumorprogression brachten, ist über dessen Proteinstruktur und der damit verbundenen Funktion in physiologischen Prozessen wenig bekannt.

In dieser Arbeit wird zum ersten Mal die Rolle von MACC1 in der Clathrin-abhängigen Endozytose (CME) untersucht. Nach massenspektrometrischer Analyse des MACC1-Interaktoms wurde die Proteinbindung von MACC1 und den CME-verbundenen Faktoren CLTC, DNM2 und AP-2α, bzw. dem CME-Cargo TfR experimentell bestätigt. Davon ausgehend wurde der Endozytoseweg von TfR und MACC1-abhängige Änderungen in dessen Oberflächenverteilung, Internalisierung, Recycling und Proteinabbau mittels neu etablierter Methoden untersucht und ergab einen deutlichen Einfluss von MACC1 auf die Internalisierung und das Recycling von TfR. Daraufhin wurden durch Sequenzanalyse der MACC1-Proteinstruktur vorhergesagte N-terminale Interaktionsbereiche mit CME-Faktoren betrachtet, die eine Clathrin-Box sowie NPF- bzw. DPF-Motive umfassen. Deletionsvarianten von MACC1 wurden zunächst auf ihre Interaktionsfähigkeit mit CLTC, DNM2 und TfR getestet, deren subzelluläre Lokalisation bestimmt, sowie deren Einfluss auf den Endozytoseweg von TfR geprüft.

Das erhöhte Recycling von TfR in Abhängigkeit von MACC1 wurde für EGFR als wichtigen Vertreter von krebsrelevanten Rezeptor-Tyrosinkinasen überprüft. Die Analyse des TfR-EGFR gekoppelten frühen Endozytosewegs ergab eine erhöhte Recyclingrate des Rezeptors in verschiedenen MACC1-überexprimierenden Zelllinien. Um den Einfluss der N-terminalen Interaktionsbereiche von MACC1 auf den Endozytoseweg von EGFR zu verstehen, wurden die MACC1-Deletionsvarianten nicht nur auf Änderungen im Verlauf der EGFR-Endozytose geprüft, sondern ebenfalls auf die Aktivierung des Rezeptors sowie nachgelagerter Signaltransduktoren wie PI3K/AKT und ERK1/2. Die Wichtigkeit der Interaktionsbereiche von MACC1 wurde durch eine Analyse der EGF-induzierten Zellproliferation bestätigt.

Die Ergebnisse dieser Arbeit, die die Rolle von MACC1 in der Endozytose beschreiben, erweitern die Interventionsmöglichkeiten gegenüber der Fernmetastasierung solider Tumore und könnten helfen, das Überleben betroffener Patienten zu verlängern.

Publications

1. **Imbastari** F, Dahlmann M, Mari T, Scholz F, Timm L, Twamely S, Migotti R, Dittmar G, Rehm A, Stein U. MACC1 regulates TfR and EGFR clathrin-mediated endocytosis and receptor recycling in colorectal cancer. In submission, 2019

2. Radhakrishnan H, Walther W, Zincke F, Kobelt D, **Imbastari** F, Erdem M, Kortüm B, Dahlmann M, Stein U. MACC1—the first decade of a key metastasis molecule from gene discovery to clinical translation. Cancer Metastasis Rev. 2018 Dec;37(4):805-820. doi: 10.1007/s10555-018-9771-8. PMID: 3060725

3. Pieraccioli M, **Imbastari** F, Antonov A, Melino G, Raschellà G. Activation of miR200 by c-Myb depends on ZEB1 expression and miR200 promoter methylation. Cell Cycle. 2013 Jul 15;12(14):2309-20. doi: 10.4161/cc.25405. PMID 24067373

Alla vita, alla sua bellezza, felicità e unicità.

Alla libertà e con essa la verità.

1. Introduction

1.1 CRC: incidence, mortality and risk factors

Cancer represents an enormous burden on societies across the world. Generally, in less developed countries the incidence and mortality of cancer are higher than in developed countries, but both have increased over the last 20 years due to the growth and aging of populations and their increasing exposure to known and newly emerging risk factors. Global statistics estimated 18.1 million new cancer cases and 9.6 million cancer deaths worldwide in 2018[1]. Cancer death rates are the most effective measure to understand research progress against cancer, and although they have been rising in the 20th century, the rates had dropped of 26% (2.3 million fewer cases in total between 1991-2015) because of the early detection and targeted treatments[2]. Nowadays, colorectal cancer (CRC) is the sixth most common cancer in men for incidence and mortality, in new estimated cases worldwide. CRC dramatically strikes more women than men. In US for example, CRC is the third-leading cause of cancer deaths (respectively 12% for women and 9% for men). Worldwide, CRC is the fourth most common cancer in new cases incidence and the fifth for mortality for women[3].Estimated global numbers of CRC-related deaths in 2018 show the highest rates in Asia and Europe, in particular in the south. The 5-year survival rate for those with localized CRC, is 80% but declines to 58%, 10 years after diagnosis. If the cancer has spread metastatically to nearby organs or lymph nodes by the time of diagnosis, 5-year survival drops to 15%[2]. The risk of CRC increases with age and drops dramatically starting around the age of 50. CRC also increases in incidence when considering factors such as obesity, physical inactivity, a diet high in red or processed meat and low in fruits and vegetables, alcohol consumption, and long-term smoking. There is a hereditary component; risk increases for those with a personal or family history of CRC and/or polyps, a personal history of chronic inflammatory bowel disease (e.g. ulcerative colitis or Crohn disease), some other inherited genetic conditions (e.g. Lynch syndrome), and type 2 diabetes[2].

1.2 Tumorigenesis and cancer progression

Tumorigenesis and progression of CRC is a slow, multistep process driven by critical genetic alterations which can be inherited (germ-line mutations) or progressively acquired (somatic mutations). These lead to a high predisposition for CRC development, often resulting in metastasis. Hereditary CRC has been categorized into two basic types with different clinical and pathological features according to the genetic background: Familial Adenomatous Polyposis (FAP) and Hereditary

Non-polyposis CRC (HNPCC)[4]. FAP is typically characterized by the loss of the gatekeeper adenomatous polyposis coli (APC) gene, while HNPCC is characterized by genetic instability and mutations in the mismatch repair process and associated genes[4]. Understanding the molecular basis of CRC has been a long and challenging process which has still not been completed. However, huge improvements were achieved in the last years to comprehend the underlying mechanism of CRC progression. As many kinds of cancer, also CRC is marked by a loss-of-function defects in tumor-suppressor genes functions or gain-of-function mutations in oncogenes.

One of the best characterized features of CRC is genomic instability, which can occur through the physical loss of a wild-type copy of a gene and its structure (e.g. APC, cellular tumor antigen p53 or the small mother against decapentaplegic (SMAD) gene[5]. A subgroup of patients exhibit an inactivation of genes involved in the mismatch repair process, inherited inactivation somatically or through the germ line, as in Lynch Syndrome (2-4% of total CRC cases, for HNPCC)[6]. The most common genes responsible in this context, are DNA mismatch repair protein 1 and 2 (MLH1, MLH2); very recently, the mutY homologue gene (MYH) was added to this list. Gene inactivation participates in tumor progression by epigenetic silencing, which is mediated by the aberrant methylation of promoters in CpG islands.

CRC develops through a sequential, multistep process, beginning with the mutational inactivation of tumor-suppressor genes, in some cases initially involving only APC, and then progressing to p53 and transforming growth factor β (TGFβ). A hyperactivation of oncogenes also contributes extensively to CRC development. RAS (small GTPase KRas) and BRAF (serine/threonine-protein kinase B-raf) are key regulators which promote tumor progression by triggering the downstream hyperactivation of the mitogen-activated protein kinase (MAPK) signaling pathway. In addition, somatic mutations of PI3KCA (the catalytic subunit of PI3K, phosphoinositide 3-kinase) and the loss of the phosphatase and tensin homolog (PTEN) account for one third of the mutations observed in CRC. The aberrant regulation of signaling pathways or receptors has also been commonly accepted as a critical step in causing adenoma to develop into carcinoma. An activation of the epidermal growth factor receptor (EGFR) or the vascular endothelial growth factor receptor (VEGFR) strongly influence the overall survival of CRC patients[7].

The last decade has seen mounting evidence that lifestyle and diet constitute risk factors for CRC. The increased consumption of red meat, for example, has been shown to increase consistently the risk of developing CRC, and this depends on heme (a combination of ferrous iron and a heterocyclic organic compound). Heme promotes cancer possibly through genetic alterations in the colorectum, affecting particularly the APC and p53 genes[8]. In particular, heme is degraded and processed by heme oxygenase, releasing free ferrous iron. This circulating iron promotes cancer in different ways,

such as, forming reactive oxygen species (ROS) and malondialdehyde via the fat peroxidation pathway[9,10].

1.3 Adenoma-carcinoma sequence

CRC development proceeds along two different pathways: the chromosomal instability (CIN, canonical pathway) or through microsatellite instability (MSI). However, only 15% of CRC gain a bi-allelic inactivation of the mismatch repair genes expressed in MSI[11,12]. Approximately 85% of CRC are characterized by CIN generated during a step-by-step acquisition of mutations in several key regulators, which finally promote cell survival and growth by evading cell apoptosis. CRC progression overlaps with progressive and increasing CIN in the adenoma-carcinoma sequence. CIN involves not only mutations but also the loss of heterozygosity (LOH) of genes, epigenetic silencing through methylation, transcriptional upregulation of oncogenes, tumor suppressor repression, translocations or chimeric fusions, resulting finally in a loss or gain of function of specific genes. Moreover, CIN is the result of early somatic mutations that provide the cell with a survival advantage, resulting in a clonal expansion that initiates evolving stages of tumor formation[13]. The adenoma-carcinoma sequence was first hypothesized by Fearon and Vogelstein, who proposed that specific genetic events are accompanied by progressive alterations of tissue (Fig. 1). The principal genetic mutations of the sequence are briefly discussed below.

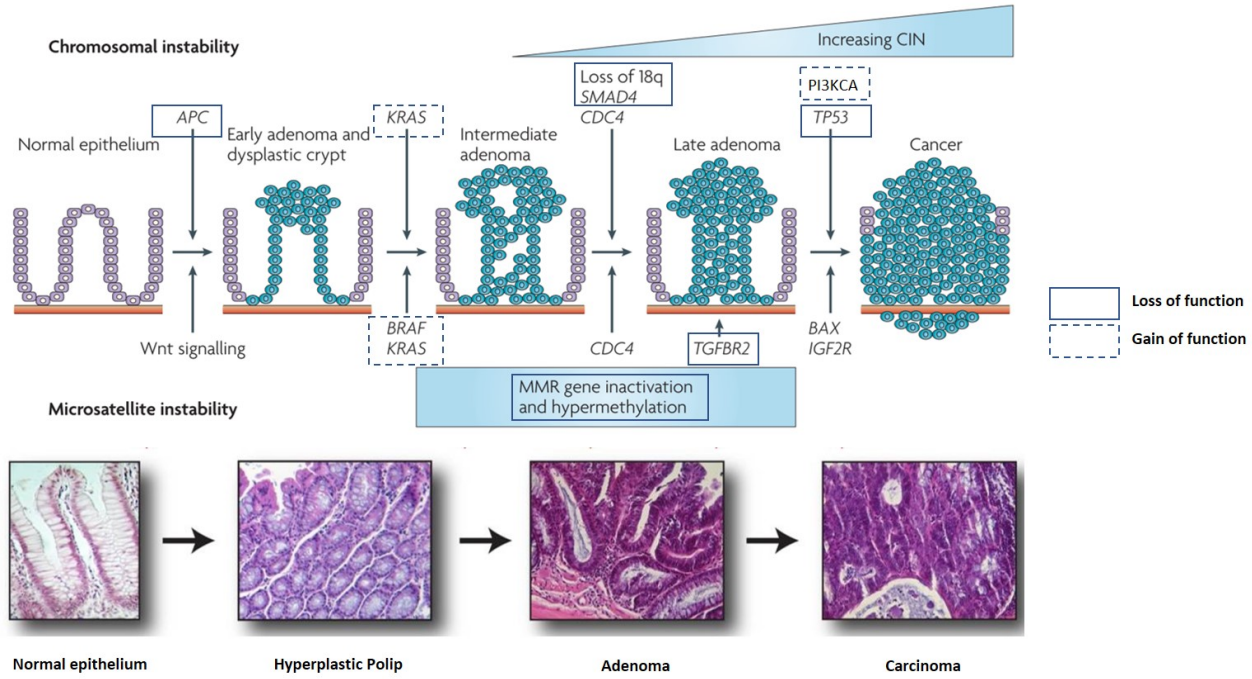

Figure 1 The CRC Adenoma-carcinoma sequence. Brief description of the model of the adenoma-carcinoma sequence summarizing all the reported visible clinical pathological changes with the genetic aberrations during the early CRC stages and later CIN progression, resulting in a sequential loss or gain of function of several genes. The first steps of the adenoma formation are characterized by loss of APC. Sequentially, adenomas undergo several mutations, such as mutations in KRAS or BRAF. These events are followed by the loss of chromosome 18q and SMAD4, downstream of TGFβ, and mutations in p53. In parallel the MSI, is characterized

by the deficiency of the mismatch repair genes and system which results in microsatellite mutations. In the lower panel, histological aspects of CRC progression from normal epithelium to carcinoma are represented. Adapted from Walther et al., Nat Rev, 2009 and Li et al., Curr Mol Pharmacol, 2009.

1.3.1 APC, β-catenin and Wnt signaling

Early stages of CRC transformation are marked by the loss of the APC function, located on chromosome 5q21. Germ line mutations in the APC gene typically lead to FAP development and CRC in 90% of the cases [14,15]. APC is the key regulator of a multi-protein complex together with the glycogen synthase kinase 3 β and axin (APC-GSK3β-axin complex) of the Wnt pathway. This complex regulates intracellular levels of β-catenin by phosphorylating it and leading the protein to the degradation in the proteasome, resulting in a modulation via Wnt signaling[16,17]. Mutations in APC result in a loss of β-catenin regulation by impairing and avoiding its degradation, migrating instead into the nucleus, and resulting in constitutively active transcription of the T-cell factor/lymphoid enhancer-binding factor (TCF/LEF) promoter and therefore enforced Wnt signaling[18].

1.3.2 KRAS, BRAF and MAPK signaling

Further genetic alterations during early stages of the adenoma-carcinoma sequence involve the small GTPase KRas (KRAS). KRAS is a GTP-binding protein located on 12p12.1, whose GTPase activity serves as an effector of several downstream pathways[19]. The mutation status of KRAS is an established predictive marker for treating CRC and determines patients response to EGFR inhibitors[20]. The EGFR ligand EGF leads to a homodimerization of the receptor and consequently to transphosphorylation of docking sites of the cytoplasmic tail (phosphorylated tyrosine -pY- e.g. 1067/1068). The docking sites bind generally to GRB2 or GAB1. These adaptors recruit the guanine nucleotide exchange factor (SOS) to activate the small GTPase RAS. KRAS activates the mitogen-activated protein 3 kinase (MAP3K, RAF), which activates MAP2K (MEK1/2) in a sequential cascade and ends in the final activation of MAPK (ERK1/2)[21–23] (Fig.2). This increases MAPK signaling and promotes cell proliferation, survival and metastasis[24]. Oncogenic mutations of these proteins are present in about 40% of CRCs. Three mutations are the most frequent[25], with different effects on the activating potential of KRAS and distinct responses to therapies[26]. KRAS mutations are independent prognostic markers in CRC associated with differential outcomes. The most studied and well-known mutations are in exon 2 (codon 12 and 13) and exon 3 (codon 61). A poorer prognosis has been associated with the glycine to valine substitution of codon 12[27]. Due to this convergence, CRC stage IV patients with

KRAS mutations react poorly to cetuximab and panitumumab and receive low benefits compared to patients with wild type KRAS[28–33].

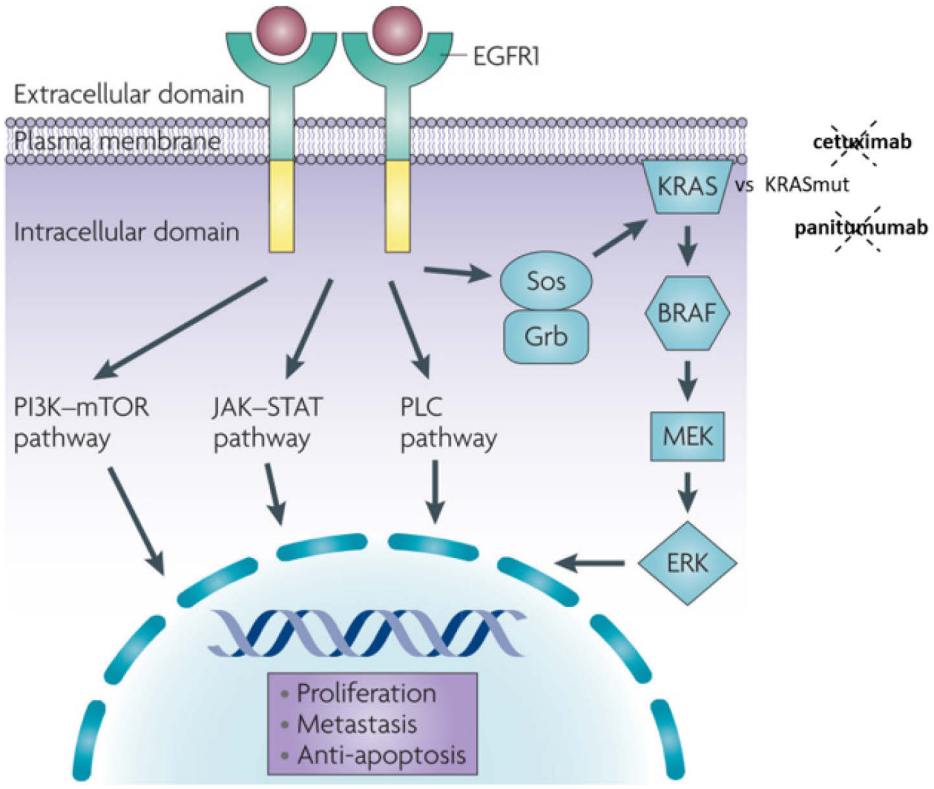

Figure 2 EGF-stimulated signaling cascades and their effects. Upon EGF binding EGFR, the receptor homodimerizes activating the tail intracellular kinase domain. In particular, the KRAS signaling cascade is then activated by the binding of the adaptor proteins GRB2 and SOS to EGFR tail, leading to a progressive phosphorylation of the downstream kinases BRAF-MEK-ERK, leading to the final effect: cell growth, proliferation and metastasis development. KRAS mutational status is predictive for CRC patients, in particular because KRAS mutated patients are resistant to cetuximab and panitumumab therapies. Adapted from Walther et al., Nat Rev, 2011.

1.3.3 p53 gene and the DNA repair balance

P53 is a tumor suppressor protein whose gene is located on the short arm of chromosome 17 (17p). P53 is the most frequently altered gene is many cancer types, also known as the "genome guardian"[34]. Its transcription is activated during cellular stress in non-pathogenic conditions, in particular, its stabilization leads to a specific DNA binding of target genes resulting in growth arrest and cell cycle arrest and cell death[35–37] (e.g. cyclin-dependent kinase inhibitor 1 -p21-, growth arrest and DNA damage inducible alpha -GADD45A-, E3 ubiquitin-protein ligase -MDM2-). During oncogenic stress or DNA damage, P53 can promote the repair of DNA via several genes such as GADD45[38]. More interestingly, after DNA damage p53 is phosphorylated by ATM, migrates into the nucleus and binds

to the p21 promoter, leading to a block of the cell cycle via cyclin-dependent kinase 4/6 and D (cdk4-cdk6/cyclin D)[39]. P53 is also able to promote cell death by promoting Noxa transcription when DNA damage is irreparable; when DNA is successfully repaired or in unstressed cell conditions, p53 is degraded from the proteasome after MDM2-mediated ubiquitination and the cell cycle is restored[39]. Pathogenic alterations of the p53 gene or the allelic loss of 17p is very common in CRC and determines the impact and potential of cancer therapy[40]. Mutations in the gene have been reported in 4-26% of adenomas, 50% in adenomatous polyps and in 50-75% of adenocarcinomas[41]. A loss of p53 is associated with the transition from adenoma to carcinoma and contributes to the late and aggressive stages of CRC.

1.3.4 18q loss and the TGFβ signaling

The deletion of the long arm of chromosome 18 is the most common cytogenetic disruption associated with a poor prognosis in CRC; 18q is lost in 10-30% of early adenomas and 60% of late adenomas[41,42]. The original candidate in this region is directly linked and responsible for CRC development, was thought to be the "deleted in CRC" (DCC) gene. Later, other tumor suppressor genes were identified in this region, including SMAD2 and SMAD4, which are involved in CRC development and as mediators of the inhibitory signal from the TGFβ signaling pathway[43,44]. Activated TGFβ signaling regulates features of the cell including growth, apoptosis, differentiation and matrix production through the transcription activation via SMAD2/4 of a myriads of target genes[45]. In CRC the deletion of SMAD2 and SMAD4, considered as tumor suppressors, or deregulation of SMAD7 (SMAD2/4 inhibitor) leads to a deregulation of the TGFβ signaling and resulting in poor prognosis of CRC by increasing the epithelial mesenchymal transition (EMT) and migrative features of the cell[46–48].

1.3.5 EMT: how CRC metastases generate during cancer progression

Surgery is still the main treatment for early stages of patients with tumors that have not yet metastasized. However, several factors influence the results, such as preoperative staging and the choice of treatment (due to UICC or TNM staging system), together with mutational screening[49,50]. CRC survival is highly dependent upon the stage and progression of the disease, and only 10% of patients show a 5-year survival rate when presenting metastasis[51]. 90% of cancer deaths overall are due to metastatic dissemination, compromising the outcome of treatments[52]. One of the hallmarks

of tumor progression is the ability to invade and metastasize[53]. Metastasis formation is an extraordinary complex process and underlies the ability of a cancer cell to disseminate through the blood flow or lymph nodes from the primary tumor to distant organs, to be able to form a clinically relevant lesion at the new secondary site[54,55]. This process is known as metastatic dissemination and is represented in Figure 3.

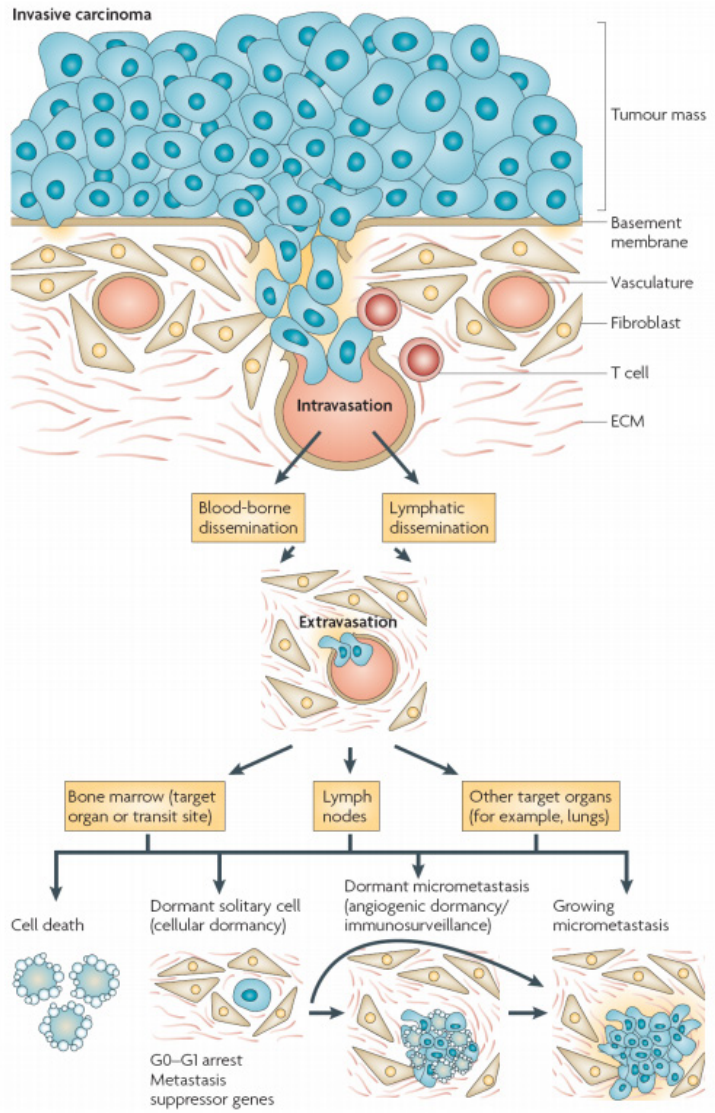

Figure 3 Principal steps of EMT. Tumor cells are enabled to migrate and invade the stroma by transcription enhancement of several markers and genes for invasiveness such as N-Cadherin, Vimentin and mesenchymal integrins. Tumor cells degrade extracellular matrix (ECM) and disseminate into the blood stream or into lymphatic routes. After dissemination, tumor cells might target several sites, as bone marrow, lymph nodes or other organs. In this sites and organs tumor cells might follow different fates as shown, but principally arise and form growing micro metastases. From Aguierro, Nat Rev Cancer, 2007

Numerous molecular alterations accompany the metastatic dissemination process[56]. One of the first is the dissolution of the tight junctions, triggered by a decrease of claudin-1 and occludin which are degraded or delocalized along with E-cadherin. Coinciding with the molecular changes, cells in this phase lose apical-basal polarity[57]. The TGFβ receptor makes a major contribution by activating EMT driving factors: zinc-finger protein (SNAIL), zinc-finger E-box-binding (ZEB) and basic helix-loop-helix (bHLH, TWIST). These transcription factors can repress epithelial genes (e.g. E-cadherin) and activate genes associated with the mesenchymal phenotype (e.g. Vimentin). During EMT, metastatic cancer cells not only change their integrin repertoire to facilitate migration but also increase the production of metalloprotease 2 and 9 (MMP2 and 9), enhancing ECM degradation and permitting invasion[58,59]. As well, many receptors and pathways are involved in EMT. In particular, an activated RAS and RAF cascade or mutations in the MAPK pathway lead to continuous activity of SNAIL and Rho-GTPase activity and increased motility[60]. EGFR is also involved in the process and when stimulated via EGF, it induces the endocytosis of E-cadherin, favouring cell movement. It also induces TWIST expression, leading to a reduction of E-cadherin levels[61,62] 2 and 9, enhancing ECM degradation and permitting invasion.[58,59] As well, many receptors and pathways are involved in EMT. In particular, an activated RAS and RAF cascade or mutations in the MAPK pathway lead to continuous activity of SNAIL and Rho-GTPase activity and increased motility.[60] EGFR is also involved in the process and when stimulated via EGF, it induces the endocytosis of E-cadherin, favouring cell movement. It also induces TWIST expression, leading to a reduction of E-cadherin levels.[61,62]

1.4 Current clinical intervention therapies for CRC

The most important known prognostic marker for CRC is the pathological stage of the primary tumor at the time of diagnosis. Currently the tumor-node-metastasis (TNM) staging system of the Union for International Cancer Control's (UICC) is used to analyze the disease and classify the extent of cancer invasion to the bowel wall and the metastatic dissemination to the lymph nodes. In particular, the primary tumor growth (T), lymph nodes infiltrations (N) or metastasis development (M) are associated with numbers (1-4 and letters a-b) to assess the CRC stage, prognosis and appropriate treatment. The 5-year survival rate for those with localized CRC, classified following the UICC staging system[63], is 80% but declines to 58%, 10 years after diagnosis. If the cancer has spread metastatically to nearby organs or lymph nodes by the time of diagnosis, 5-year survival drops to 15%[64,65].

The most common line of diagnosis and treatment for CRC in the absence of metastatic dissemination is first, the correct staging and a subsequent resection/surgery (colectomy). Colectomy

is an efficient and curative method, if associated with a radiation pre- and post-operative (neoadjuvant and adjuvant therapies). Patients with early, localized stages of CRC (TNM 0-I) show a 5-year survival of 90%[52]. For stage II-III patients, in whom the primary tumor has already invaded the surrounding tissue and lymph node metastases, resection is followed by adjuvant chemotherapy treatment. Milestones of CRC treatment have been the use of fluorouracil (5-FU) and leucovorin and Capecitabine. Respectively the first two are administered together; 5-FU is a fluorinated pyrimidine, that inhibits the thymidylate synthetase and consequently pyrimidine nucleotide synthesis. 5-FU is normally administered together with leucovorin, a reduced folate that stabilizes the binding between 5-FU and thymidylate synthetase.

Their synergistic effect finally inhibits DNA synthetase and induces cell cycle arrest and apoptosis. Capecitabine is a pro-drug that undergoes enzymatic conversion to 5-FU. All three drugs cause major side effects including neutropenia, stomatitis, diarrhea, nausea and vomiting. Several other drugs have been approved by the FDA for later stages of CRC: Irinotecan stabilizes DNA breaks and oxaliplatin induces apoptosis via the formation of DNA bulky structures[65].

In advanced stages (IV) of CRC metastatic dissemination limits the success of the treatment and it is the cause of a severe drop in the 5-year survival rate, to 12-15%[52]. To improve this situation, the FDA has approved several other treatment combinations which are already in clinical use. The most common is FOLFOX (oxaliplatin, fluorouracil, and leucovorin). Unfortunately, it causes neuropathy in 92% of patients. New targeted therapies involve monoclonal antibodies against specific targets such as EGFR on cancer cells, which aim to block or inhibit cellular pathways essential for tumor growth. Further FDA-approved therapies include cetuximab and panitumumab (ABX-EGF), monoclonal antibodies designed to target the extracellular domain of EGFR, inhibiting ligand-induced downstream signaling, and bevacizumab, targeting the vascular endothelial growth factor to inhibit tumor vascularization.[66,67]

The aim of these inhibitors is to improve CRC treatment by targeting VEGF/VEGFR triggered PI3K/AKT- FAK- and MAPK signaling pathways at different levels affecting migration, cell cycle progression, survival and proliferation of tumor cells.[68] Nevertheless, several studies conducted on cetuximab have revealed limitations. Cetuximab is effective only whether the patient bears a wild-type form of KRAS or EGFR. When KRAS or EGFR are mutated at the onset of metastasis, resistance is dependent on the hyperactivation of the downstream cascade, due to constitutively active upstream KRAS.[33,69,70] New targeted therapies are needed to overcome the effect of these mutations and constitutive hyperactivation of the EGFR pathway due to its negative impact on treatment outcomes.

1.5 MACC1: a newly identified prognostic and predictive marker for CRC

In 2009, the group of Prof. Stein identified MACC1 (Metastasis associated in colon cancer 1) as a prognostic and predictive marker in CRC through a genome-wide RT-PCR analysis of the normal mucosa, primary tumors and metastases of patients. MACC1 mRNA expression is higher in malignant tissue than in adenomas or normal mucosa, and levels in the primary tumor correlate positively with metachronous distant metastasis formation and negatively with metastasis-free survival. The 5-year survival rate for stage I-III CRC patients with high MACC1 expression in the primary tumor is only 15% compared to subjects with low MACC1 expression which show a higher 5-year survival rate (80%). There is increasing evidence that MACC1 plays pivotal roles in development and progression of entities beyond CRC, particularly in lung adenocarcinoma, esophageal cancer, ovarian cancer, glioblastoma, glioma, pancreatic cancer, squamous cell carcinoma, renal pelvis carcinoma, bladder urothelial carcinoma, cervical cancer, osteosarcoma, breast, esophageal and gastric cancer[71–78], totalizing 22 different entities. However, the underlying mechanisms by which MACC1 mediates progression in many of these solid tumor entities are still vague. Functionally, MACC1 regulates the mRNA expression of the HGF receptor MET, increasing its transcription via the MET promoter. Prior work has identified MACC1 as a prognostic and predictive biomarker, not only in CRC, but in diverse type of cancers. Its effects include increases of cell motility and migration via MACC1/HGF/MET, PI3K/AKT and MEK/ERK, Wnt/β-catenin axes coordinating EMT[79,80] (Fig. 4).

Furthermore, MACC1 overexpression leads to cell invasion and angiogenesis, and induces tumor growth and metastasis formation in xenograft mice [81,82]. Recently our group proved also, that MACC1-dependent tumor progression depends on increased activation of pluripotency mediated by the MACC1/Nanog/Oct4 axis driven by Wnt-β-catenin signaling[83]. MACC1 overexpression appears to decrease 5-FU and cisplatin sensitivity in gastric cancer via MCT1-upregulated expression affecting the results of therapy and the relapse of the cancer, but showing treatment-predicting traits[84–87]. We recently used high-throughput screening to identify two new potent MACC1 transcriptional inhibitors: Rottlerin and Lovastatin, resulting in reduced MACC1 mRNA and protein expression and leading to reduced cell motility[88].

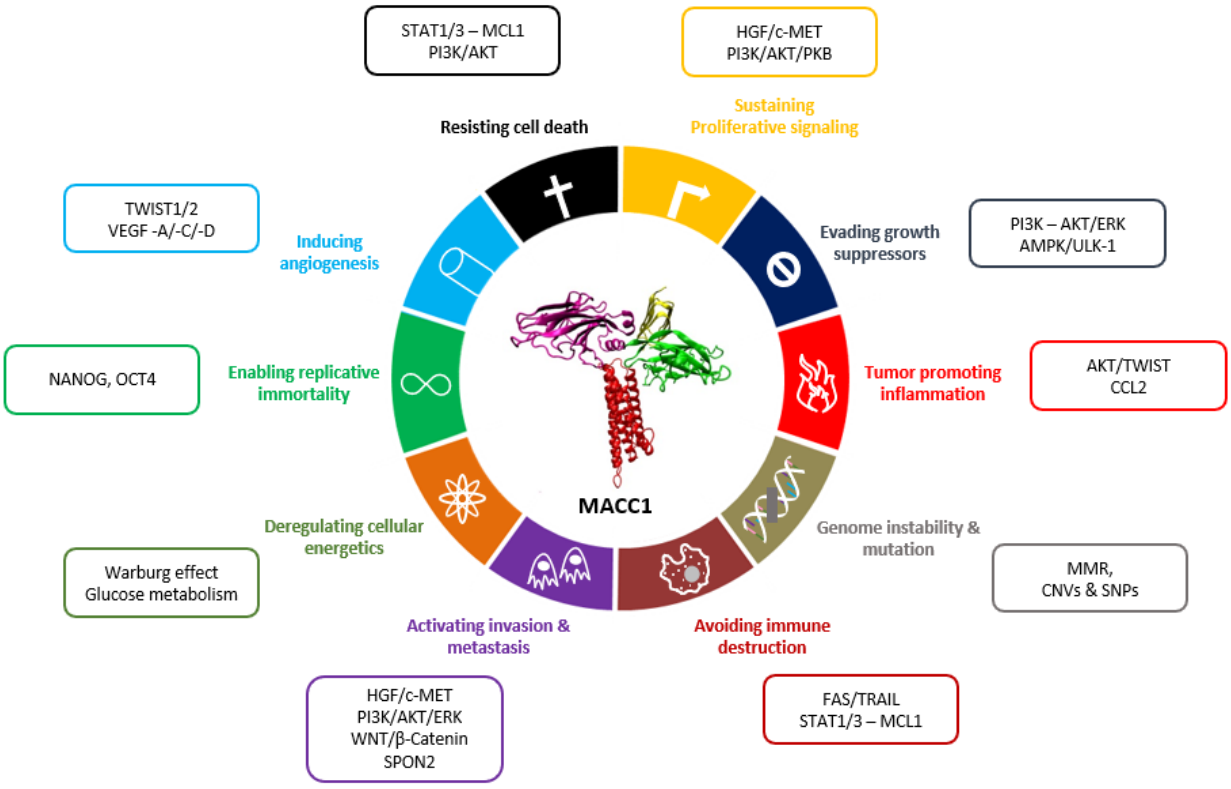

Figure 4 MACC1 3D structure and impact on cancer hallmarks and associated pathways. MACC1 impact has been related to cancer hallmarks by characterizing its involvement in several signaling pathways and relating it to the biological characteristics of cancer. Many pathways are involved in the MACC1-mediated effect on cancer cells. From Radhakrishnan et al., Cancer and metastasis Review, 2018

1.5.1 MACC1 structure and roles related to pathways

The MACC1 gene is located on the human chromosome 7 (7p21.1)[89]. The unspliced MACC1 transcript contains seven exons and six introns, resulting after splicing in a final coding cDNA of 2,559 nucleotides. The gene encodes for a protein of 852 amino acids. Several domains have been predicted in the protein structure of MACC1 (Fig. 6)[90].

The N-terminal domain of the protein contains a clathrin box, two Epsin 15 Homology interaction motifs (NPF), and an interaction motif (DPF) for adaptor protein 2α (AP-2α). The N-terminal domain presents is then followed by domain present in zona occludens 1 (ZO-1) and uncoordinated-5 proteins (ZU5 domain), and a domain conserved in ankyrins domain (UPA domain). These domains are shown in Figure 5.

The C-terminal region of MACC1 includes a SH3 domain which is generally important for interactions between proteins in particular with the proline rich domain (KxxPxxP, PRD) and signalosome proteins such as growth factor receptor bound protein 2 (GRB2), E3 ubiquitin-ligase (c-Cbl), and proto-oncogene tyrosine kinase (Src)[91] (Fig.5). It is also known that the SH3 domain typically interacts with proline rich domains (PRD) of other proteins, such has dynamin[92,93]. Interestingly, the location of MACC1 on chromosome 7 is near the TWIST gene which is involved in CRC and tumorigenesis. MACC1 is able to upregulate the TWIST1/2 genes promoting vasculogenic mimicry, but also to induce the activation of the TWIST/VEGF signaling pathway in gastric cancer[94,95].

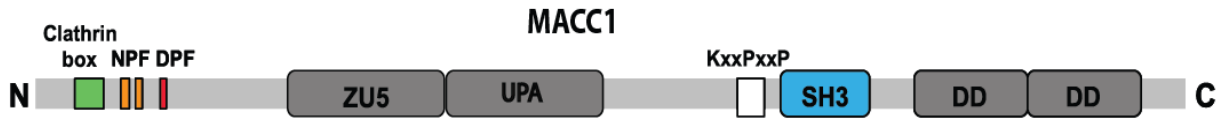

Figure 5 Schematic overview of MACC1 protein structure. MACC1 shows several clathrin-mediated endocytosis domains at its N-Terminus and C-Terminus. At the N-Terminus: the clathrin box, two NPFs motifs, and the DPF motif. Centrally: ZU5 and UPA domains. At the C-Terminus: the proline-rich domain (KxxPxxP), the SH3 domain and two death domains (DD).

One of the recently discovered targets of MACC1 is β-catenin and Wnt signaling; in nasopharyngeal carcinoma and CRC, MACC1 and β-catenin are positively correlated; knocking down both inhibits proliferation, migration and invasion. Silencing MACC1 inhibits β-catenin and c-Myc but doesn't affect ERK1/2 expression in NPC.

Accordingly, in CRC MACC1 overexpression upregulates MET, β-catenin, c-Myc, cyclin D1 and MMP9 expression and the upstream factor p-GSK3β. In HCT116 CRC cells, MACC1 overexpression causes a suppression of E-cadherin and increases vimentin, the first step for a cell undergoing EMT. Taken together these data show a prominent role of MACC1 in tumorigenesis and EMT via Wnt/β-catenin signaling[72,96].

Very recently, MACC1 has been characterized regarding another fundamental pathway: PI3K/AKT. Although no effect of MACC1 overexpression on the PI3K/AKT pathway has been shown in CRC[89], another effect has been described in gastric cancer and hepatocellular carcinoma. In gastric cancer, MACC1 overexpression predicts poor prognosis and enhances proliferation, migration, invasion;

additionally, it induces trastuzumab resistance in GC cell lines, enhancing their resistance to the metabolic stress via the Warburg effect and activating PI3K/AKT signaling[97,98].

MACC1 is also involved in the HGF/MET pathway as a key regulator; our lab identified MET as a transcriptional target of MACC1. In CRC it is also known that MET-promoting tumorigenic progression depends on a collaboration and balance between MACC1 and miR-1[99]. This microRNA has generally a suppressive role but Giordano's group has shown that in metastatic tumors, its downregulation correlates with the overexpression of MET and MACC1, favoring MET-induced tumor growth[99]. Furthermore, MACC1 has been identified very recently as a regulator of the MAPK/ERK pathway; in pancreatic cancer MACC1 is not only an indicator of poor prognosis but its inhibition suppresses proliferation and migration.

When MACC1 is downregulated, pancreatic cell lines are more sensitive to gemcitabine treatment via inhibition of the ERK signaling pathway[100]. In the ovarian cancer cell line SKOV-3, it has been shown that silencing MACC1 leads to a higher sensitivity of the cells to cisplatin, increased cisplatin-induced apoptosis, and decreases in p-ERK1/2 expression[84]. In gastric cardia adenocarcinoma, MACC1 might contribute to cancer progression as well; it has been predicted as a target of miR-141, which suppresses MACC1 by binding its 3'-UTR, leading to an effect on MAPK/ERK and P38 MAPK signaling pathway[101]. In summary, over the last 10 years the role of MACC1 has been dissected in several cancer types and has been implicated in pathways such as the HGF/MET axis, MAPK/ERK, VEGF, TWIST1/2, Wnt/β-catenin and PI3K/AKT.

1.5.2 Role of MACC1 in cancer progression and metastasis

MACC1 has been identified as a prognostic and predictive marker for many solid cancer entities. Its overexpression promotes proliferation, invasion, migration, and colony formation[72,74,77,78,100,102–107]. In vivo studies with several mouse models showed that the intrasplenic injection of SW480 cells overexpressing MACC1 clearly increases tumor growth and liver metastasis compared to the empty vector, confirming its tumorigenic and metastatic capabilities[89]. Recently, reports have shown that silencing MACC1 with target specific shRNA (SW620/shMACC1) decreases tumor formation and metastasis in xenografted mice[81]. MACC1's role in cancer and its effect has been also investigated with regard to another characterized prognostic marker: the cysteine-rich protein 61 (CYR61). Silencing both by targeting them with miRNA (miR-100 and miR-143), inhibited the EMT process that promotes apoptosis in CRC cell lines and decreases tumor growth. Targeting MACC1 and CYR61 decreased not only the rates of invasion and metastasis formation but also the size and growth of the

tumor, thereby increasing the overall survival of tumor-bearing mice. In conclusion, targeting MACC1 in combination with CYR61 via miRNAs may be a useful therapeutic strategy to treat CRC in future years[82].

1.5.3 MACC1 is a target of many miRNAs

An abnormal expression of specific miRNAs contributes to cancer development by regulating proliferation, apoptosis and drug resistance in cancer cells. A dysregulation of the silencing effects of other miRNAs may cause tumor progression and metastasis formation[108]. The relationship between MACC1 and miRNAs has been widely explored in the last 4 years. Many papers show direct miRNA effects on proliferation, invasion and migration via targeting MACC1. Recently, MACC1 was identified as a target of miR-994. In gastric cancer cells, miRNA-994 inhibits EMT and metastasis formation but the re-expression of MACC1 rescued the effect, restoring EMT probably via the MET/AKT pathway[109]. In CRC cells, MACC1 has also been shown to be a target of miR-433. The tumor-suppressive characteristics of this miRNA lie in its ability to reduce viability and promote apoptosis in CRC cell lines by targeting MACC1 expression[110].

A novel therapeutic approach for treating liver metastasis in CRC has been suggested through the negative regulation of MACC1 expression targeted by Hsa-miR-574-5p. After an *in silico* analysis this miRNA was identified as a negative regulator of MACC1; its knockdown increased colony formation, cell invasion and spheroid formation of HCT116 cells, compared to the control group. Mimic transfected SW1116 cells showed the opposite effect. Finally, these effects were studied in a mouse model of liver metastasis after intrasplenic injection of GFP-labeled SW1116 and HCT116 cells, and the incidence of liver metastasis was increased[111].

miR-338 has exhibited a prominent suppressive behavior by targeting MACC1 in several cancer types. In HCC, miR-338-3p shows a negative correlation with MACC1, VEGF and β-catenin; its suppression corresponds to an increase in angiogenesis. In normal brain and glioma tissues, miR-338-3p also regulates tumor progression by silencing MACC1. In glioma cell lines the miRNA increases apoptosis and slightly inhibits proliferation, while MACC1 partially rescues this effect. In conclusion, in glioma cells this miR regulates aggressive cancer by targeting MACC1, engaging a tumor-suppressive and balancing role. More relevantly, in gastric cancer miR-338-3p silences ZEB2 and MACC1, inhibiting migration and invasion and upregulating the expression of EMT markers such as E-cadherin. By targeting MACC1, miR-338-3p inhibits also the MET/AKT pathway, whereas a re-expression of MACC1 and ZEB2 in this context reverted the cancer-inhibitory effects on EMT[79,112,113]. To conclude, MACC1

has become a widely studied prognostic marker and a number of aspects of its relationships to miRNAs remain to be explored. This suggests that targeted and combined therapies might constitute a promising avenue for new therapies.

1.6 Hints about MACC1 functions from its homologue SH3BP4

In this thesis, SH3BP4 was studied as an homologue of MACC1; they share a 43.7% sequence homology[91]. In particular, they own similar clathrin boxes NPFs motifs, DPF motif and a SH3 domain. In this study we dissected the role of MACC1 in endocytosis using SH3BP4 as reference and positive control, considering the homology. Other proteins with similar to MACC1 in the domain composition include ANK, UNC5, UNC5CL[71,89,90]. The MACC1 homologue SH3BP4 (also named Transferrin Trafficking Protein, or TTP), is a SH3-domain binding protein first identified in 1999 through a genome-screen in corneal fibroblasts[114]. It is expressed in pancreas, placenta, heart and kidney. Its localization has been studied via FISH and the gene for SH3BP4 was found in 2q37.1-q37.2. The translated protein contains 963 amino acids (107.5 kDa) and belongs to the EH–network family of endocytosis proteins. Its structure contains several motifs including three NPFs, a DPF and a P-x-x-P motif, two SH3 domains, several tyrosine phosphorylation sites and death domains at its C-terminus[115] (Fig. 6).

Figure 6 Schematic structure of SH3BP4. In different colours from the N-Terminus: the CB, an SH3 domain, three NPFs, a PxxP domain, the ZU5 domain, the UPA domain, a second SH3 domain, two DD domains.

The 1999 study suggested an involvement of SH3BP4 during endocytosis, a role confirmed in a number of subsequent studies. SH3BP4 localizes mainly at the plasma membrane (PM) and in early and late endosomes in retinal pigment epithelial cells. One of its identified regulators is the 14-3-3 protein[114]. The two proteins interact directly at Ser^{245}, a residue essential for their association. SH3BP4 is responsive to oxidative stress and is phosphorylated on Ser^{245} by the AKT kinase, the downstream target of PI3K, to promote the association with 14-3-3[116–120]. The first clear indication on SH3BP4 function was introduced by Tosoni's group[121]. SH3BP4 interacts with clathrin, dynamin, epsin 15, and the AP-2 complex. It has been found in transferrin receptor-clathrin coated pits and coated

vesicles (TfR-CCPs and TfR-CCVs), and the colocalization of SH3BP4 with CLTC and TfR within these vesicles is dependent on the SH3 domain of TTP. SH3BP4 specifically regulates TfR endocytosis without perturbing the internalization of EGFR and low-density lipoprotein receptor (LDLR). Its knockdown or overexpression leads to a decreased rate of TfR internalization without affecting the recycling route. SH3BP4 specifically regulates TfR cargo loading on the vesicle through phosphorylation events and it has also been hypothesized that this might exclude SH3BP4 from EGFR-containing pits. Three models have been proposed of SH3BP4 function during TfR endocytosis[121] (Fig. 7) without perturbing the EGFR and LDLR. Its knockdown or overexpression lead to a decreased rate of TfR internalization without affecting the recycling route. SH3BP4 specifically regulates TfR cargo loading on the vesicle through phosphorylation events and it has also been hypothesized that this might exclude SH3BP4 from EGFR-containing pits. Three models have been proposed of SH3BP4 function during TfR endocytosis[121] (Fig. 7)

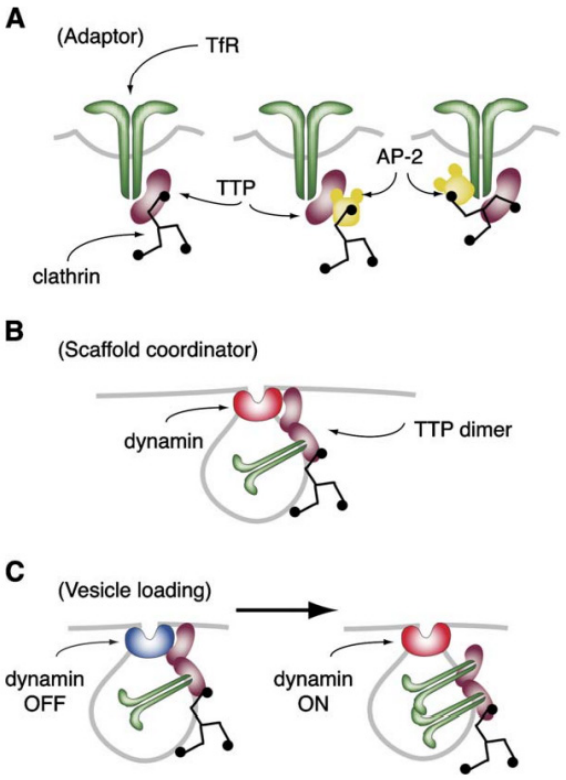

Figure 7 SH3BP4 functions and speculated working models during TfR-CCV formation. (A) Adaptor model: TTP links TfR to CLTC (directly, left) or via AP-2 (indirectly, center) or with AP-2 (right). (B) Scaffold coordinator: TTP recruits dynamin regulating the fission machinery, TTP might bind CLTC directly. (C) Vesicle loading model: TTP acts as in (B) but switches off dynamin until TfR is not loaded into the pit. After TfR is loaded TfR excludes TTP from the machinery, allowing the activation of dynamin. The three models are not exclusive, and have been adapted from Tosoni et al., Cell, 2005.

Further work has shown that SH3BP4 has functions related to the fibroblast growth factor receptor 2b receptor (FGFR2b). Olsen's group showed that SH3BP4 acts as a molecular switch of the FGFR2b

receptor and is recruited at the signalosome of the FGFR2b receptor depending on whether the stimulus is FGF-7 or FGF-10. The result is two different but aggressive cellular outputs. When FGFR2b is stimulated with FGF-10, the receptor is phosphorylated at the cytoplasmic tail (on the tyrosine 734), allowing the recruitment of PI3K via SH3BP4 at the signalosome. This stimulates the recycling of the receptor to the PM, leading to sustained signaling and cell migration as a final result. In contrast, when FGFR2b is stimulated by FGF-7, SH3BP4 is not recruited and PI3K does not phosphorylate Y734. This leads to transient signaling and to the degradation of the FGF2b receptor and the final outcome is a switch to cell proliferation[122] (Fig. 8).

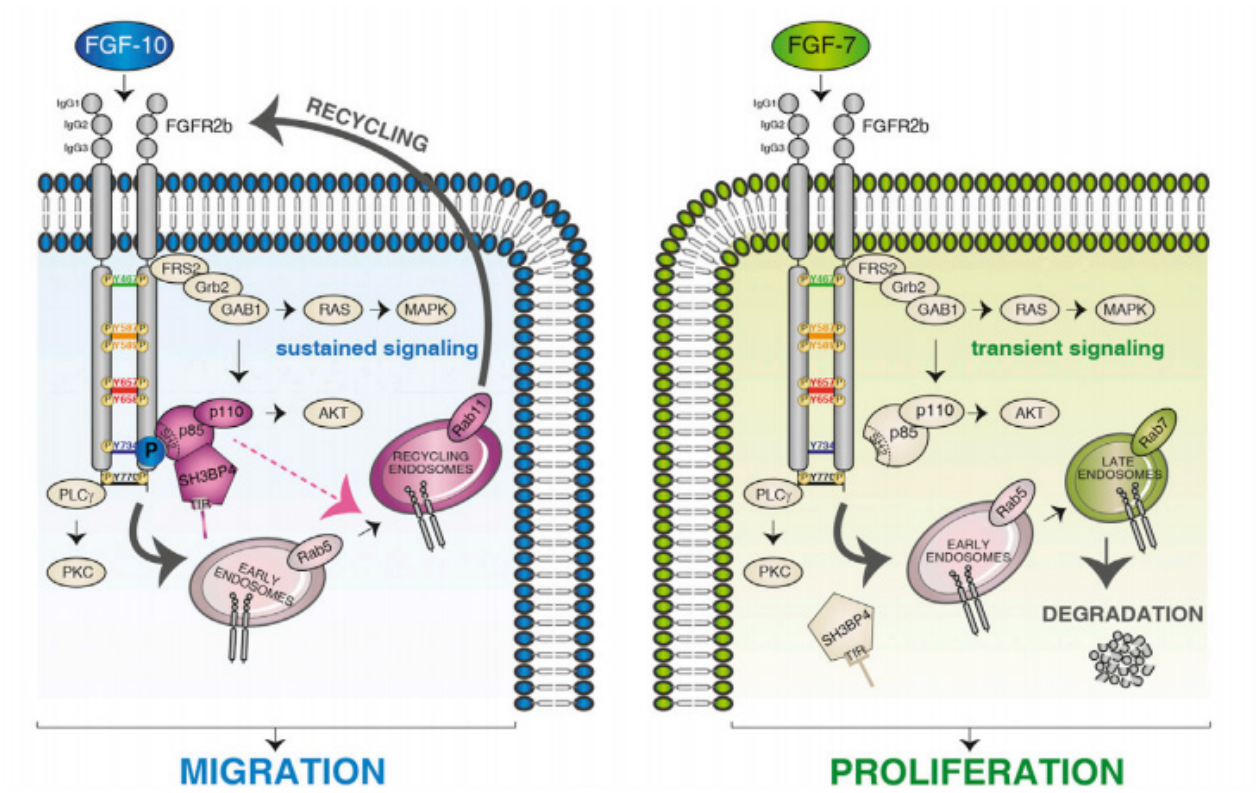

Figure 8 SH3BP4 sustains migration, signaling and recycling of FGFR2b receptor. Schematic representation of the proposed model from the Olsen' group. FGF10 ligand-mediated stimulation of the FGFR2b determines a phosphorylation of the Y734, and an interaction with the catalytic unit of PI3K (p85) and the subsequent recruitment of SH3BP4. SH3BP4 is responsible for the FGFR2b sorting at the endosomal level towards TfR-positive compartments and endocytic recycling compartments (ERC). On the contrary, FGF7 ligand-stimulated clathrin-mediated endocytosis (CME) of FGFR2b only determines a transient signaling, the Y734 is not phosphorylated upon stimulation, and therefore p85 not recruited, together with SH3BP4, at the FGFR2b tail. The receptor is targeted to degradation. Adapted from Francavilla et al., Molecular Cell, 2013.

A number of additional roles have been identified for SH3BP4. An active role for this protein has been hypothesized during apoptosis in ARPE-19 cells[118]. Transfection of these cells with its C-terminal DD-domains stimulates the cells to progress more quickly toward apoptosis. Furthermore, this protein has been recently shown to be targeted by miR-125b as a novel melanogenesis-regulator

gene in melanoma cell lines. miR-125b binds directly to the 3'-UTR of SH3BP4, thereby decreasing its expression. SH3BP4 is positively regulated by MITF, a master gene in melanocytic cells[123].

1.7 Endocytosis: biological role and tumorigenic involvement

Endocytosis is a physiological process by which cells takes up nutrients and material from the environment through well-organized structures. It regulates the lipid and protein composition of the plasma membrane. A number of endocytic processes have been identified over the last years and can be subdivided in two branches: CME and clathrin-independent mechanisms (NCE). The most studied clathrin-independent mechanisms in mammalian cells are those that are caveolin-dependent[124,125], GRAF-1-dependent (CLIC/GEEC)[126,127], flotillin- and Arf6-dependent[128,129] and Il-2 receptor-dependent.

Very recently, Di Fiore's studies showed that NCE and CME are not exclusive, when considering the EGFR receptor. It is well-established that EGFR is internalized and targeted to degradation, mediating signaling attenuation. Di Fiore's pioneering researched showed instead, that CME-internalized EGFR is targeted to recycling, while NCE-internalized EGFR is sorted for degradation, modifying the nature of the signaling attenuation or enforcement[130].Thus, endocytosis controls numerous biological processes including cell signaling. In this thesis the focus will be CME-mediated signaling and its impact on cell physiological endocytic processes.

CME is important for many reasons; it is fundamental to neurotransmission, signal transduction and the plasticity of the plasma membrane in response to distinct stimuli. The intake of receptors from the plasma membrane into the cells during CME results in the formation of vesicles in sequential and well-regulated steps that place the receptor in a protective "cage" along with adaptors; they are then transported into other organelles to perform their biological actions. Briefly, clathrin vesicle formation is divided into the sequential steps of nucleation, cargo selection, coat assembly, scission and uncoating [131–133].

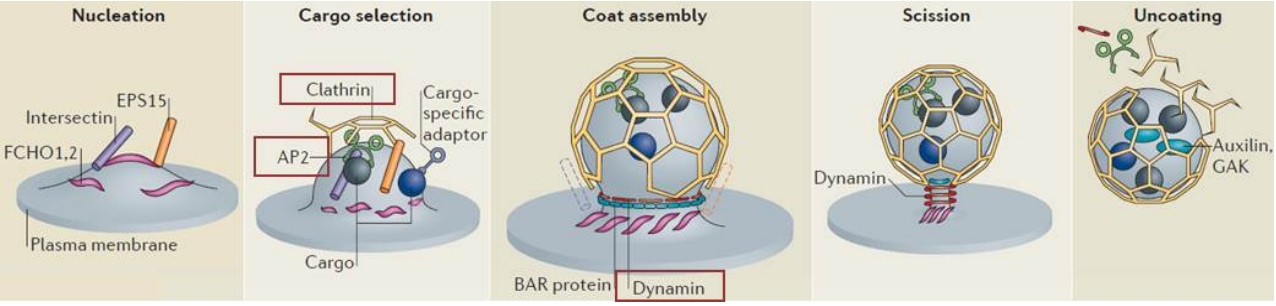

Figure 9 Clathrin coated vesicle formation stages. Sequential representation of the CCV assembly is shown. The formation of a CCV is divided in five stages, in total the entire process is carried out in 45-60 sec. ca. and involves more than 100 different proteins. In red, the proteins will be considered in this thesis: clathrin, AP-2, dynamin. Many other proteins have been identified in this process such as: intersectin, EPS15, F-BAR domain-containing Fer/Cip4 homology domain-only proteins 1 and 2 bar domain only 1,2 (FCHO1,2),

Bin/amphiphysin/Rvs protein (BAR protein), Auxilin and the G-associated kinase (GAK). Adapted from McMahon et al., Nat Rev, 2011.

The first stage of a CCV formation is nucleation and is characterized by proteins including FCHO1,2, intersectin and EPS15 (Fig. 9). These proteins are involved in the first step before the formation of the vesicle and are recognized as "nucleators". They create a first interaction hub during the curvature of the plasma membrane while the "pit" is formed, preparing the plasma membrane before the main scaffolding "clathrin-AP-2" hub is constructed to finalize CCV formation[134–136]. During the cargo selection step clathrin and AP-2 cooperate simultaneously to orchestrate the maturation of the pit. AP-2 acts as a major hub to modulate the recruitment of several adaptors, the phosphatidylinositol 4,5-bisphosphate (PIP_2) and the cargo receptor, and support the clathrin initial coating of the pit. During coat assembly and scission, dynamin and BAR proteins cooperate to mediate the curvature of the CCV and the neck formation, which allows the vesicle to be pinched off the cytoplasm. Sequentially Auxilin and GAK mediate the vesicle uncoating in the cytoplasm. Below the structures and roles of clathrin and AP-2 before describing the final stages of CCV formation will be briefly and concisely analyzed [131].

1.7.1 Clathrin structure, biological and tumorigenic function

Clathrin was first identified in 1975 by the postdoc Barbara Pearse. Her original aim was to identify and purify tubulin, but she then discovered and characterized clathrin coated cages (Fig. 10). CCVs are hexagonal and pentagonal lattices that can self-organize in cages of triskelia. Clathrin is a trimer made of three heavy chains (CHC; 190kDa) associated with three light chains (CLC; 23kDa). The most relevant part of clathrin is the terminal domain (CTD, Fig. 10), a region protruding inward from the clathrin cage which comes in contact not only with adaptors throughout CCV formation but also other membrane interacting proteins. The terminal domain is constituted by a β-propeller structure and can interact with a consensus motif (LΦXΦD/E, Φ hydrophobic residue), which is recognized as "the clathrin box", on interacting proteins[133,137–139].

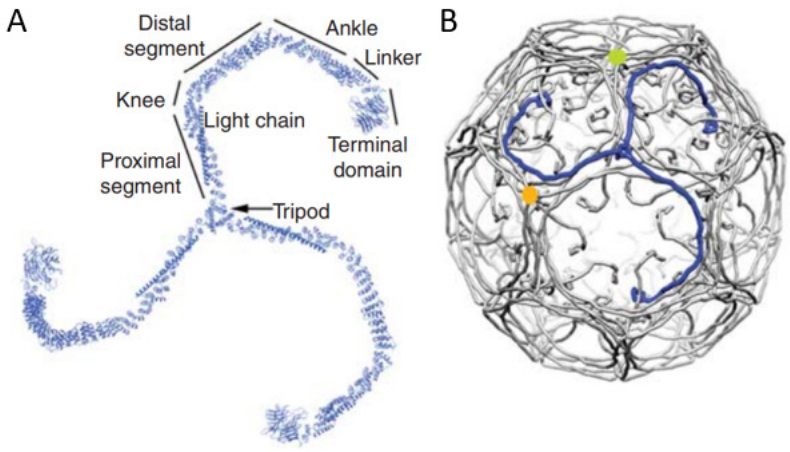

Figure 10 Clathrin structure. (A) The clathrin triskelion is represented. All the CHC domains are reported in the figure, including the most relevant one: the terminal domain. (B) 3D structure and packing of the CCV. Adapted from Kirchhausen et al., CSH Perspect Biol, 2014

Clathrin's involvement in tumorigenic processes has not been fully clarified, but a direct involvement of clathrin in tumors was recently shown, providing evidence of chromosome fusion (chromosome 2 and 17) in hemopoietic tumors. Further, an evidence for clathrin as an oncogenic-driving protein has been pointed out in the inflammatory myofibroblastic tumor (IMT) in which ALK and the clathrin heavy chain gene (ALK-CLTC) are fused[140].

1.7.2 AP-2 structure, biological and tumorigenic function

The adaptor protein 2 (AP-2) was first identified 30 years ago, as a "basket assembly" protein, able to promote the formation of a clathrin coat from purified triskelia. Nowadays, AP-2 is known to be one of the major components of CCV but also the main driver of receptor internalization. The adaptor protein family is constituted of 5 members termed AP-1 to AP-5. Only AP-2 takes an active part in CCV formation during CME, while the others regulate the traffic between endosomes and the trans-Golgi network[141,142]. AP-2 is associated with the plasma membrane and consists of two larges subunits (α and β2, 100-130 kDa), two medium (μ2, 50 kDa) subunits, and one small (σ2, 20 kDa) subunit. The main subunits conserve small flexible appendages which can associate with clathrin via their clathrin boxes or DPF motifs. In summary AP-2 is recruited to the PM and oscillates between a closed and an open conformation; the latter is able to bind PIP_2 and exposes additional sites important for CCV formation. Interactions with cargos stabilize the open conformation of AP-2,

leading to clathrin recruitment. The entire sequence of events takes globally 2 minutes. During CCV formation, the coat undergoes maturation. BAR proteins mediate the invagination of the plasma membrane and dynamin regulates the final step of vesicle scission.

1.7.3 Dynamin 2 structure, biological and tumorigenic functions

The dynamin super-family comprises several multi-domain GTPases with low affinity for guanine nucleosides and a number of characteristics related to self-assembly. The dynamin protein weighs around 70kDa and has diverse functions in cells. Dynamin's main function is to participate in membrane-remodeling events by forming self-assembling rings/helix-like structures around the neck of vesicles. Dynamin regulates the rate-limiting step of CCV fission and the fusion of intracellular trafficking vesicle into other endosomal organelles, influencing strongly endocytic traffic. An example is the transport of recycling vesicles from the tubular endosome to the plasma membrane, as occurs with the TfR[143–145].

Several isoforms of dynamin are known; here the focus will be restricted to known functions of dynamin 2 (DNM2). DNM2 has been identified as an important player during CME, regulating the rate-limiting step in pinching off the CCV and therefore directly regulating endosomal trafficking (Fig. 11). Alterations in the guanosine triphosphate hydrolase (GTPase activity) of DNM2 lead not only to aberrant CCV formation but also strongly impair downstream signaling of activated receptors (e.g. EGFR)[146]. Several isoforms of dynamin are known; here the focus will be restricted to known functions of DNM2.

DNM2 has been identified as an important player during CME, regulating the rate-limiting step in pinching off the CCV and therefore directly regulating endosomal trafficking. This leads to a general dysregulation of the process and increases tumorigenic effects on cancer cells.[147,148] Recently DNM2 has been determined to regulate actin dynamics at lamellipodia/invadopodia and focal adhesions, leading to suggestions that DNM2 might become an interesting therapeutic target in metastasizing solid cancers. There the remodeling of cell architecture is promoted by migration and is the key to aggressiveness.[149–152]

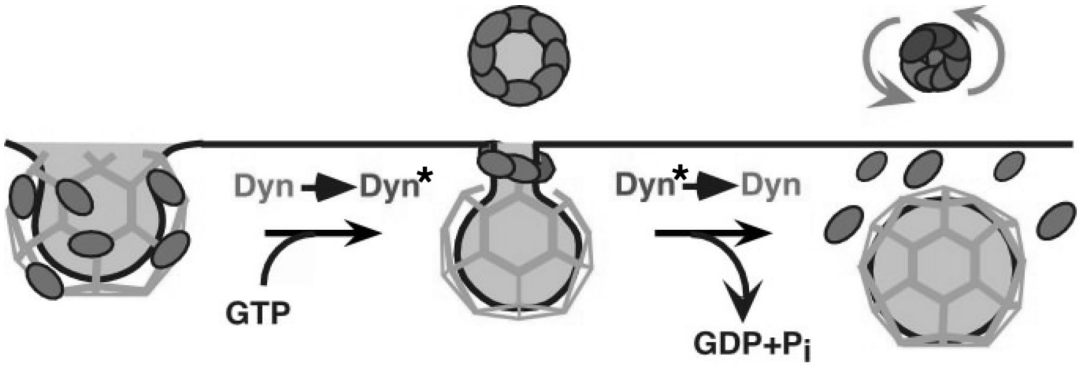

Figure 11 Dynamin GTP-mediated fission of clathrin coated vesicle. Dynamin binding to GTP triggers the assembly of dynamin units in a neck. After the collar assembly, the dynamin-mediated hydrolysis of GTP in GDP changes, its transformation and conformation, closing the neck resulting in the CCV pinching off into the cytoplasm. From Mettlen et al., Biochem Soc Trans, 2009

1.8 Endocytosis and Signaling

Endocytosis has recently emerged as a crucial factor in cancer. The effective internalization and intracellular traffic of plasma membrane proteins such as receptors and their endocytic and signaling adaptors have long been considered critical check-points in mediating an attenuation of signaling after stimulation by an extracellular ligand. Considerable evidence has been gathered to show that cell proliferation and migration are also results of aberrant and derailed endocytosis, as shown in Figure 12. In the case of receptor tyrosine kinases (RTKs) and integrins, the recycling process has an impact on sustaining signaling during proliferation or mediating the turnover of anchoring sites, respectively. In the case of integrins this contributes to malignant transformation[153,154].

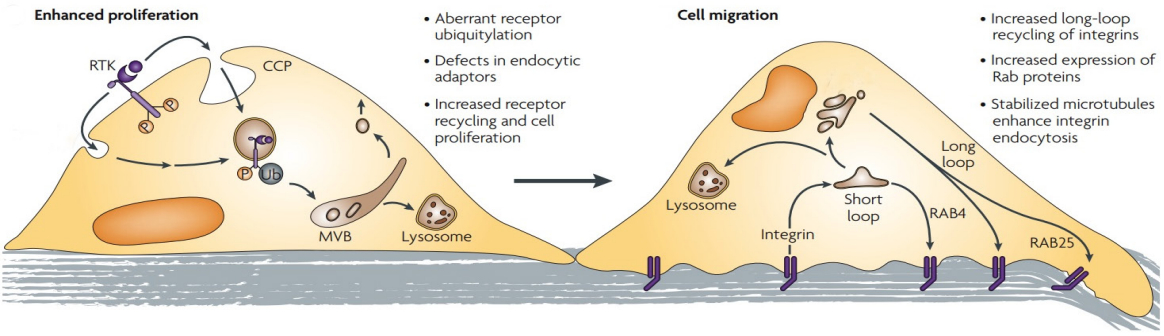

Figure 12 Derailed endocytosis in the biological processes of proliferation and migration. (Left panel) Derailed endocytosis is responsible for enhanced proliferation and cell migration. In particular, increased cellular

proliferation depends on aberrant receptor ubiquitination, which avoids the receptor target to degradation, increase receptor recycling to PM, or defects in endocytic adaptors. (Right panel) A derailed endocytosis enhances also the integrin-mediated migration of cancer cells. In particular, integrin increased recycling via RAS-related protein 4 or 25, or stabilized microtubular structures. From Mosesson et al., Nat Rev Cancer, 2008

CME modulates signaling of receptors that have been stimulated at various stages. This guarantees different signaling outputs depending on the plasticity of endocytic compartments. As shown in Figure 13 the early endocytic control of signaling begins at the plasma membrane and typically depends on the fidelity of the endocytic machinery assembly during the fission of a CCV[155156]. Beyond the availability of the receptor and its ligand at the plasma membrane, the correct recruitment of the endocytic machinery during the formation and the fission of CCVs directly influences the prolongation of active signaling. This depends mainly on the recruitment of dynamin and AP-2. In more detail, dynamin recruitment is a prerequisite for a productive CCP maturation, while the role of AP-2 is dispensable[157].

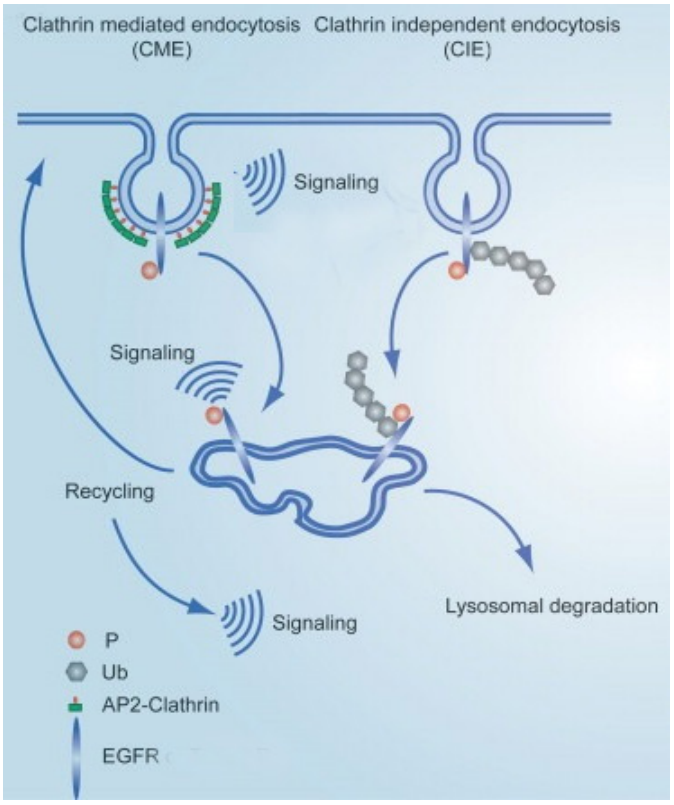

Figure 13 Endocytic "check points" of the EGFR receptor. Representation of the EGFR signaling check point after EGF-stimulated endocytosis triggered both via CME and NCE. (Left) EGF-activated EGFR is internalized via CME, and regulates the signaling during vesicle formation, at endosomal sites and via recycling. EGF-triggered NCE endocytosis leads the EGFR to ubiquitination and degradation, attenuating the signal. P - phosphorylated receptor; Ub - ubiquitinated receptor. Adapted from Disanza et al., Molecular Oncology, 2009

The expression of specific mutants of dynamin or dynamin depletion leads to a complete disruption of the EGFR endocytosis and thus to the attenuation of EGF-dependent EGFR activation and degradation with consequent attenuation of ERK1/2 and PI3K downstream pathways[146]. This makes the internalization of EGFR an important step for a sufficient activation of signaling. Endosome-associated internalized EGFR also supports cell survival by recruiting signaling machinery (such as GRB2, SHC and PI3K) to the endosome and sustaining the active signaling cascade directly from this compartment [158].

1.9 Biology of the Transferrin receptor

TfR is the most commonly used model to investigate the individual steps in CME and their regulation by the cell. TfR is a 90-95 kDa transmembrane glycoprotein involved in the cellular uptake of iron and thereby the regulation of cell growth[159]. Knockouts of TfR in early embryonic development lead to a severe dysregulation of erythropoiesis and neural development[160]. At the PM, TfR is present as a homodimer connected by disulfide bridges. The extracellular part of the receptor contains the binding site for transferrin (Tf)[161,162]. An overview of TfR protein structure can be seen in Figure 14. TfR expression is regulated at the post-transcriptional level in response to intracellular iron deposits. TfR is ubiquitously expressed at low levels in most cells but is highly expressed in cells with a high proliferative rate[159,163–167]. TfR expression in cancer cells is higher compared to healthy counterparts. This higher TfR expression has been shown to be due to an increased need for iron as a cofactor of the ribonucleotide reductase enzyme involved in DNA synthesis in highly proliferative cancer cells[159,166–170].

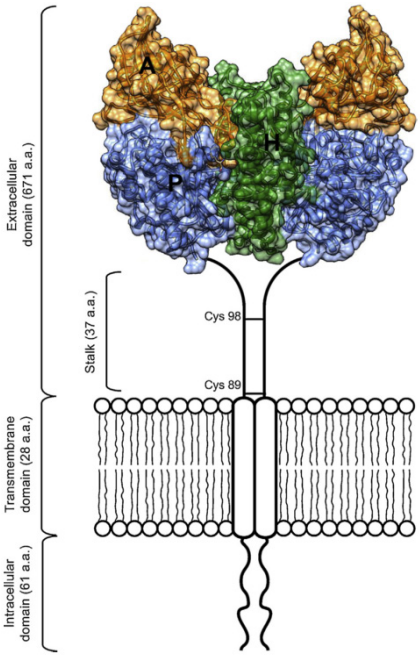

Figure 14 The TfR structure. This scheme represents a type II transmembrane transferrin receptor homodimer consisting of two monomers linked by disulfide bridges at cysteines 89 and 98. The TfR1 contains an intracellular domain, a transmembrane domain, and a large extracellular domain. This structural model of the extracellular domain consists of three subdomains: apical (A, orange), helical (H, green) and protease-like domain (P, blue). Adapted from Luria-Perez et al., Biol Med Hosp Inf Mex, 2016

TfR trafficking in the cell has been extensively explored; iron-binding transferrin (ferric transferrin, h-Tf) binds the receptor and is internalized via CME. Through the acidification of pH in endosomes, Tf changes its conformation releases the bound iron and stays as apo-Tf bound to the TfR. This complex can be recycled back to the cell surface, where neutral pH triggers apo-Tf release[162,171,172]. In contrast to receptors such as EGFR, TfR is constitutively internalized independently of the binding of h-Tf. After internalization, TfR is sorted into early endosomes either for recycling or degradation. 95% of TfR/apo-Tf complexes are recycled back to the cell surface; the remaining 5% are degraded in lysosomes[173].

1.10 Involvement if TfR in CRC and targeted therapy

Iron is a primary nutrient that regulates cell growth and proliferation, but an overload may cause accumulation/toxicity, mutations and oxidative stress. This has led to the identification of excess iron as a risk factor for CRC[174,175]. The overexpression of TfR on the surfaces of cancer cells confers a growth advantage and increases their malignancy[168]. The relationship between iron uptake in CRC and cell growth was first introduced by Zorbas' group, who tested CRC cell lines (HCT116, RKO, CBS and GEO) for their growth sensitivity to Tf, EGF and insulin. Poorly differentiated HCT116 and RKO

cells acquire growth capability in the presence of Tf or insulin, or both, but only in combination with EGF; they are insensitive to EGF alone. More differentiated cell lines (CBS and GEO) still respond to EGF but require at least Tf and insulin to support their growth. Moreover, HCT116 cells respond to Tf and insulin in growth media by increasing the expression of EGF receptors at the cell surface.[176]

TfR density has been studied to date in 23 colon tumors (adenoma and malignant villous tumors) and their respective healthy mucosa after surgical resection. Analysis of the Tf binding capacity of tumor cells has shown that it increases compared to the control mucosa, leading to the introduction of TfR as a reliable prognostic marker that can be used to estimate the growth rate of tumors in CRC. In contrast to this role for TfR in CRC, Zarkovic's group has highlighted a differential expression of TfR: a higher expression of TfR in CRC samples classified as Dukes A and B (well differentiated) and a lower expression in carcinoma samples Dukes C and D (poorly differentiated), the prevalent types to develop metastasis[177].

A recent interesting study of 11 CRC carried out by the Tselepis' group revealed a general increase in the expression of iron import proteins (e.g. DMT1 and TfR) in these tumors compared to the respective normal mucosa. In Caco-2 and SW480 cells, proliferation rates increase whether or not this is supported by loading the cells with iron along with an increased repression of E-cadherin at the protein and mRNA level[178].

Intensive studies of TfR has been accepted as a prognostic marker for several cancer types including CRC, and its high accessibility on the cell surface renders it a promising target for delivering cytotoxic agents specifically to tumor cells. The most studied intervention to inhibit proliferation or to stimulate apoptosis in cancer cells is an anti-TfR-targeted monoclonal antibody. From the early 1980s, several murine antibodies have been used against TfR on the cell surface; some have been very efficient but not all of them are reliable in blocking uptake without causing secondary effects such as cytotoxicity[162]. However, the use of murine antibodies against TfR for targeted therapies in humans produce severe side effects. The short half-life of the murine antibodies requires continual administration that may cause the production of human anti-mouse antibodies (HAMA) and allergic reactions. Murine anti-TfR antibodies and chimeric fusion proteins are not the only targeted therapy being used to modulate TfR-mediated cell proliferation. The short half-lives of the antibodies and the limitations in direct conjugation, have made it mandatory to develop new delivery methods. A recent study has suggested the use of Tf-nanoparticles (100 nm ca.) and liposomes as directed delivery systems. Tf-nanoparticles that are doxorubicin-conjugated are the most developed class, generally leading to a higher intracellular uptake of doxorubicin with a strong reduction in tumor growth.[179] In agreement with this, one of the most recent studies published on TfR-targeted delivery shows the importance of this receptor in its diffusing ability into the brain by overcoming the blood-brain

barrier. Because the inhibition of cell proliferation and growth is a primary aim for cancer therapy, TfR inhibition or targeted-drug delivery via TfR have emerged as promising anti-cancer therapeutic strategies which merit further development.

1.11 The epidermal growth factor receptor, a prognostic marker for CRC

EGFR, also known as ErbB1 belongs to the ErbB family receptors. This super-family of receptors includes three less studied members: ErbB2, ErbB3, and ErbB4. EGFR is a transmembrane receptor consisting of an extracellular ligand binding domain, a transmembrane domain and an intracellular domain with intrinsic tyrosine kinase activity[180]. It has recently been shown that upon EGF stimulation, the dimeric EGFR/EGF complex is internalized for intracellular sorting, a process which regulates downstream signaling pathways and cell fates[181]. Alongside EGF, ErbB receptors have also been shown to bind the transforming growth factor receptor α (TGFα). Both TGFα and EGF bind EGFR, albeit with different affinities that depend on the pH-determined sensitivity of the ligands. EGFR is influenced directly at the level of endosomal sorting, decreasing its ability to recycle back to the plasma membrane according to its binding stability[181,182]. EGFR's fate after ligand-stimulated internalization is determined by a series of events and recruitment that involve cargo adaptors, kinases and sorting proteins at the signalosome. A recent model of EGFR internalization and sorting has been proposed by Stang ’s group (Figure 15)[183].

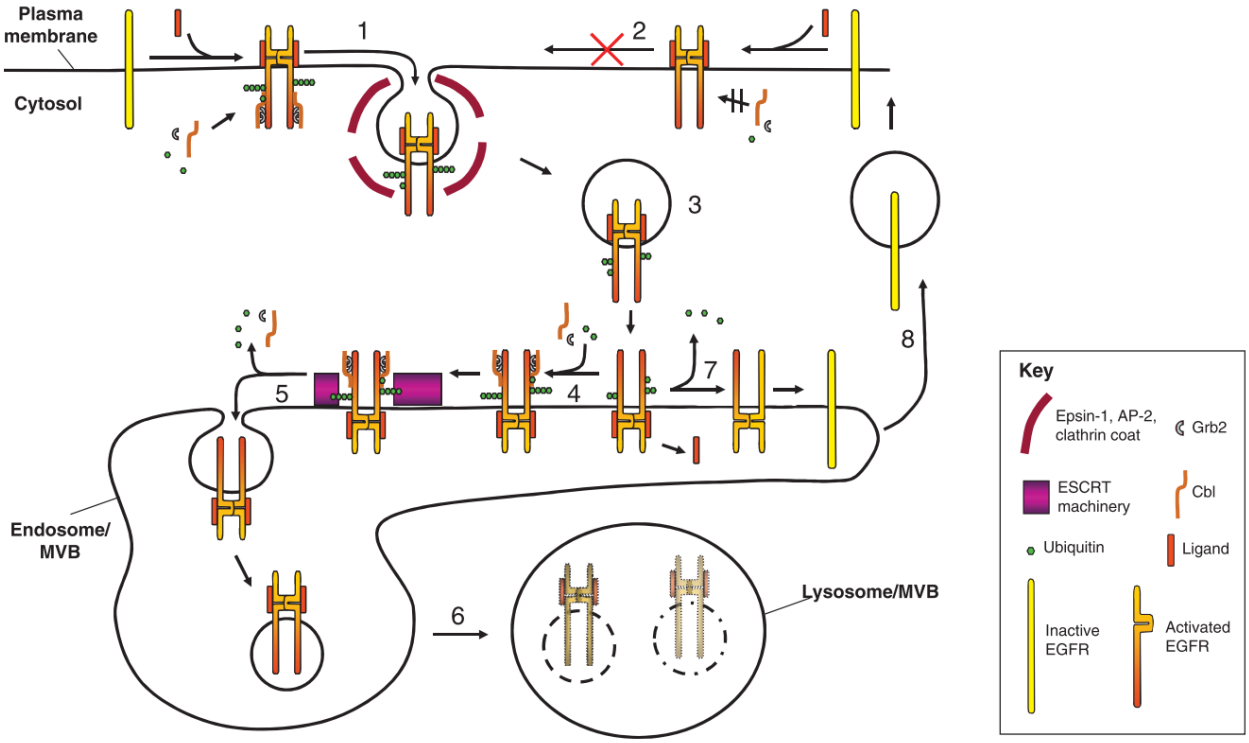

Figure 15 EGFR trafficking model. (1) Upon EGF-stimulated CME, EGFR is activated, ubiquitinated and transported into CCV. (2) The block of ubiquitination of the receptor inhibits its internalization. (3) During the trafficking in vesicles EGFR is partially deubiquitinated and reaches the endosomes (4) where the ligand-bound EGFR is re-ubiquitinated and interacting with the endosomal sorting complexes required for transport (ESCRT) machinery, is sorted to the inner vesicles of endosomes to MVB (5) and lysosome (6). Alternatively (7), if the EGF-ligand complex dissociates at low pH in endosomes the receptor is deactivated and deubiquitinated, transported to ERC and recycled back to PM (7-8). From Madshus et al., JCS 2009.

Ligand-stimulated EGFR is internalized via CME and is targeted to early endosomes and later to sorting endosomes tubovesicular structures that dynamically matures mediating the receptor sorting into different routes. The receptor will be then delivered to ERC and recycled or degraded into lysosome-associated membrane glycorotein 1 (LAMP-1) marked compartments. Once at the sorting endosomes, EGFR is delivered to multi vesicular bodies (MVBs) for lysosomal degradation, leading to a downregulation of EGFR signaling and proliferation which ultimately segregates the kinase tail from the signalosome molecules. Recently it has also been shown that a monoubiquitination of RTKs upon ligand binding suffices to target the receptor to lysosomes[184]. Interestingly, mutations of c-Cbl on its binding site on EGFR (Tyr1045) impair the receptor ubiquitination, but not its internalization, leading to decreased degradation and increased recycling[184]. Alternatively, once EGFR is internalized and reaches the sorting endosomes, it might be targeted for recycling. This path is less that understood but it has become clear that EGFR fate depends on the endosomal sorting complexes required for transport (ESCRT) complexes, in particular I and III[185]. EGFR fate also depends on the ligand stability. Initially the binding of EGF and TGFα to EGFR can promote polyubiquitination with the same intensity

at the PM. EGF remains stably bound to EGFR at endosomes, maintaining the kinase activity and the ubiquitination and degradation. TGFα does not, it dissociates from the receptor mediating a transient ubiquitination and thereby allowing EGFR recycling to PM. c-Cbl seems to dissociate from the receptor as well. Thus, the EGF-induced ubiquitination of EGFR is important in allowing the EGFR tail to stably bind c-Cbl and target EGFR for degradation. In contrast, TGFα leads to less stable binding to the receptor in acidic compartments, ultimately leading to a disassembly and to the recycling route of EGFR to the PM[183].

Until recently, EGFR internalization has been considered a well-known example of how CME works and how it influences receptor-intrinsic signaling by driving its phosphorylation. CME has long been recognized purely as a mechanism to attenuate signaling, but recent studies have led to the surprising suggestion that CME might not be a straightforward way to degrade EGFR[130]; depending on the concentration of the extracellular ligand (EGF), the fate of the receptor might change. These latest studies revealed the importance of the correct CME internalization of EGFR that happens for low doses of EGF-stimulated endocytosis (20 ng/ml), in contrast to a NCE which normally targets EGFR to degradation for high doses of EGF-stimulated endocytosis (100 ng/ml)[130]. Low and high EGF dose on EGFR show different consequences for EGFR activity and the downstream signaling. For low EGF-stimulated internalization, a sustained signaling is possible through the EGFR recycling to PM via CME. For high EGF-stimulated internalization, the internalized EGFR are targeted to degradation, resulting in an impairment of the signaling. Signaling induced by ligand-binding receptors drives cell type-specific responses such as cellular proliferation and differentiation, depending on the receptor involved. This has made it important to understand how EGFR CME influences signaling via its differential sorting. Ligand binding, the recruitment of specific adaptors and correct trafficking is fundamental for EGFR signaling, recycling and degradation. EGF-mediated EGFR signaling is further under strict regulation by dynamin. In cells overexpressing a dominant negative version of dynamin (dynamin-K44A), defective in GTP binding, the EGF-stimulated EGFR endocytosis was completely abolished compared to the control cell line overexpressing a wild type isoform of dynamin. This led to an intracellular accumulation of EGF that was degraded after 10 minutes. Furthermore, EGF stimulated endocytosis in dynamin-K44A overexpressing cells does not following the classical ligand-induced trafficking to degradation but recycles instead. Importantly, dynamin-K44A overexpressing cells showed increased EGF-dependent proliferation compared to the wild type control[186]. Recently, Li's group showed that EGFR cooperates with TfR via its activation to achieve an increased surface distribution of TfR in non-small cell lung cancer. More importantly, supplementing the cells with ferric citrate (non-Tf bound) iron rescued the inhibition of EGFR-promoted proliferation caused by tyrosine-kinase inhibitor treatment, concluding that the EGFR positively regulates intracellular iron levels and the membrane expression of TfR [187]. To conclude, dynamin-defective CME and TfR have an

impact not only on EGFR routing and surface distribution in the cell, but also stimulate enhanced proliferation. This might be the mechanistic basis by which a cancer cell escapes the attenuative role of CME.

2. Aims of the thesis

MACC1 has been identified in 2009 as a driver for cancer progression and metastasis formation for CRC, but also as a prognostic marker for metastasis and metastasis free survival[89]. In the last 10 years, MACC1 has become a referring prognostic and predictive marker also for several other types of cancer[188]. Besides promoting cell proliferation, migration, and invasion, as well as regulating MET expression, MACC1 promotes epithelium dependent angiogenesis in gastric cancer via TWIST/VEGF-A[95]. In addition, several studies highlighted the importance of silencing MACC1, resulting in decreased cell proliferation, migration, and invasion, as well as reduced tumour formation and metastasis in xenograft mouse models. However, little is known about the protein structure and function of MACC1, besides prediction analyses of structural domains and linear interaction motifs. Therefore, the main aims of this study are as follow:

a. Elucidation of the role of MACC1 in TfR CME. The thesis will investigate first the interaction of MACC1 with CME proteins (clathrin, dynamin, adaptor complex 2) and then the impact of MACC1 on TfR endocytic traffic.

b. Identification and characterization of MACC1 CME specific domains and elucidation of their importance in this physiological process. This part of the thesis will dissect first the importance of the interaction of these domains (clathrin box, NPFs and DPF) in their binding with MACC1 after deletion. In the second part, this thesis will characterize the impact of MACC1 predicted CME domains deletions, during TfR CME.

c. To conclude, in the last part of this thesis, MACC1 impact on CME will be investigated regarding an additional receptor (EGFR). Similarities between the MACC1 impact on TfR and EGFR during the endocytic traffic will be analysed. Also, we will study the impact of the CME domains of MACC1 on EGFR signaling during endocytosis.

3. Material and Methods

3.1 Cell culture

Cell culture media, phosphate-buffered saline washing (PBS; 137 mM NaCl, 2.7 mM KCl, 10 mM Na_2HPO_4, 2 mM KH_2PO_4 pH 7.4) and Trypsin/EDTA solution were obtained from Life Technologies. All human CRC cell lines used in our study (Table 3.1) were obtained from the American Type Culture Collection (ATCC). Cells were grown in RPMI-1640 or DMEM (Invitrogen), supplemented with 10% fetal bovine serum (FCS; Bio&Cell, Germany). All cells were maintained at 37°C in a humidified, 5% CO_2 ventilated incubator. Cells were trypsinized and diluted in a 1:6-8 ratio every 2-3 days. All cells were negative for mycoplasma, verified regularly using the MycoAlert® Mycoplasma detection kit (Lonza). The cell lines used in this study were recently authenticated by short tandem repeat profiling (DSMZ, Braunschweig, Germany).

Table 3.1 Summary of all CRC cell lines used in this study

Cell line	***Medium***	***ATCC number***
SW480	RPMI-1640, 10% FBS	CCL-227
SW620	DMEM, 10% FBS	CCL-228
HCT116	DMEM, 10% FBS	CCL-247
HCT15	RPMI-1640, 10% FBS	CCL-225

All cell lines are registered in the American type culture collection (ATCC).

3.2 Derivative cell lines

The cell lines SW480/e.v., SW480/MACC1, and SW480/SH3BP4 were previously generated by stable transfection of SW480 cells with pcDNA3.1, pcDNA3.1-pCMV-MACC1-V5-His, and pcDNA3.1-SH3BP4 plasmids, respectively, and antibiotic selection of G418, (ThermoFisher, 1 mg/ml) of single clones. SW620/sh control and SW620/sh MACC1 cells were obtained by lentiviral transduction of SW620 cells with pRFP-CB-CMV-driven sh control, sh MACC1 tagged with RFP constructs (Origene, US), were kept under antibiotic selection of Blasticidin (Invitrogen, 1 mg/ml). The derivative cell lines are listed in Table 3.2. The description of the MACC1 CME mutants will be reported in the next paragraph.

Table 3.2 Summary of derivative cell lines used in this study

Cell line	*Medium*
SW480/empty vector (e.v.)	RPMI, 10% FBS
SW480/MACC1	RPMI, 10% FBS
SW480/SH3BP4	RPMI, 10% FBS
SW620/sh control (sh cnt)	DMEM, 10% FBS
SW620/sh MACC1	DMEM, 10% FBS
HCT116/GFP	DMEM, 10% FBS
HCT116/MACC1-GFP	DMEM, 10% FBS

3.3 Cloning of MACC1 mutants

Cell lines containing mutated versions of the MACC1 open reading frame (ORF) are listed in Table 3.3. The MACC1 N-terminal DNA fragment with deletions (ΔNT) of potential interaction motifs of factors associated with CME (clathrin box, NPFs and DPF) was synthesized ad hoc (gBlocks® Gene Fragment; Integrated DNA Technology, IDT). The DNA fragment was designed with 5'- and 3'- regions of 80 bp, homologous to the target vector, to enable homologous recombination. A schematic representation of the ΔNT fragment location within the MACC1 ORF can be found in Figure 16, all the deleted sequences are reported in Figure 17 and its newly generated (from gBlocks®) complete sequence is given in Table 3.5.

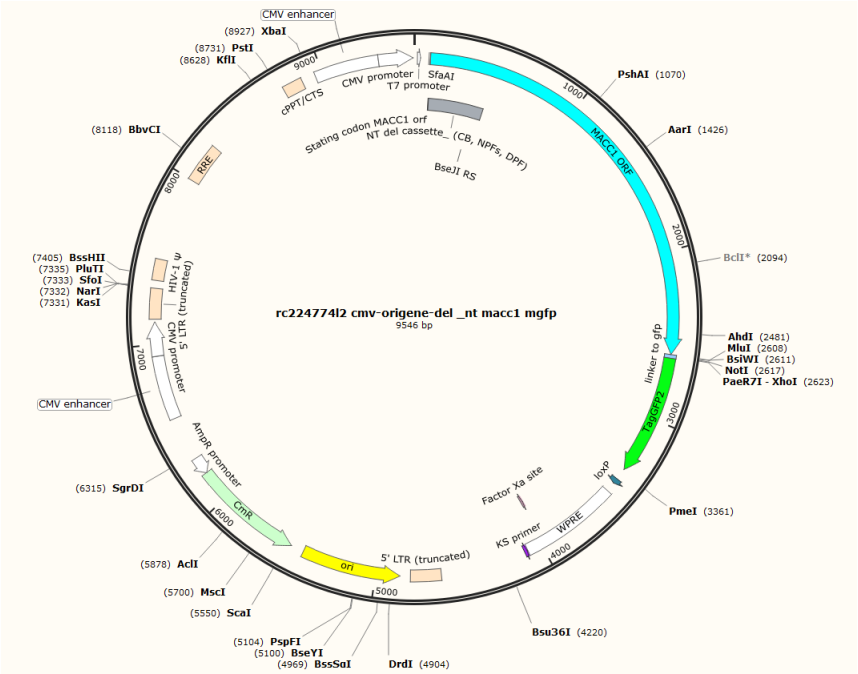

Figure 16 Schematic representation of the MACC1 ORF. The appropriate location of the N-terminal DNA fragment with specific CME deletions is reported (in figure: ΔNT cassette, in grey; in brackets the sequential deletions of cassettes deleted: clathrin box, NPFs, DPF).

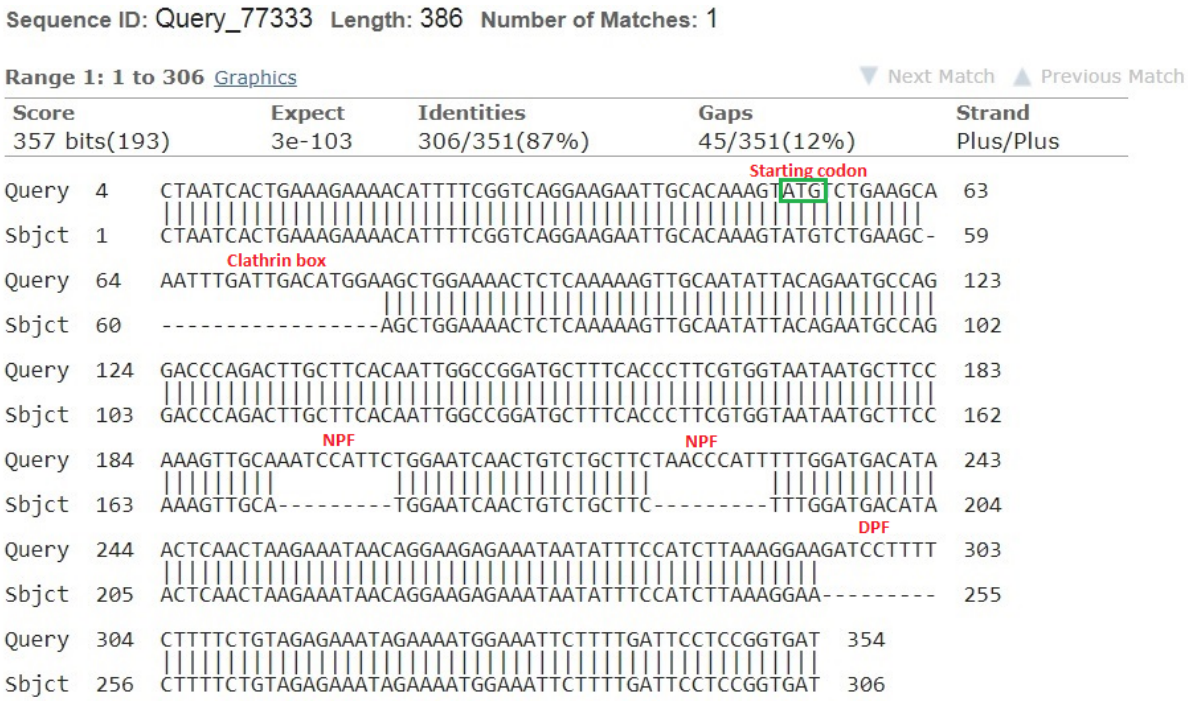

Figure 17 MACC1 N-terminal nucleotide sequence. The MACC1 deleted CME cassettes (in red) are reported. In order the MACC1 start codon (ATG, in green) as reference. Sequentially reported in red the clathrin box deleted sequence, the two NPFs and the DPF sequences.

All plasmids and sequences used in this thesis are listed in Table 3.4. The lentiviral vector rc224774l2 cmv-macc1-mgfp (OriGene, US) containing the MACC1 ORF tagged with GFP was digested with SfaAI and BseJI (Fast Digest, Thermo Scientific) following manufacturer's instruction. All restriction enzymes used are listed in Table 3.6. Homologous recombination of the synthesized MACC1-DNA fragment with N-terminal deletions and the target vector occurred via Gibson Assembly® (New England Biolabs), according to manufacturer's instruction. The reaction was incubated at 50°C for 65 min, and was then chemically transformed into NEB® Stable competent bacteria (New England Biolabs). After shaking at 37°C for 1 hr, transformed bacteria were selected on LB agar plates (10 g Trypton, 5 g yeast extract, 5 g NaCl, 15 g Agar) containing chloramphenicol (1 µg/ml, Sigma Aldrich). Plasmid DNA, from overnight cultures of picked colonies grown at 37°C in 2 ml LB medium (10 g Trypton, 5 g yeast extract, 5 g NaCl), was isolated with the PureYield™ Plasmid Miniprep System (Promega). A control digestion of the resulting DNA with SfaAI and BseJI was tested on a 1% agarose gel (Roth) for specific bands that indicate the correct recombination of the DNA fragment, generating rc224774l2 cmv-macc1-deltaNT-mgfp (**MACC1ΔNT-GFP** construct). In a second cloning step, we chose the previously generated deleted SH3-domain of MACC1[89] construct (51–amino acid in-frame deletion), containing the unique restriction sites XhoI and PshAI of MACC1. This MACC1 fragment was amplified by polymerase chain reaction (PCR) using *PfuUltra* High-Fidelity DNA Polymerase (Agilent Technologies) according to the manufacturer´s protocol. The primers used for this reaction

are listed in Table 3.5. To insert the amplified region into the target vector by Gibson Assembly, homologous ends were attached by first amplifying short flanking DNA fragments with suitable overlaps for the site of insertion and the MACC1 SH3-deletion fragment in 2 sequential steps (primers for PCR amplification 1 are: Fwd_amplif sh3frag_PshAI/Primer_R; for the PCR amplification 2 are Primer_F/Rev_amplif sh3frag_XHOI, all the sequences from BioTez, Berlin; reported in Table 3.5). The flanking regions and the SH3-deletion fragment were mixed in stoichiometric amounts (3:1) and are fused by PCR amplification, using the primer set Fwd_amplif sh3frag_PshAI / Rev_amplif sh3frag_XHOI (PCR amplification 3). The PCR reaction was performed using using *PfuUltra* High-Fidelity DNA Polymerase (Agilent Technologies) according to the manufacturer´s protocol with the following parameters:

Step	**Cycles**	**Temperature (°C)**	**Time**
1	1	95°C	2 min
2	30	95°C	45 sec
		63°C	30 sec
		72°C	2 min
3	1	72°C	10 min
4	1	4°C	hold

The generation of the lentiviral vectors rc224774l2 cmv-macc1-deltaSH3-mgfp (**MACC1ΔSH3-GFP** construct, Figure 3) and rc224774l2 cmv-macc1-deltaNTdeltaSH3-mgfp (**MACC1ΔNTΔSH3-GFP** construct, Figure 18, upper panel) was again performed by homologous recombination of the amplified flanked SH3-deletion construct into the PshAI/XhoI digested target vectors rc224774l2 cmv-macc1-mgfp and rc224774l2 cmv-macc1-deltaNT-mgfp, respectively (the enzymes used are listed n table 3.6).

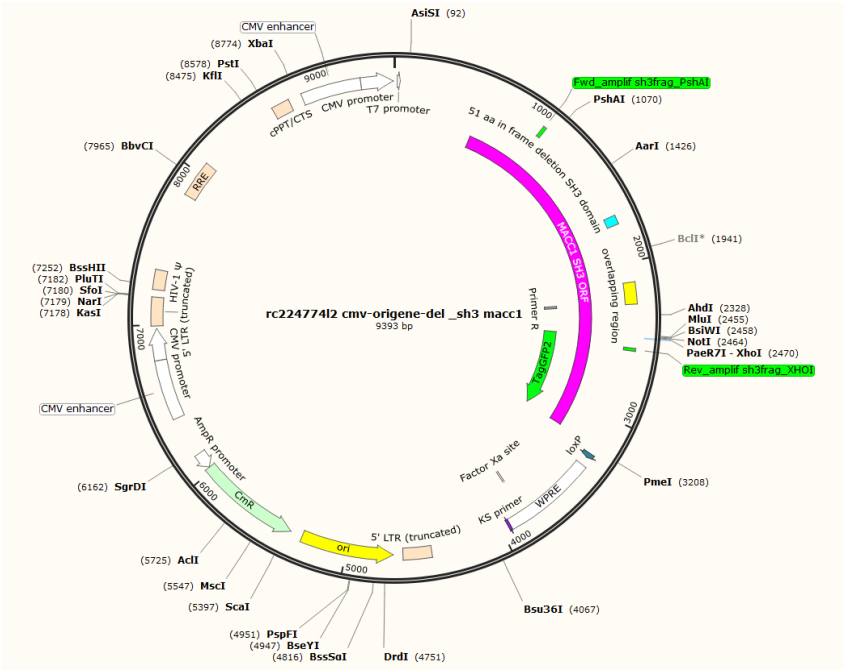

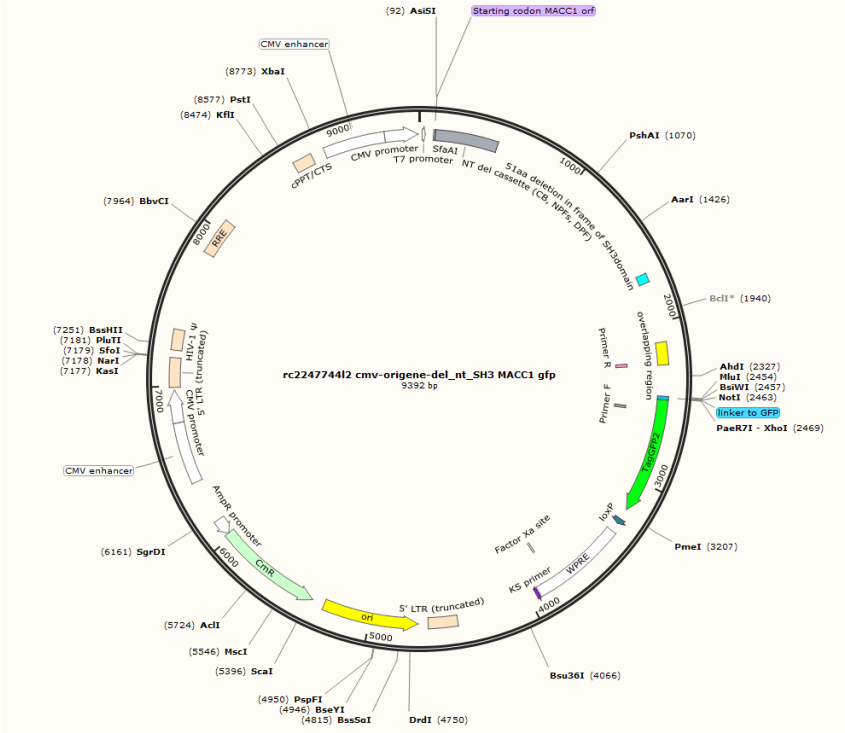

Figure 18 Schematic representation of the MACC1 ΔSH3 mutant (top panel), and the MACC1 ΔNTΔSH3 (bottom panel) mutant construct. In the maps, all the primers location for the entire cloning of the ΔSH3 mutant (top), and (bottom) the location of the N-terminus deleted region together with the SH3-deleted region are reported.

GFP and MACC1-GFP constructs were stably transduced by lentiviral particles (kindly provided and performed by Dr. Kobelt) and cells with high transgene expression levels were selected via FACS, generating SW480/GFP, SW480/MACC1-GFP, SW480/MACC1ΔNT-GFP, SW480/MACC1ΔSH3-GFP and SW480/MACC1ΔNTΔSH3-GFP cells, respectively.

Table 3.3 Establishment of GFP-control, full length MACC1- GFP and mutants of MACC1 CME cassettes

Cell line	***Medium***
SW480/GFP	RPMI, 10% FBS
SW480/MACC1-GFP	RPMI, 10% FBS
SW480/MACC1ΔNT-GFP	RPMI, 10% FBS
SW480/MACC1ΔSH3-GFP	RPMI, 10% FBS
SW480/MACC1ΔNTΔSH3-GFP	RPMI, 10% FBS

Table 3.4 Summary of plasmids and fragments

Plasmid	***Company***
CME Deleted MACC1 N-Terminal Fragment (Gib_Frag_del_NT, gBlocks ®)	IDT
pcDNA3.1_ MACC1 his V5 7a5 del SH3	Amplification
rc224774l2 cmv-macc1-mgfp	Origene
rc224774l2 cmv-gfp	Origene

Table 3.5 Sequences and primers for the generation of the MACC1 mutants

Sequence or Primer	***Name***	***Size***	***Purpose***
5'-*GTGAACCGTCAGAATTTTGTAATACGACTCACTATAGG GCGGCCGGGAATTCGTCGACTGGATCCGGTACCGAGG AGATCTGCCGCCGCGATCGCC*ATG*CTAATCACTGAAA GAAAACATTTTCGGTCAGGAAGAATTGCACAAAGTAT GTCTGAAGCAGCTGGAAAACTCTCAAAAAG*TTGCAAT ATTACAGAATGCCAGGACCCAGACTTGCTTCACAATTG GCCGGATGCTTTCACCCTTCGTGGTAATAATGCTTCCA AAGTTGCATGGAATCAACTGTCTGCTTCTTTGGATGAC ATAACTCAACTAAGAAATAACAGGAAGAGAAATAATA TTTCCATCTTAAAGGAACTTTTCTGTAGAGAAATAGAA AATGGAAATTCTTTTGATTCCTCCGGTGATGAACTTGA TGTGCATCAGTTACTTAGGCAGACTTCCTCAAGAAATT CTGGAAGATCTAAAAGTGTTTCAGAACTTCTGGA-3'	Gib_frag_del_NT	512bp	MACC1 N-terminus containing deletion of the clathrin box, two NPF sites and a DPF. In evidence: MACC1 starting codon (green).

PCR amplification 1: 51-amino acid in-frame mutated SH3 amplification

5’-CTTGGGTAAAGAAGGCCCTT-3’	Fwd_amplif sh3frag_PshAI	Amplification of the in-frame mutated SH3 domain upstream PshAI RS and XhoI from the original plasmid (Stein et al., Nature Med 2009)
5'-AGGCAGGTTTCCACATCATC-3'	Primer_R	
PCR amplification 2: MACC1 GFP ORF end amplification from the recipient GFP plasmid		
5’-GCTGTCAAGCTTGGAAAAGG-3'	Primer_F	Amplification of the region upstream the XhoI site and the end of the MACC1-GFP tag region
5'-GAACTTGTGGCCGTGCAC-3'	Rev_amplif sh3frag_XHOI	
PCR amplification 3: Amplification of the SH3 deletion fragment of the upstream and downstream flanking regions		
5’-CTTGGGTAAAGAAGGCCCTT-3’	Fwd_amplif sh3frag_PshAI	Amplification of the fused DNA fragments using the complementarity of the overlapping region (139 bp). The total amplification results in a 1567 bp fragment.
5'-GAACTTGTGGCCGTGCAC-3'	Rev_amplif sh3frag_XHOI	

Table 3.6 Restriction enzymes and their reaction temperatures

Restriction Enzyme	***Working temperature and thermal inactivation***	***Company***
SfaAI	37°C (thermal inactivation 80°C 5 min)	Fast Digest, Thermo Scientific
BseJI	65°C (no thermal inactivation)	Fast Digest, Thermo Scientific
PshAI	37°C (thermal inactivation 80°C 20 min)	Fast Digest, Thermo Scientific
XhoI	37°C (thermal inactivation 80°C 5 min)	Fast Digest, Thermo Scientific

3.4 Gene expression analysis

3.4.1 RNA isolation and reverse transcription

Cells (3 - 5 x 10^5) were seeded into a 6 well plate, washed with PBS and trypsinized. Total RNA was isolated using TRIzol reagent (Invitrogen, Thermo Scientific) according to manufacturer’s instructions.

RNA concentrations were determined by spectrophotometry on a Nanodrop device (Peqlab, Erlangen, Germany). 50 ng of RNA was reverse transcribed with random hexamers in a reaction mix (10 mM $MgCl_2$, 1 x PCR Buffer II, 0.25 µM pooled dNTPs, 1 U RNAse inhibitor, 2.5 U Moloney murine leukemia virus reverse transcriptase; all from Applied Biosystems). Reaction was performed at 42°C for 15 min, 99°C for 5 min, and subsequent cooling at 5°C for 5 min. Reverse transcripts were either stored at -20°C or directly used for quantitative real-time PCR.

3.4.2 Quantitative real-time PCR

Reverse transcripts were diluted (1:3) and amplified using the Go Taq® Master mix (Promega). Primers used for gene specific quantitative real-time (q)PCR amplification were obtained from Biotez (Berlin, Buch) and are listed in Table 3.7. Each PCR reaction was performed in a total volume of 10 µl in 96-well-plates in the LightCycler 480 (Roche Diagnostics). The PCR protocol includes a pre-incubation step at 95°C for 2 min followed by 45 cycles of (a) denaturation at 95°C for 7 sec, (b) annealing at 60°C for 10 sec and (c) elongation at 72°C for 20 sec. Each qPCR reaction was performed in duplicates. In parallel, cDNA quantification of the housekeeping gene GAPDH was used for normalization of gene expression. Data analysis was performed with LightCycler 480 Software release 1.5.0 SP3 (Roche Diagnostics). Mean values were calculated from duplicate qPCR reactions. Each mean value of the expressed gene was normalized to the respective mean GAPDH expression. Data were analyzed using the ΔΔCt method for relative amounts of gene expression. All expression analyses were performed three times independently.

Table 3.7: Primers used for quantitative real-time PCR

Primer name	Sequence
MACC1 Fwd	5‘-TTCTTTTGATTCCTCCGGTGA-3‘
MACC1 Rev	5’-ACTCTGATGGGCATGTGCTG-3’
TfR Fwd	5’-GGCTACTTGGGCTATTGTAAAGG-3’
TfR Rev	5’-CAGTTTCTCCGACAACTTTCTCT-3’
SH3BP4 Fwd	5’-ACAACACCACCGAAATGGG-3’
SH3BP4 Rev	5’-ATCATACCGCTGTCACTCAGT-3’
EGFR Fwd	5’-AGG CAC GAG TAA CAA GCT CAC-3’
EGFR Rev	5’-ATG AGG ACA TAA CCA GCC ACC-3’
GADPH Fwd	5’-GAAGATGGTGATGGGATTTC-3’
GADPH Rev	5’-GAAGGTGAAGGTCGGAGT-3’

3.5 Protein Analysis

3.5.1 Protein extraction

For total protein extraction, 3-5 x 10^6 cells per well were seeded in 6-well plates. After 48 hr, cultured cells washed in PBS were scraped off the well, collected in 1.5 ml tubes and pelleted at 1,200 rpm (161 rcf) for 5 min. The pellet was either frozen at -20°C or immediately subjected to protein extraction. For total protein extraction cells were lysed with RIPA buffer (50 mM Tris–HCl at pH 7.5, 150 mM NaCl, 1% NP-40; supplemented with protease and phosphatase inhibitor cocktail tablets; Roche Diagnostics, Germany) for 30 min on ice. Cell debris was pelleted at 14,000 rpm for 15 min at 4°C. The supernatant was transferred to a new tube, stored at -20°C or directly subjected to Western blot (WB) analysis.

3.5.2 Protein quantification

Protein concentration was determined before samples were applied to WB analysis. Quantification was performed with Bicinchoninic Acid Protein Assay Reagent (BCA; Invitrogen, Thermo Scientific), according to the manufacturer's instructions, using serial dilutions starting from 2 mg/ml of BCA solution for the standard curve. BCA reaction was incubated at 37°C for 15 min and absorption was measured at 560 nm in a SpectraFluor Plus II (Tecan) plate reader. Samples of equal amount were boiled at 98°C for 5 min in NuPAGE loading buffer supplemented with 10% DTT (all Life Technologies, Thermo Scientific, Darmstadt, Germany) according to the manufacturer's instructions. To analyze protein expression levels samples were separated with sodium dodecyl sulfate-polyacrylamide gel electrophoresis (SDS-PAGE).

3.5.3 Western Blot analysis

Separation with SDS-PAGE and WB was used to analyze protein expression levels. Protein extracts were diluted with RIPA to obtain 10-20 µg of total protein in 1x NuPAGE® loading buffer and 10% DTT. Protein samples were loaded onto a self-casted 10% gel and calculated using an on-line calculator (https://www.cytographica.com/lab/acryl2.html). For the 6% stacking gel: 40% acrylamide, 0.5 M Tris pH 6.8, 10% ammonium persulfate (APS), 10% sodium dodecyl sulfate (SDS), Tetramethyl ethylenediamine (TEMED) ddH_2O; for the 10% separating gel: 40% Acrylamide, 1.5 M Tris pH 8.8,

10% APS, 10% SDS, TEMED, ddH_2O). Protein electrophoresis was carried out in 1x Laemmli running buffer (25 mM Tris, 192 mM Glycine, 0.1% SDS) buffer at 120 V for 1.5 hr within the EasyPhor Page Mini system (Biozym®). Pre-stained Spectra™ Multicolor high Range Protein Ladder (Thermo Scientific) was used to determine the band size. Semi-dry electrotransfer blotting of proteins onto the nitrocellulose membrane (Amersham, GE healthcare) occurred in Trans-blot® Turbo system (Bio-Rad) in Trans-Blot Turbo Transfer Buffer (at 25 V for 10 min. Quality of the protein transfer was analyzed by protein staining with Ponceau S solution (Sigma-Aldrich). The membrane was washed with TBS-T (50 mM Tris-HCl pH 7.5, 150 mM NaCl, 0.05% tween 20,) and blocked for 1 hr at room temperature (RT) with blocking buffer (6% milk powder in TBS-T, Roth). Membranes were then incubated overnight at 4°C with primary antibody in 6% milk (Table 3.8) followed by 3 washes with TBS-T 0.05% tween and an incubation for 1 hr at RTwith horseradish peroxidase (HRP)-conjugated secondary antibody. Secondary Antibodies diluted in TBS-T with 5% BSA. Antibody-protein complexes were visualized with WesternBright (Advansta, Menlo Park, CA, USA) and subsequent exposure to Fuji medical X-ray film SuperRX (Fujifilm, Tokyo, Japan). WB for β-actin served as protein loading control.

Table 3.8: Antibodies used for Western blot analysis, their dilutions and their origins

Target	Dilution	Company
Primary antibodies		
Anti-β-Actin (clone AC-15)	1:20.000	Mouse monoclonal, Pierce
Anti-MACC1	1:1000	Rabbit polyclonal, Sigma
Anti-TfR (13-6800)	1:1000	Mouse monoclonal, Thermo Scientific
Anti-CLTC (c-20)	1:1000	Goat polyclonal, Santa Cruz
Anti-DNM2 (c-18)	1:1000	Goat polyclonal, Santa Cruz
Anti-AP2α (c-8)	1:1000	Mouse monoclonal, Santa Cruz
Anti-SH3BP4	1:1000	Rabbit polyclonal, Thermo Scientific
Anti-EGFR (1005)	1:1000	Rabbit polyclonal, Santa Cruz
Anti-EGFR (A-10)	1:1000	Mouse monoclonal, Santa Cruz
Anti-p-EGFR (Tyr 1068)	1:1000	Rabbit polyclonal, Cell Signaling
Anti-AKT	1:1000	Rabbit polyclonal, Cell Signaling
Anti-Phospho-AKT (Ser473)	1:1000	Rabbit polyclonal, Cell Signaling
Anti-p44/42	1:1000	Rabbit polyclonal, Cell Signaling
Anti- Phospho-p44/42	1:1000	Rabbit polyclonal, Cell Signaling
Secondary antibodies		
Anti-rabbit-HRP (W401B)	1:10.000	HRP conjugated antibody, Promega
Anti-mouse-HRP	1:10.000	HRP conjugated antibody, Pierce

Anti-goat-HRP (sc-2020)	1:10.000	HRP conjugated antibody, Santa Cruz

3.6 Co-Immunoprecipitation assay

To analyze MACC1 interacting proteins, 80–90% confluent cells of 10-cm dishes were washed once in ice-cold PBS and then lysed in co-IP lysis buffer (20 mM Tris-HCl pH 7.5, 150 mM NaCl, 0.1% NP40, 1 mM EDTA, 1% Triton, supplemented with complete protease inhibitor tablets; Roche) for 30 min on ice. Extracts were centrifuged for 10 min at 14.000 rpm at 4°C and incubated overnight with 4 µg of target specific antibodies (listed in Table 3.9.). Antibody-bound protein complexes were pulled down using Protein G Agarose beads (Alpha Diagnostic), washed three times with ice-cold co-IP lysis buffer, and denatured in NuPAGE loading buffer at 98°C for 10 min. Interaction of the precipitated proteins with MACC1 was analysed by WB and immunostaining for MACC1.

Table 3.9: Antibodies used for co-IP analysis, their dilutions and their origins

Target	Dilution	Company
Anti-Transferrin receptor (13-6800)	4 µg	Mouse monoclonal, Thermo Scientific
Anti-EGFR (1005)	4 ug	Rabbit polyclonal, Santa Cruz
Anti-Clathrin (c-20)	4 ug	Goat polyclonal, Santa Cruz
Anti-DNM2 (c-18)	4 ug	Goat polyclonal, Santa Cruz
Anti- AP2α (c-8)	4 ug	Mouse monoclonal, Santa Cruz
Anti-Met (25H2)	4 ug	Mouse monoclonal, Cell Signaling

3.7 Immunofluorescence and data analysis

Cells were seeded onto glass coverslips (VWR ®, 13 mm diameter, 1.5 µm thickness) at 1 x 10^4 cells/ml in 24 well plates. After 48 hr cells were starved in serum-free media (SF-MEM media, Life Technologies) without FBS supplement. Cells were treated depending on the experiment with human holo-Transferrin (h-TF, Sigma-Aldrich), or with EGF (Sigma-Aldrich), and then washed twice with PBS. Stained cells were fixed with 4% paraformaldehyde (PolyScience) in PBS for 15 min at RT. Fixed cells were quenched for 10 min with 0.1 M Glycine (Roth), washed twice with 0.2% tween 20 in PBS (PBS-T) and permeabilized with 0.2% Triton X-100 in PBS (PBS-X) for 10 min. After washing with PBS-T, the coverslips were incubated 1 hr in 5% albumin IgG free in PBS (Roth) at RT, were washed twice with PBS-T, followed by the incubation with protein specific primary antibodies in 2.5% albumin IgG free in PBS at 4°C overnight. The antibodies used for the immunofluorescence are listed in Table 3.10.

After 3x washing with PBS-T, the coverslips were incubated with their respective secondary antibodies for 1 hr at RT. After 3x washing with PBS-T the coverslips were incubated with 4',6-diamidin-2-fenilindolo (DAPI; Biosciences) for 3 min at RT, and washed twice with PBS-T before they were mounted with Dako Fluorescent mounting media (Agilent).

Table 3.10: Antibodies used for immunofluorescence

Target	Dilution	Company
Primary antibodies		
Anti-MACC1 (D-15)	1:50	Goat polyclonal, Santa Cruz
Anti-MACC1	1:100	Rabbit polyclonal, Sigma-Aldrich
Anti-Transferrin receptor (13-6800)	1:50	Mouse monoclonal, Thermo Scientific
Anti-Clathrin (X22)	1:400	Mouse monoclonal, Abcam
Anti-Clathrin (CLTC)	1:100	Goat polyclonal, Sicgen antibodies
Anti-Clathrin (D3C6)	1:100	Rabbit polyclonal, Cell Signaling
Anti- α-Adaptin (AP6)	1:100	Mouse monoclonal, Abcam
Anti-DNM2 (#3457)	1:100	Rabbit polyclonal, Abcam
Anti-EGFR (1005)	1:50	Rabbit polyclonal, Santa Cruz
Anti-EGFR (A-10)	1:50	Mouse monoclonal, Santa Cruz
Anti-human HGF/c-MET (AF276)	1:100	Goat polyclonal, R&D Systems
Endosomal markers kit (EEA1, RAB11, CLTC)	1:100	Cell Signaling
Anti-Lamp1 (D2D11) XP®	1:100	NEB
Secondary antibodies		
Anti-goat Alexa Fluor® 488 conjugated	1:200	Thermo Scientific
Anti-mouse Alexa Fluor® 555 conjugated	1:200	Thermo Scientific
Anti-rabbit Alexa Fluor® 647 conjugated	1:200	Thermo Scientific

Slides were imaged with a Leica SP5 confocal microscope (Leica, Microsystem), equipped with an argon laser having a 488 nm emission, one helium neon laser with 633 nm emission, a diode laser with a 405 nm emission and a diode-pumped solid state (DPSS) with 405 nm emission. Images were sampled at a resolution of 1024 by 1024 pixels, using a 63x (NA 1.5) objective, a 5 times software zoom and a 10-20 z-step size of 0.2-0.3 µm. Images were saved in the Leica image file (.lif) format and quantification was performed on a NDVIA GeForce GTX 1070 PC workstation with an Intelcore i7-4930, 64 GB, 3,4 GhZ using Imaris 8 (Bitplane, South Windsor,

CT, USA). Quantification of the fluorescence overlap was measured with IMARIS (v.8) using the background automatic threshold.

3.8 Endocytic-related functional and trafficking assays

3.8.1 Surface staining and uptake of TfR

Cells (1 x 10^6) were cultured in 60 mm dishes until 80 –90% confluency and were starved in SF-MEM at 37°C before the assay to deplete the supply of culture-born Tf. Cells were then washed once in ice-cold PBS, harvested and resuspended in cold RPMI supplemented with 0.2% bovin serum albumin (BSA) containing 25 mg/ml Alexa® Fluor 647-conjugated Transferrin (Tf-Alexa® Fluor 647; Life technologies). The cells were incubated for 1 hr on ice to stain the surface located receptors. Receptor internalization was allowed by shifting the pre-stained cells to 37°C. Mean fluorescence intensity (MFI) of internalized TfR was determined by stopping the internalization after 10 and 20 min in ice-cold PBS. After cells were fixed (1 mM EDTA, 1% glutaraldehyde in PBS), Tf/EGF-Alexa® Fluor 647 fluorescence was analysed using the FACS LSR Fortessa™ (BD Bioscience), quantifying the signal intensities in the APC channel. Unstained cells were used as background while the internalized signal was calculated by virtual stripping of the surface signal.

3.8.2 Surface staining and recycling of EGFR

Cells (1 x 10^5) were cultured in 6-well plates and were starved in SF-MEM at 37°C before the assay to deplete the supply of culture-born EGF. For the EGFR surface quantification cells were washed once in ice-cold PBS, harvested and resuspended in cold PBS supplemented with 0.2% BSA containing 2.5 mg/ml Alexa® Fluor 647-conjugated EGF (EGF-Alexa® Fluor 647; Life technologies). The cells were incubated for 1 hr on ice to stain the surface located receptors. Fluorescence intensity of recycled EGFR was determined by stopping the clathrin-mediated endocytosis with 20ng/ml EGF (Sigma) after 30 min in ice-cold PBS and staining with 2.5 µg/ml Alexa® Fluor 647-conjugated EGF, with or without pre-treating the cells for 4 hr with monensin (10 µM, Sigma) as controls. After cell washing with cold-PBS, cells were fixed (1 mM EDTA, 1% glutaraldehyde in PBS), and EGF-Alexa® Fluor 647 fluorescence

was analyzed using the FACS LSR Fortessa™ (BD Bioscience), quantifying the signal intensities in the APC channel. Unstained cells were used as background.

3.8.3 Transferrin and EGF receptor endocytic trafficking assays

For analysis of internalized receptor/ligand complexes and their subsequent localization and quantification in acidic cellular compartments, we obtained Tf and EGF labelled with the pH-sensitive red fluorescent dye pHrodo™ (Tf-pHrodo™ and EGF-pHrodo™; Thermo Fisher Scientific). These innovative fluorogenic dyes enable to detect and measure the fluorescence increase of the complex (receptor/ligand) while trafficking into the cell when reaching compartments with increasing and acid pH. Cells were cultured in 96-well plates (Corning) until they were approximately 80–90% confluent, and were starved before the assay in SF-MEM overnight at 37°C to deplete the supply of culture-born Tf or EGF. Cells were washed twice in ice-cold PBS. pHrodo™ Red-labelled Tf/EGF in Live Cell Imaging solution (LCIS, Life Technologies) were added to the plate with the relative controls at the indicated concentrations (Table 3.11 and Table 3.12). The plates were transferred into the IncuCyte ZOOM® platform located in a cell culture incubator at 37°C/5% CO_2. At least two images per well from at least two technical replicates were taken every 5-15 min for 3-4 hr, using a 20X objective lens and then analyzed using the IncuCyte™ Basic Software. The acquisition time for phase contrast and emission intensities in the red channel was set to 2200 ms. In phase contrast, cell segmentation was achieved by applying a confluence mask. An area filter was applied to exclude objects below 50 μm^2. Red channel background noise was subtracted with the Top-Hat method of background, and the integrated fluorescence signal was quantified by the software after applying a mask.

Table 3.11: IncuCyte® ZOOM Live-cell Analysis System compound working concentrations

Target receptor	Dilution	Compound
Tf receptor	50 μg/ml	pHrodo™ Red-labelled Tf, Thermo Scientific
EGF receptor	5 ug/ml	pHrodo™ Red-labelled EGF, Thermo Scientific

Table 3.12: IncuCyte® ZOOM Live-cell Analysis System used inhibitors and working concentrations

Target receptor	Dilution	Compound
Monensin	10 μM	Control treatment for recycling inhibition, Sigma-Aldrich
Bafilomycin	100 nM	Control treatment for degradation inhibition, Sigma-Aldrich
Dynasore	80 μM	Control treatment for internalization inhibition, Abcam

3.8.4 Transferrin Recycling assay

Cells were cultured in 100-mm dishes until they were approximately 80 –90% confluent and starved before the assay in SF-MEM for 1 hr at 37°C to deplete the supply of culture-born Tf. Cells were then washed once in ice-cold PBS, harvested and resuspended in cold RPMI with 0.2% BSA containing 25 µg/ml Tf-Alexa® Fluor 647. Cells were incubated for 15 min at 37°C. The endocytosis was stopped with ice-cold PBS. Cells were centrifuged and washed with ice-cold PBS and resuspended in cold RPMI 10% FBS h-Tf (250 ug/ml). The reaction was stopped at indicated time points. The cells were collected and washed twice with ice-cold PBS and fixed (1 mM EDTA, 1% glutaraldehyde in PBS). Tf-Alexa® Fluor 647 fluorescence was analyzed using the FACS LSR Fortessa™ (BD Bioscience), quantifying the signal intensities in the APC channel. Data were analyzed considering the endocytosed Tf-Alexa® Fluor 647 as 100% of the internalized TfR. A reduction of Tf-Alexa® Fluor 647 signal intensity over time was used to evaluate the rate of TfR/ Tf-Alexa® Fluor 647 recycling to the plasma membrane, where the Tf-Alexa® Fluor 647 was released from TfR and washed off. The protocol has been kindly provided from Dr. Armin Rehm[189].

3.8.5 TfR degradation assay

For the TfR degradation assay, cells were grown to 80–90 % confluency and starved at 37°C in SF-MEM (Invitrogen). Cells were treated for 10 and 20 min with 50 µg/ml h-Tf (Sigma), with or without pre-treatment of bafilomycin A1 (100 nM; Sigma). Total TfR protein was immunoblotted as previously described.

3.9 Proliferation assay

For the determination of anchorage-dependent cell proliferation, 1 x 10^4 cells were plated into 96-well-plates and were allowed to accommodate for 6 h before treatment. Treated cells were grown for 2-4 days in 20 ng/ml EGF RPMI supplemented with 2% FBS. The proliferation rate was observed via IncuCyte® ZOOM Live-cell Analysis System (Essen BioScience) at 37°C. Each cell proliferation experiment was performed in duplicates, for three independent times.

3.10 EGFR downstream cell signaling analysis

For the signaling analysis, cells were seeded in 6-well plates for 48 h, and after starvation with SF-MEM cells were stimulated with 20 ng/ml EGF in RPMI (Sigma) for the indicated time points. Cell lysates were subjected to WB and immunostaining as previously described.

3.11 High throughput analysis for Mass Spec data and other software

For identification of the MACC1 interactome by mass spectrometry (MS) (shot-gun proteomics), immunoprecipitation of SW620 cells with two polyclonal rabbit anti-human MACC1 antibodies (HPA020103, HPA020081, Sigma, St. Louis, USA, 2 µg) was performed 4 times independently. Samples were eluted from the affinity beads using denaturing buffer (6 M urea, 2 M thiourea, 20 mM HEPES, pH 8.0, Sigma). Proteins were converted to peptides in a two-step digestion using endopeptidase LysC (Wako, Japan) and trypsin (Promega, Madison, WI, USA). The peptides were desalted using Stage-Tips following a protocol by Rappsilber et al[190]. The purified peptides were then resuspended in 3% trifluor acetic acid / 5% acetonitrile buffer (Sigma, Merck) and separated on a reversed-phase column (20 cm length, 75 µm ID, 3 µm Reprosil-C18, Dr. Maisch) with a gradient from 5 to 45% acetonitrile in 122 min. Peptides were ionized on a Proxeon ion source and directly sprayed into the mass spectrometer (Q-Exactive, Thermo Fisher). The recorded spectra were analyzed using the MaxQuant software package (Version, 1.2.2.5) with fixed modifications set to carbamylation of cysteines and variable modifications set to phosphorylation of serine, threonine, and tyrosine, and methionine oxidation. The false-discovery rate was set to 1% on protein and peptide level. Statistical analysis of the data set was performed using the R-statistical software package. These analyses were performed in cooperation with Dr. Gunnar Dittmar, MDC, Head of Mass Spectrometry Core Facility, before the start of this project.

Interactors of MACC1 identified by mass spectrometry were classified by DAVID (Database for Annotation, Visualization, and Integrated Discovery) Bioinformatics Resources tool (v6.7)[191]. For functional annotation clustering of gene ontology terms (GO terms), we set the following parameters: classification stringency “medium” and EASE=1, interactors selected had a p-value<0.05. We set interesting clusters with a fold enrichment of $\log_2$>1.5.

3.12 Statistical analysis

Statistical analysis was performed using GraphPad prism software (v5.01, GraphPad software, La Jolla, CA, USA) using either unpaired two-tailed Student t-tests, one-way or two-way ANOVA followed by posthoc Bonferroni correction, depending on the obtained datasets. Signal half-lives

were calculated using non-linear regression. P-values below 0.05 were considered statistically significant.

4.Results

4.1 Identification of MACC1 CME interactors

4.1.1 MACC1 protein structure and CME interactome analysis

MACC1 contains several putative domains as shown (Fig. 19, A) which have been predicted and identified in 2009 by our group[89]. In order to study MACC1 interactome and its role in CME process in CRC cells, a pull down of MACC1 from SW620 cells was performed followed by mass spectrometry (MS). This analysis allowed us to identify MACC1 potential interacting proteins. Of note, the SW620 cell line of metastatic CRC was chosen as model system due to high endogenous MACC1 expression[89] (cooperation with G. Dittmar, head of mass spectrometry core facility, MDC). MACC1 interactors were categorized using DAVID (Database for Annotation, Visualization, and Integrated Discovery) Bioinformatics Resources tool (v6.7)[191] (Figure 1; R analysis handled by Tommaso Mari, Prof. Selbach Group at MDC). Only proteins with a p-value<0.05 were considered and validated in further analysis.

MACC1 interactome analysis showed 1103 potential interaction partners and 27 interesting GO Terms or gene clusters enriched (fold enrichment>0.5 (Log2)) in biological processes, cellular components and molecular functions, all related to endocytosis and vesicle transport (Fig.19, B). We focused our attention on a subcategory of proteins (in red, Fig.19), that were reporting CME interactors interesting for our research. These CME proteins of interest have been selected considering the presence of CME motifs MACC1 protein structure in particular the clathrin box, NPFs and DPF motifs (Fig. 19, A).

Furthermore, to understand at which steps MACC1 might have been involved in CME processes MACC1 potential interactors were involved during CME we also analyzed the MS list using another reliable tool: the KEGG PATHWAY (https://www.genome.jp/kegg/pathway.html). This is a reference database system for pathways mapping. The MS list analysis showed MACC1 enrichment in many different pathways, showing also several MACC1 potential CME interactors. The specific GO terms containing MACC1 CME interactors considered in this thesis are marked with red stars (Supplementary Figure 1, and 10). In conclusion, MACC1 shows GO enrichment in CME-related proteins which have been identified as potential interaction partners.

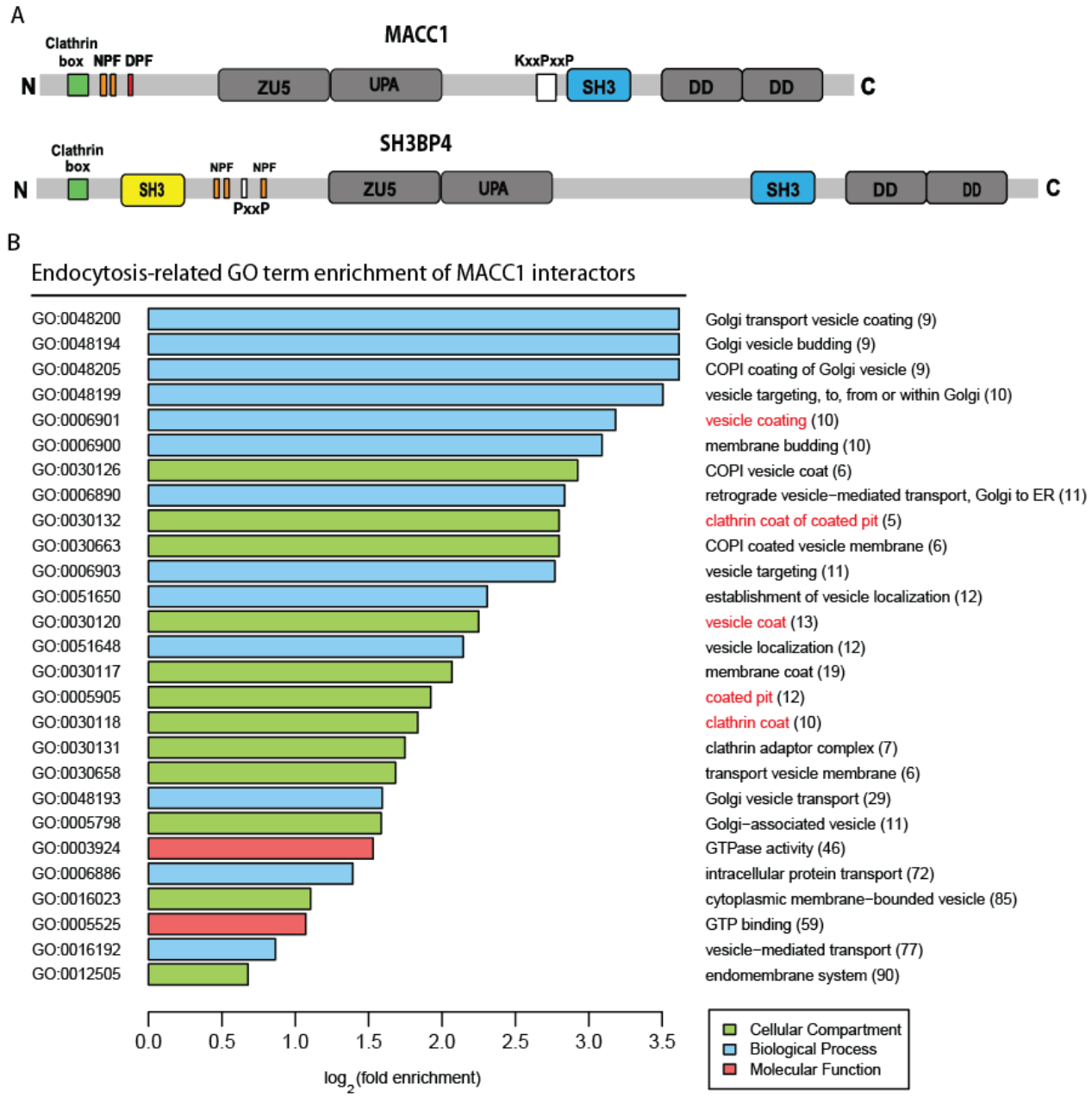

Figure 19 MACC1 protein structure and CME interactome analysis. (A) MACC1 and SH3BP4 protein structures are shown; MACC1 and SH3BP4 share a 43.7% protein homology and several endocytosis cassettes. MACC1 (in color) motifs at the N-terminus: clathrin box (binds clathrin terminal domain, CTD); NPF, the Epsin 15 homology motif interacting site (Asn-Pro-Phe motif binds epsin homology (EH) domain); DPF, α-adaptin binding domain of AP-2α, Asp-Pro-Phe motifs are shown. Motif at the C-terminus: SH3, SRC homology 3 domain (interacts with proline-rich domains, PRD is shown. (B) Endogenously expressed MACC1 was pulled down via coimmunoprecipitation (coIP) in SW620 cells and its interactome was analyzed via DAVID. In (B) MACC1 endocytosis-related GO term enrichment analysis is shown and subdivided in cellular compartments, biological processes and molecular functions categories. The GO terms containing the CME proteins discussed in this thesis are shown in red.

4.1.2 MACC1 interacts with several CME factors and with TfR in different CRC cell lines

The previous data indicates a possible role for MACC1 during CME traffic. In order to investigate and characterize MACC1 protein interactors and its involvement in CME process, we choose a set of CRC cell lines (SW480, SW620, HCT15, HCT116) as a model system. At first, we confirmed the expression of CME related proteins in all the chosen cell lines. The following Figure (20, A) shows indeed that CME related proteins such as: CLTC, DNM2, and AP-2α are highly and similarly expressed across all the cell lines. Thus, to identify and assess MACC1 involvement in CME, we further validated our MS results via coIP. For this purpose, CME proteins were pulled down and used as bait in three different CRC cell lines, respectively: SW620 (endogenously overexpressing MACC1), SW480/MACC1 (ectopically overexpressing MACC1), SW480/MACC1-GFP (ectopically overexpressing GFP-tagged MACC1). As shown (Fig. 20 B-D), MACC1 coimmunoprecipitates with CLTC, DNM2, AP-2α and TfR. Globally, these data confirm the direct or indirect interaction of MACC1 with CLTC, DNM2, AP-2α and TfR in different CRC cell lines.

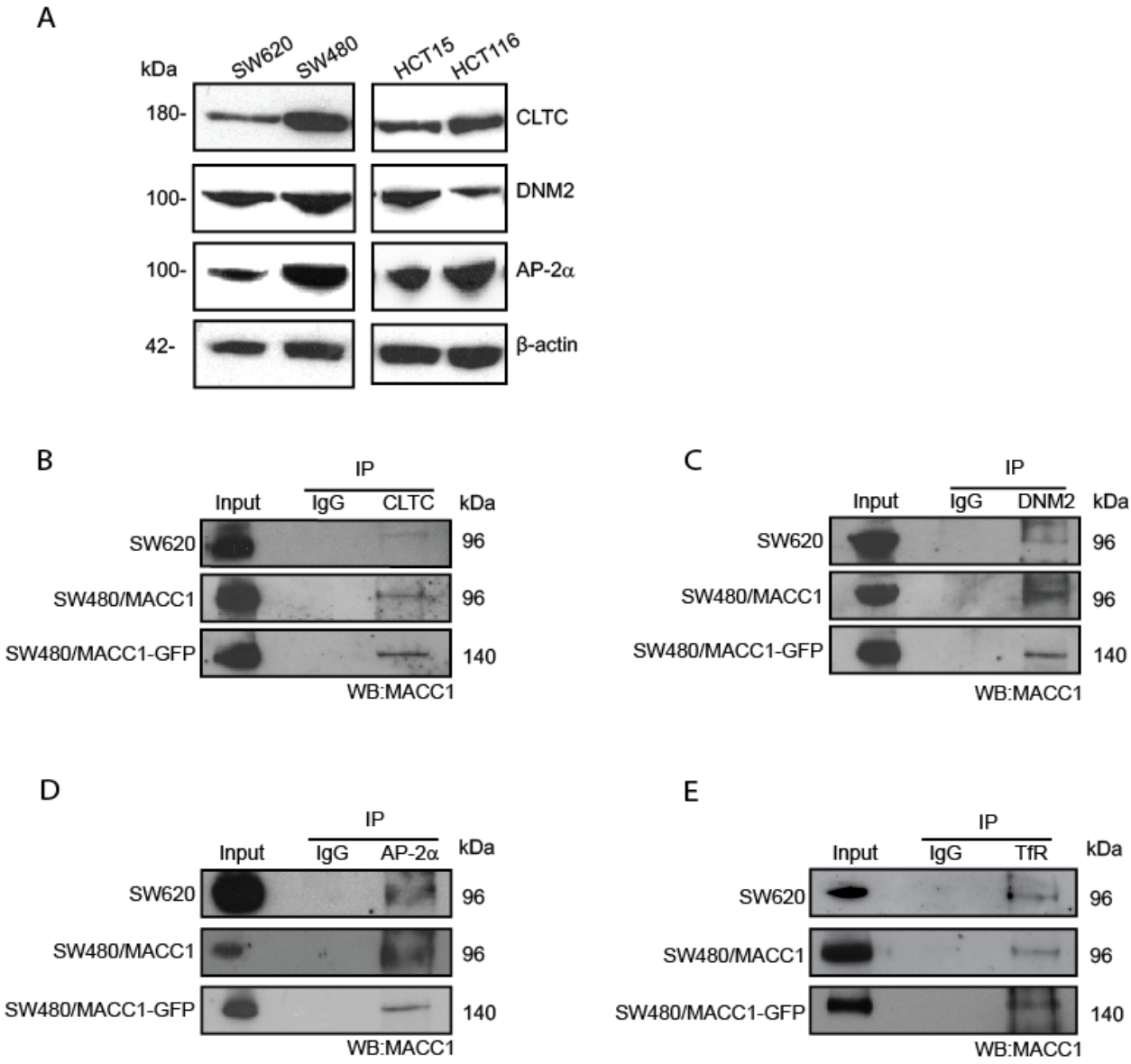

Figure 20 MACC1 interacts with several CME factors and with TfR in different CRC cell lines. (A) CME-involved proteins were evaluated for their protein expression via WB, in different CRC cell lines (SW620, SW480, HCT15, HCT116). After seeding (3 x 10^5), cells were harvested, lysed in RIPA buffer and the cell lysates were immunoblotted for CLTC, DNM2, AP-2α and β-actin as a loading control. Represented (A, left panel) are the protein expressions of CLTC, DNM, AP-2α in SW480 and SW620 cells. In parallel (A, right panel) protein expressions of CLTC, DNM2 and AP-2α in HCT15 and HCT116 cells. (B-E) MACC1 CME binders validated via coIP in three different cell lines: SW620, SW480/MACC1, and SW480/MACC1-GFP. After seeding, cells (4 x 10^6) were harvested and lysed in coIP lysis buffer (see material and methods for details). Cell lysates were coIP with control IgG or indicated against individual CME proteins and immunoblotted for MACC1. The binding of MACC1 and CLTC (B), DNM2 (C), AP-2α (D) is shown, while the binding between MACC1 and TfR (E) has been also determined.

4.1.3 Ligand-stimulated TfR internalization alters MACC1 colocalization and correlation with CME proteins

Plasma membrane receptors play a key role in cell homeostasis by regulating cell signaling (in both attenuation and enforcement) and nutrient uptake[132,192,193]. Receptor fate changes dynamically during the principal steps of CME such as internalization, recycling and degradation. Hence, it has become pivotal to decipher the role of CME-associated proteins in deciding receptor routes during endocytosis. A first effective adopted approach was to investigate their recruitment to the endocytic machinery, in order to understand their impact during receptor fate decision. For this end, we elucidated MACC1 impact on CME regulation, in particular we analysed MACC1 changes in distribution, correlation and colocalization with CME interactors validated beforehand (CLTC, DNM2, AP-2α, TfR).

TfR is a well-known model receptor that is constitutively internalized via CME[194]. To confirm MACC1 involvement during CME and to investigate its correlation with CME proteins belonging to early or late stages of CCV formation, SW480/MACC1 cells were treated with h-Tf for 15 min following 1 h starvation (to deplete circulating TfR). After triggering TfR internalization and trafficking to endosomes (within 15 min of stimulation), MACC1 correlation with CME proteins, before and after TfR-stimulated internalization, was screened via immunofluorescence (IF) and analyzed using confocal microscopy. All the screened IFs are representative of a central section of the cell (Figure 21, top panel).

Interestingly, both colocalization and correlation of MACC1 with TfR and the CME-associated factors CLTC and DNM2 changes upon ligand-stimulated TfR internalization (Fig. 21, A-C). More specifically, the Pearson's correlation increased significantly for MACC1 colocalization with TfR and CLTC after the stimulation. In contrast, the Pearson's correlation for MACC1 colocalization with DNM2 or AP-2α decreased. Furthermore, MACC1 colocalization with TfR and CLTC, as shown in Figure 21 (A-B) is strikingly increased in punctate structures in the cytoplasm. While, MACC1 and DNM2 initially colocalizing at PM (Figure 21, C) show a decreased correlation and distribution at PM after ligand-stimulated TfR internalization. MACC1 and AP-2α correlation decreased upon TfR stimulated-internalization, leading us to exclude this protein from any further analysis in this thesis, because of the secondary and probably indirect role with MACC1.

Together, our data show that upon Tf-triggered internalization of TfR, MACC1 changes its distribution and correlation with different endocytic proteins. In particular, MACC1 colocalization was found increased with DNM2 at the PM before the stimulation and decreased after the stimulation. In contrast, after TfR-stimulated internalization MACC1 colocalization is increased in the cytoplasm with

CLTC and TfR and displayed in punctate structures. In conclusion, MACC1 shows a stimuli-dependent changes in the localization and correlation with several CME proteins confirming its involvement during CME and in CCPs or CCVs.

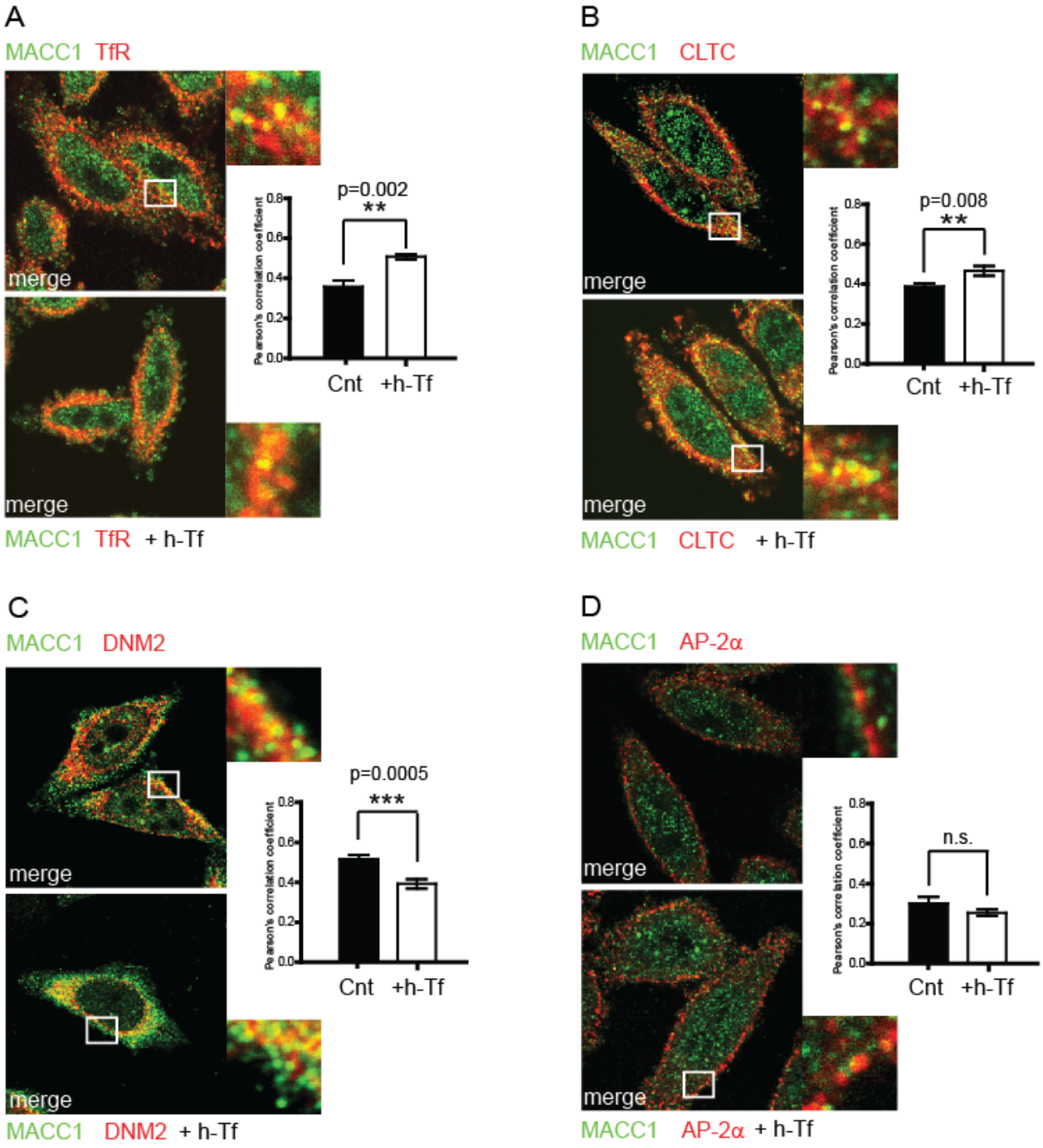

Figure 21 Ligand-stimulated TfR internalization alters MACC1 colocalization and correlation with CME proteins. A confluent monolayer of SW480/MACC1 cells (1x10^4) was seeded, serum starved (1 hr) and treated for 15 min h-Tf (250 ug/ml) in order to measure the distribution and correlation of MACC1 with endocytic proteins by immunofluorescence. (A-D) Colocalization of MACC1 and TfR (A), CLTC (B), DNM2 (C) and AP-2α (D) in SW480/MACC1 cells before (upper panel) and after (lower panel) 15 min stimulation of TfR internalization with h-Tf. Scale bar = 10 µm. Indicated regions are displayed enlarged (10x). Statistical analysis of Pearson

correlation coefficients (n > 60 cells, mean ± SEM, n=3) are performed by Student's t-tests. Single channel images are provided in Supplementary Figure 2.

4.1.4 MACC1 marks TfR containing vesicles and colocalizes with endosomes and TfR, upon h-Tf triggered TfR CME internalization

TfR has been widely characterized for its internalization process, and together with LDLR they represent the classic examples for CME[195]. TfR receptor recycling to the PM after internalization seems to be the default path[171]. Moreover, in order to be recycled back to the PM, TfR does not require any specific consensus sequence on its cytoplasmic tail.[196] Thus, considering its simplicity and its extensive characterization in literature, we focused on understanding MACC1 impact on TfR endocytic trafficking.

TfR is internalized in CCVs, that after their uncoating, fuse with highly dynamic compartments known as endosomes, marked by EEA1[162,171]. SW480/MACC1 cells were used to accurately assess and screen the MACC1 involvement in the first endocytic steps and during TfR sorting. For this purpose, SW480/MACC1 cells were stimulated to induce the TfR-selected internalization with h-Tf, and immunostained with fluorescence-labelled antibodies for the vesicle compartment (CLTC) and the endosomal compartment (EEA1) (Figure 22, A-B). Triple colocalization has been spatially analyzed by measuring and representing the three different fluorescence intensities (red, blue, green), on the histogram in the lower panel (Figure 22, A-B), while the unstimulated condition is represented in the upper panels of Figure 22 (A-B). Our data show that MACC1 not only marks TfR-containing CCV (Figure 22, A), but also colocalizes with TfR at the endosomal compartment after 15 min stimulation (Figure 22, B). To conclude, MACC1 was found in TfR-containing vesicles and endosomes, therefore, it is involved in the earliest and later stages of TfR internalization. MACC1 might shuttle from the PM to endosomes in CCV together with TfR. Thus, MACC1 follows the TfR internalization from the PM to CCVs, towards endosomes as a cargo protein.

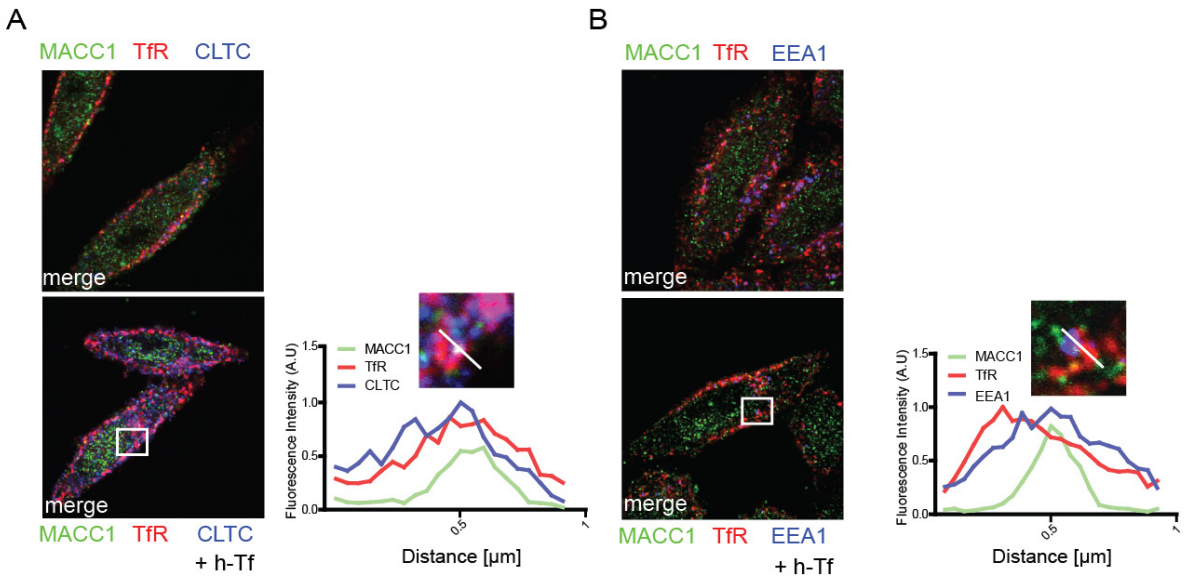

Figure 22 MACC1 marks TfR-containing vesicles and TfR-containing endosomes, upon h-Tf triggered TfR CME internalization. A confluent monolayer of SW480/MACC1 ($1x10^4$) was seeded, serum starved (1 hr) and treated for 15 min with h-Tf (250 ug/ml) (A-B) Colocalization of MACC1, TfR and CLTC (A) or EEA1 (B) after triple-staining of SW480/MACC1 cells before (upper panel) and after (lower panel) 15 min stimulation of TfR internalization with h-Tf. Scale bar = 10 µm. Indicated regions are displayed enlarged 10x, and histograms show the spatial distribution of the signal intensities across indicated sections (n = 30 cells). All panels show merged images. Single channel images are provided in Supplementary Figure 3.

4.2 Characterization of MACC1 involvement during TfR endocytosis

4.2.1 MACC1 overexpression and knockdown are not affecting TfR nor SH3BP4 mRNA expression

Several proteins have been identified as receptor-fate "switchers", but for our purpose we will focus on the well-characterized SH3BP4. SH3BP4 regulation of TfR, via DNM2, has been already elucidated[121]. MACC1 and SH3BP4 share 43.7% protein homology (Fig. 23, A) and several CME-involved domains, together with the protein signature. To exclude any biological interdependence or effect of MACC1 overexpression and knockdown on TfR or SH3BP4 gene expression, we assessed their mRNA expression in these two MACC1 conditions.

We first analyzed the expression of MACC1, SH3BP4 and TfR in SW480/e.v., SW480/MACC1 and SW480/SH3BP4, via qRT-PCR and WB. We observed no altered expression levels except for MACC1 in SW480/MACC1 and SH3BP4 in SW480/SH3BP4 as compared to SW480/e.v. (Fig. 23, A-B). Similarly, we evaluated MACC1, SH3BP4 and TfR gene expression in SW620 control cells (SW620/sh cnt) and in the MACC1 knock-down (KD) cell line (SW620/sh MACC1). we observed only an altered gene expression level of MACC1 in the KD cell lines while no alteration in the protein levels was detected (Fig. 23, C-D).

Tumors differently express TfR depending on their stage and their aggressive nature. TfR mRNA and protein levels are important to understand the endocytic receptor dynamics in terms of internalization, recycling and degradation. As previously reported for CRC, TfR is differently expressed in well (Dukes A and B) or poor differentiated (Dukes C or D) carcinoma samples or cell lines[177]. Therefore, to compare the CRC cell lines in focus (SW480 and SW620) and their TfR expression, we employed qRT-PCR and WB. As previously reported, we could confirm an altered CRC stage-dependent TfR mRNA expression in SW480 (Duke B) and SW620 (Duke C). These cell lines originate from the same patient and from primary lymph node metastasis respectively (Fig. 23, E-F). TfR is abundantly expressed in SW480 cells, confirming previous data[177], however, an even higher expression of TfR was found in SW620 cells. Also, a reduced TfR protein expression in SW480 as compared to SW620 cells was observed, matching the TfR/CRC staging only in SW480 cells, as previously mentioned[177].

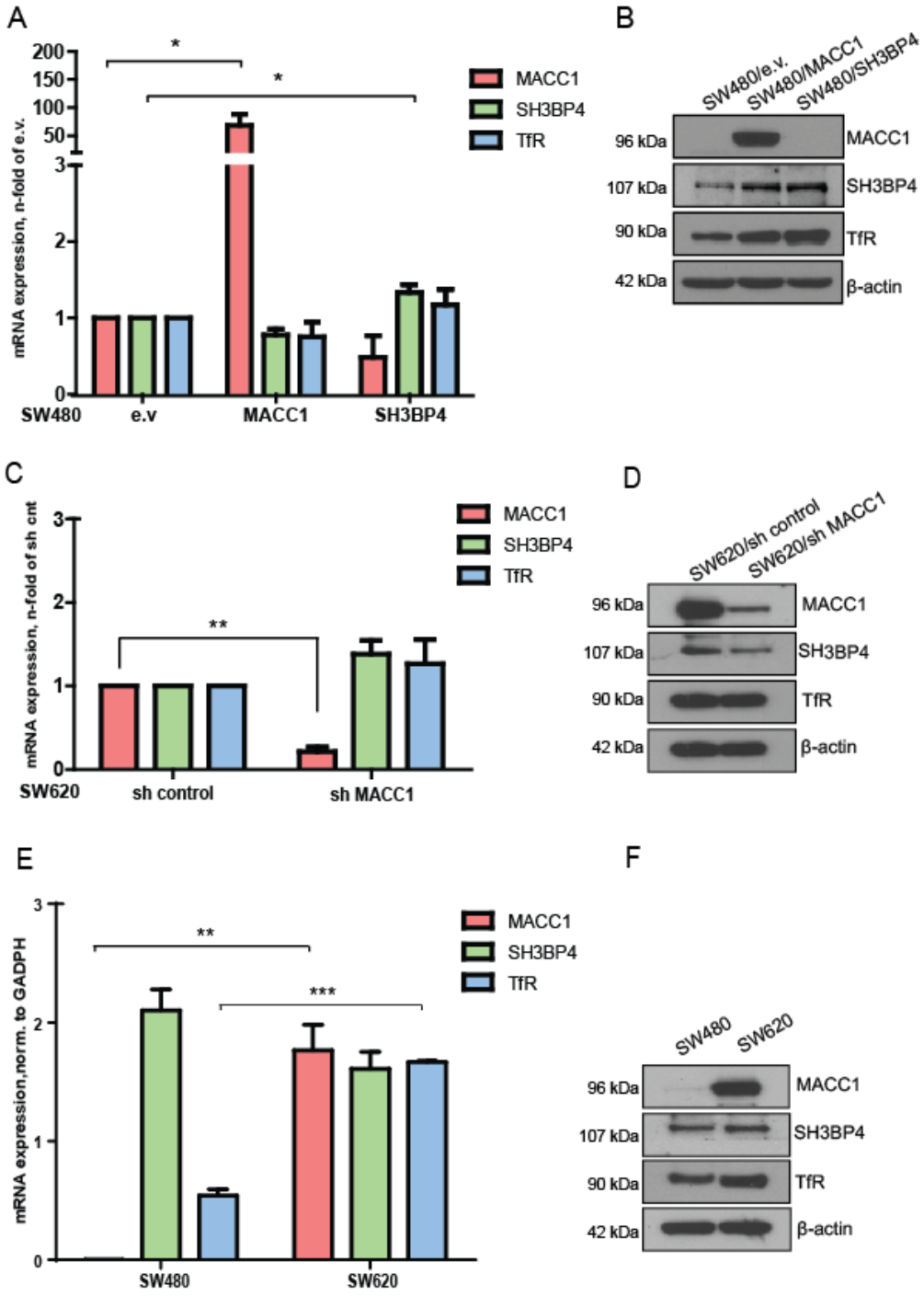

Figure 23 MACC1 overexpression and knockdown are not affecting TfR nor SH3BP4 mRNA expression. MACC1, TfR and SH3BP4 mRNA and protein expression were studied in SW480/e.v., SW480/MACC1, SW480/SH3BP4 (A-B) and SW620/sh cnt, SW620/sh MACC1 (C-D) and SW620 and SW480 (E-F) to exclude any MACC1-interdependence or MACC1 dependent-effect on mRNA and protein expression levels. Thus, 48 hr after seeding cells ($3x10^5$), total RNA was extracted, reverse transcribed and quantified by real time q-PCR. (A, C, E) MACC1, TfR and SH3BP4 mRNA expressions were validated in SW480/e.v., SW480/MACC1, SW480/SH3BP4 and SW620/sh cnt, SW620/sh MACC1 and SW480 and SW620 cells. Results are first normalized to GADPH and then represented as n-fold of the control cell line respect to the gene of interest. Results are shown as means ± SEM of three independent experiments. (B-D-F) For the MACC1, TfR and SH3PB4 protein expression analysis, after seeding ($3x10^5$), cells were harvest, lysed in RIPA lysis buffer (see material and methods for details). Cell lysates were quantified and each sample immunoblotted on nitrocellulose membrane, for MACC1, TfR, SH3BP4 and β-

actin as loading control. A representative blot of three independent experiments is shown. *p < 0.05, **p < 0.01, ***p < 0.001

4.2.2 Ectopic overexpression of MACC1 decreases TfR surface distribution and affects TfR internalization in SW480 cells

SH3BP4 involvement during CME has been already reported from Tosoni's group and from Olsen's group[121,122]. Briefly, SH3BP4 perturbation affects TfR during internalization[121]. The SH3BP4-mediated impact on TfR internalization is SH3-domain dependent and is rescued by DNM2 overexpression. This finding confirms the mutual action of SH3BP4 and its SH3 domain during the DNM2- mediated rate limiting step of endocytosis[121,122]. To investigate the role of MACC1 in the CME-dependent internalization of TfR, in comparison to the reported effects of SH3BP4, we analyzed SW480 cells with MACC1 ectopic overexpression (SW480/MACC1), of SH3BP4 (SW480/SH3BP4), and SW480 cells harboring the empty vector (SW480/e.v.), using both respectively as controls.

Surface abundance of TfR and its rate of internalization were determined by indirectly labeling extracellular surface TfR with fluorescence-labeled Tf-647 at 0°C to impede endocytosis, and for the time resolved uptake of the receptor-ligand-complex, after shifting the cells to 37°C (Fig. 24, A-B). Signal has been detected using FACS.

After carrying out the assay we observed a reduced surface abundance TfR-Tf-647 complex in SW480/MACC1 cells (Fig. 24, A), as well as in SW480/SH3BP4 cells but not relevantly, compared to SW480/e.v. cells. After shifting surface-marked cells to 37°C, the TfR uptake resulted in a significant interference in SW480/MACC1 cells, compared to SW480/e.v. cells, with a similar tendency in SW480/SH3BP4 cells at the time points 10 min and 20 min (Fig. 24, B). SW480/SH3BP4 cells were used as a positive control as previously reported[121].

To conclude SW480/MACC1 and SW480/SH3BP4 cells show a significantly lower internalized Tf-647 after 20 min, compared to SW480/e.v.. MACC1 overexpression affects, as SH3BP4, TfR-Tf-647 internalization, and this suggest MACC1 might participates during TfR internalization. However, further experiments are required to understand how MACC1 affects TfR endocytic traffic, and at which step.

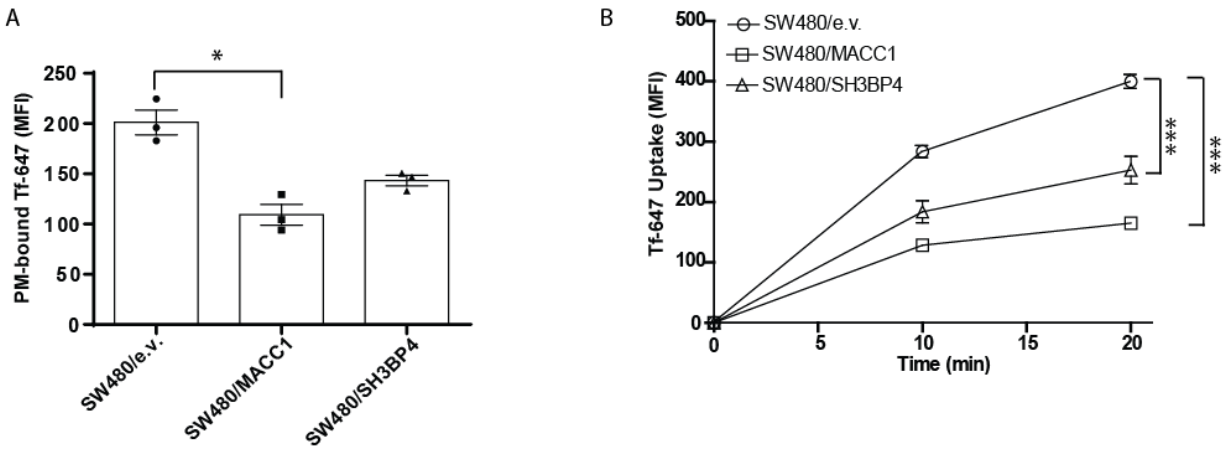

Figure 24 Ectopic overexpression of MACC1 decreases the surface distribution of TfR and affects TfR internalization. After cell seeding ($1x10^6$) and starvation, cells were harvest and marked with Tf-647 (25 µg/ml) at 0°C on ice to impede endocytosis and then shifted at 37°C (see Material and Methods for details). (A) Surface staining of TfR with Tf-647 (25 µg/ml) of SW480-derived cell lines is represented. Total surface Tf-647 signal intensities were determined by FACS. (B) Internalized Tf-647 signal intensities after temperature shift for subsequent time points. Data represent mean ± SEM of three independent experiments. *$p < 0.05$, **$p < 0.01$, ***$p < 0.001$

4.2.3 MACC1 overexpression prevents the endocytic TfR traffic into degradative compartments

To investigate the role of MACC1 during TfR internalization, we extended our previous knowledge by further validating our results (Figure 25 A-C) using a newly established technique: IncuCyte®. After the establishment of the technique, we could carry out live-cell imaging and time-dependent analysis by using the transferrin pH sensitive compound (pHrodo-Tf). As previous works showed already, the compound is able to track the internalization of TfR, in particular in endosomes and in more acidic/late endocytic compartments[187,197–20]. The TfR-Tf complex is normally 95% recycled back to the PM where it dissociates and releases (apo-)Tf into the medium[171].

The compound is designed to be brightly fluorescent and activated at low pHs, especially in degradative compartments such as MVBs and lysosomes. We adjusted the protocol to our conditions: after starving and feeding the cells with the compound, we moved the samples in the IncuCyte® shifting the temperature from 0°C to 37°C and the live-cell fluorescence signal was detected in a time-dependent manner (0-180, every 30min).

We observed an increased integrated fluorescent signal and accumulation in acidic compartments of the pHrodo-Tf in SW480/e.v. cells after 180 min (Fig. 25, A, B-1). In contrast, SW480/MACC1 cells showed a reduced intensity of the signal (Fig. 25, A, B-2), diverging from the control after 1 h. Moreover, a decreased red fluorescence signal was detected after 180 min (Fig. 25, B-2) in SW480/MACC1 cells as compared to the control cell line (Fig. 25, B-1).

In conclusion, our data show that MACC1 overexpression avoids the accumulation over time of the pHrodo-Tf-TfR complex in low pH and degradative compartments, while in the control (SW480/e.v.), a relevant accumulation of the pHrodo-Tf-TfR and the red fluorescence signal was observed after 180 min.

However, further experiments are required to understand whether MACC1 impact by avoiding TfR accumulation in acidic compartments in due to its intervention on the internalization, recycling or degradation step.

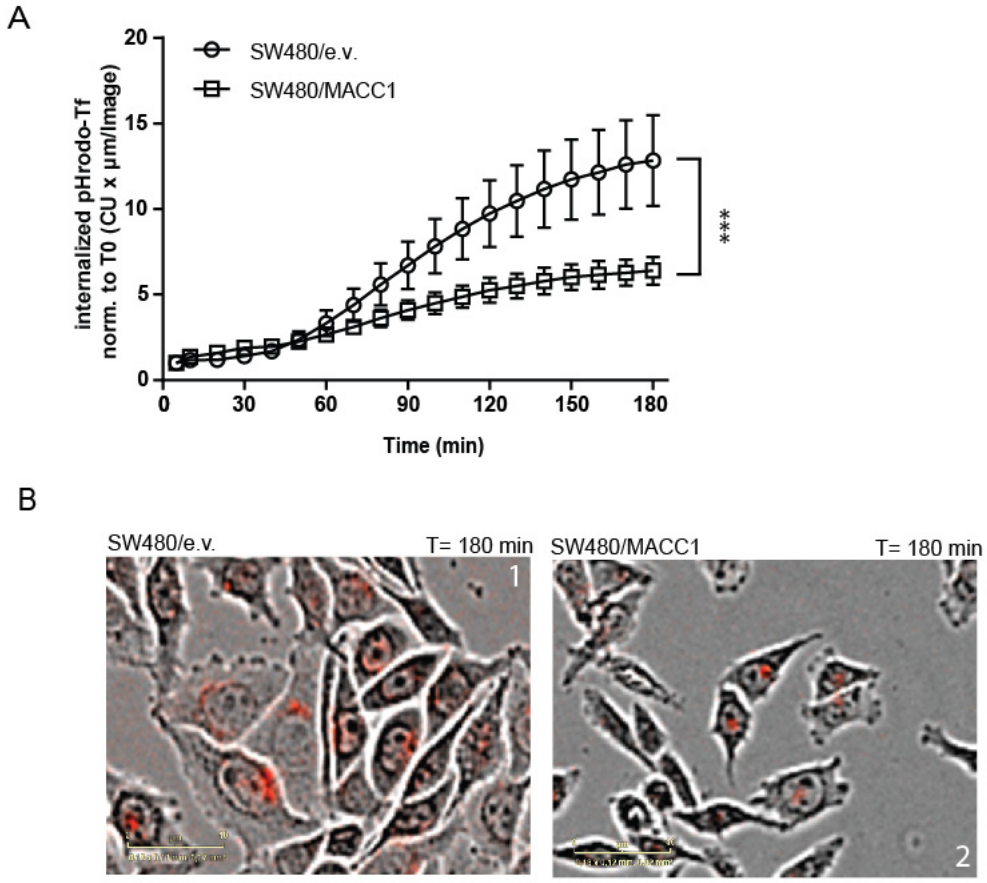

Figure 25 MACC1 overexpression prevents the endocytic TfR traffic into degradative compartments. Cells were seeded ($1x10^4$) in a 96-well plate and after starvation, were fed with pHrodo-Tf (50 ug/ml) and the integrated fluorescence signal was observed in a time-dependent manner. (A) Integrated pH-sensitive signal intensities of internalized pHrodo-Tf over time. Results are shown as means ± SEM of four independent experiments. ***$p < 0.001$. (B) Representative pictures from IncuCyte® live imaging system of SW480 e.v. (1) and SW480/MACC1 (2) and the pHrodo compound after 3 h of the endocytic assay.

4.2.4 MACC1 overexpression mediates a faster TfR recycling leaving RAB11 expression unaltered, while in the control cell line is degraded

The MACC1 overexpression prevents the TfR-pHrodo-Tf complex from being processed towards low pH and degradative compartments (Fig. 25). Hence, to understand whether MACC1 was also involved in the recycling of TfR to the PM we studied the recycling rate (observable as a loss of fluorescent signal and measured by FACS) of the TfR-Tf-647 marked complex over time. As shown (Fig. 26, A), MACC1 overexpression in SW480 generates the faster signal loss of Tf-647, compared to the control cell line SW480/e.v..

SW480/SH3BP4 cells showed no enhanced TfR recycling as compared to SW480/e.v. which is in line with previous data which showed no recycling effect of SH3BP4 ovexpression[121]. Moreover, when internalized, the TfR can be processed via two different recycling routes: a fast RAB4-mediated processing route directly from endosomes, and a slow RAB11-mediated route from ERC[195,196,203]. In our MACC1-CME interactome analysis we could find a putative interaction of MACC1 with a Ras-related protein (RAB) (Supplementary Figure 1, 10), in particular RAB11A.

Therefore, to exclude a RAB11A-altered activity on the TfR faster recycling to the PM, we checked the protein level in SW480/e.v and SW480/MACC1 cells and as reported (Fig. 26, B), no difference in RAB11 protein expression was observed between SW480/MACC1 and the control cell line.

Moreover, we also studied TfR degradation over time by analyzing the loss of TfR total protein after stimulation with h-Tf. SW480/e.v. cells show decreased total TfR protein levels over time (Fig. 26, C-D) following the stimulation of TfR uptake. On the other hand, SW480/MACC1 cells did not show apparently any loss of the protein over time. To conclude, these observations lead us to speculate a MACC1-mediated increased of TfR recycling in RAB11 endocytic recycling compartments.

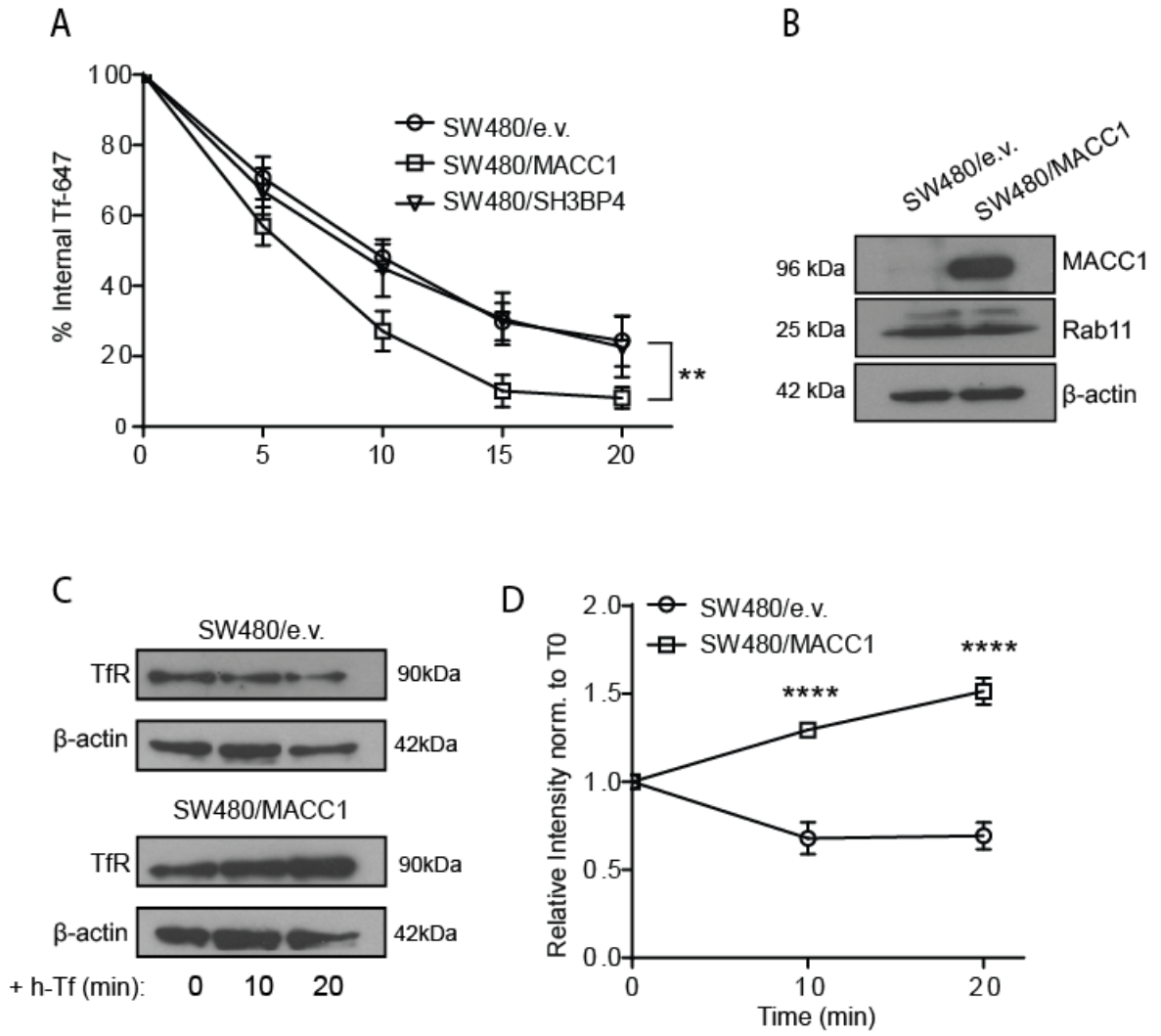

Figure 26 MACC1 overexpression mediates a faster TfR recycling leaving RAB11 expression unaltered, while in the control cell line is degraded. (A) After seeding and starving cells, the recycling assay was carried out as previously described[189] (see Material and method for details). Briefly, after marking cells surface with fluorescence-labelled Tf-647 (25 ug/ml), the shift of the cells from 0°C to 37°C in the incubator, allowed the loading of endosomes with Tf-647. Signal loss over time, due to recycling of the TfR to the PM has been quantified via FACS (MFI). (B) RAB11 protein level has been checked at steady state in SW480/MACC1 and SW480/e.v. cells. Representative Western blot of three independent experiments, β-actin has been used as loading control. (C) TfR degradation was studied, after seeding and starvation, cells ($3x10^5$) we fed with h-Tf (50 ug/ml) for 10 and 20 min. Representative Western blot of three independent experiments. (D) Quantification of TfR/β-actin ratio level upon h-Tf stimulation, after quantification of WB signal intensities and normalization to t = 0 min. MFI – mean fluorescence intensity; RAB11 – Ras-related protein Rab11; **p < 0.01, ****p<0.0001

4.2.5 MACC1 recruitment during TfR-stimulated CME increases the receptor colocalization into RAB11-marked compartments and decreases its colocalization in LAMP1-marked degradative compartments

Once we established a faster MACC1-induced recycling effect (Fig. 26, A), we confirmed and tested the ability of MACC1 to lead TfR to target RAB11 recycling compartments. To understand the fate of the internalized TfR, we compared TfR localization in SW480/e.v. and SW480/MACC1 cells, not only in RAB11-marked compartments, but also in degradative compartments, marked with the lysosomal membrane protein (LAMP1). For this purpose, immunofluorescence and confocal microscopy approaches were used.

In the end, to confirm a role of MACC1 during internalization, we blocked both the slow and fast recycling routes with the ionophore monensin and analysed the TfR endosomal accumulation after treatment [158,195–197]. Our data show that upon TfR-stimulated internalization, MACC1 overexpression in SW480 cells drives TfR to increased colocalization in RAB11-marked compartments, compared to SW480/e.v. cells (Fig. 27, A-D).

Accordingly, the results showed that in SW480/MACC1 cells TfR colocalization with LAMP1 decreased after 30 min of TfR internalization with h-Tf as compared to SW480/e.v. cells (Fig. 10, B-D). Furthermore, observing both SW480/e.v. and SW480/MACC1 cells, the overall colocalization of TfR in LAMP1 compartments is lower than in RAB11 compartments, supporting the classical sustained TfR routing into recycling compartments in both the cell lines.

However, we also used the recycling inhibitor monensin to evaluate the TfR accumulation in EEA1-marked endosomes overtime, thus, blocking both the recycling routes. As expected, considering the MACC1-mediated interference on the TfR uptake (Fig. 6, A-B-C), no accumulation between SW480/e.v. or SW480/MACC1 was observed whilst a decreased colocalization of TfR in EEA1 compartments was noticed. This confirms the MACC1-mediated interference on TfR uptake (Fig. 6). To conclude, our findings show a MACC1-mediated enhancement of the TfR trafficking into RAB11 recycling compartments and its interference during ligand-stimulated TfR internalization.

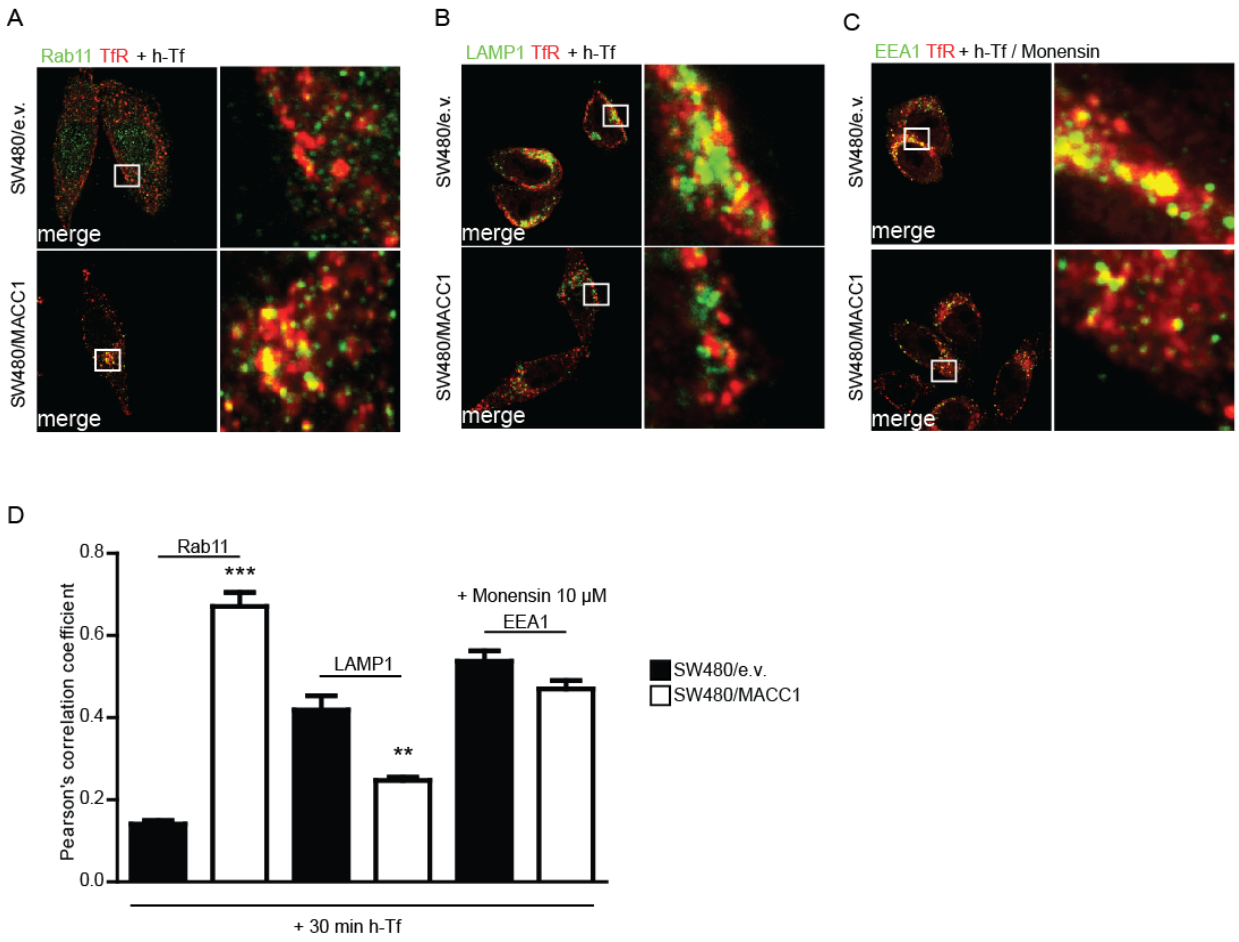

Figure 27 MACC1 recruitment during TfR-stimulated CME increases the receptor colocalization into RAB11-marked compartments and decreases its colocalization in LAMP1-marked degradative compartments. A confluent monolayer of SW480/e.v. and SW480/MACC1 cells ($1x10^4$) was seeded, serum starved and treated for 30 min with h-Tf (50 ug/ml) to measure the immunofluorescence distribution of TfR in RAB11 or LAMP1 marked endocytic compartments. (A-C) Colocalization of MACC1 and RAB11 (A), LAMP1 (B), EEA1 (C) in SW480/e.v. and SW480/MACC1 cells after 30 min stimulation of TfR internalization with h-Tf. Scale bar = 10 µm. Indicated regions are displayed enlarged (10x). (D) Statistical analyses of Persons correlation coefficients (mean ±SEM), are performed by Student's t-tests. Single channel images are provided in the supplementary Figures 4. RAB11 – Ras-related protein Rab11; LAMP1 – lysosomal membrane protein; EEA1 – early endocytic antigen 1; **p < 0.01, ***p < 0.001

4.2.6 MACC1 knockdown is not altering TfR surface abundance in SW620 cell lines but interferes with the TfR uptake

After we assessed the effect of MACC1 overexpression on TfR endocytic traffic (Fig. 25, A-B-C), we tested the effect of MACC1 knockdown (KD) on TfR internalization and surface distribution, using cell lines previously established in our lab[81]: SW620/sh cnt and SW620/sh MACC1 respectively. After lentiviral transduction, SW620 cells displayed a stable silencing for MACC1 mRNA expression (SW620/sh MACC1) (Fig. 23, C-D).

No MACC1 KD dependent alterations of mRNA and protein levels of TfR and SH3BP4 were observed in SW620/sh MACC1 cells and the respective control cell line (SW620/sh cnt) (Fig. 23, C-D). Hence, the surface abundance of TfR at PM in SW620/sh MACC1 and SW620/sh cnt cells was indirectly assessed. As shown (Fig. 28, A), no difference was observed for the TfR-Tf-647 bound to PM in SW620/sh MACC1 and the control cell line.

Consequently, the MACC1 KD-dependent effect on TfR CME uptake was elucidated. The internalization was determined by specifically labeling indirectly the TfR at PM with Tf-647 at 0°C to impede endocytosis, and the time resolved uptake of the receptor-ligand-complex was determined after shifting the cells to 37°C, (Fig. 28, A-B). As expected, MACC1 KD interferes with TfR internalization after 20 minutes, (Fig. 28, B). These data confirm MACC1 as a regulator of the TfR internalization.

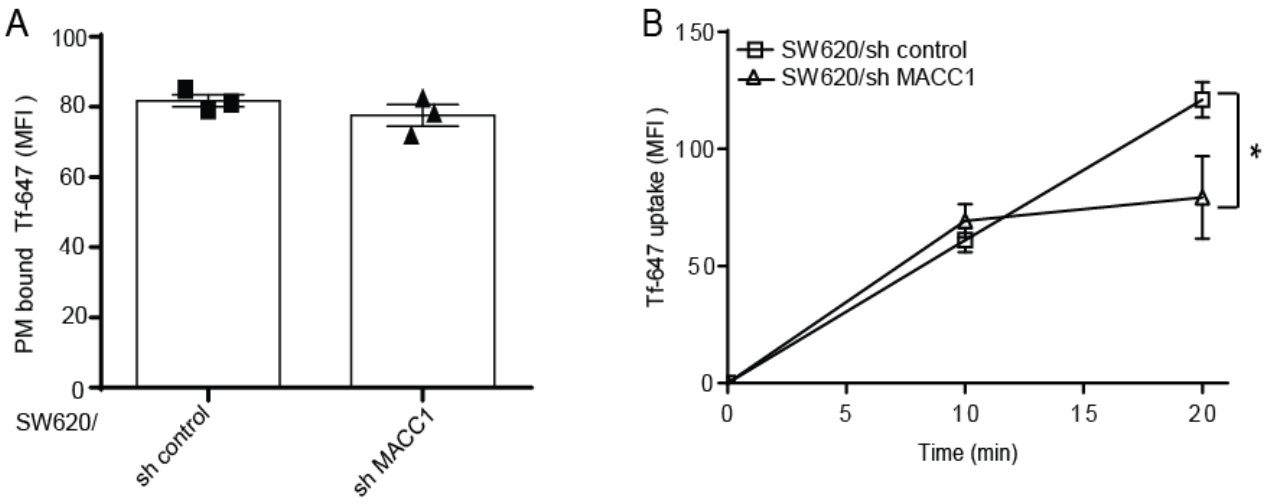

Figure 28 MACC1 knockdown is not altering TfR surface abundance in SW620 cell lines but interferes with the TfR uptake. After cell seeding ($1x10^6$) and starvation, cells were harvested and marked with Tf-647 (25 µg/ml) at 0°C and then shifted at 37°C for determining the internalized signal (see Material and Methods for details). (A) Surface staining of TfR indirectly marked with Tf-647 of SW620-derived cell lines is represented. Total surface Tf-647 signal intensities were determined indirectly by FACS. (B) Internalized Tf-647 signal intensities after temperature shift for subsequent time points. Data represent mean ± SEM of three independent experiments. *p < 0.05.

4.2.7 MACC1 knockdown targets TfR to degradative compartments

As previously shown, MACC1 recruitment during TfR internalization generates a faster TfR recycling to PM which is independent from changes in RAB11 protein expression (Fig. 26, A-B). To complete our knowledge on TfR fate after internalization in MACC1 overexpressing and knock-down conditions, we used the IncuCyte® Live-imaging system, with the pH sensitive compound pHrodo-Tf.

As expected, after feeding the cells with the pHrodo-Tf and shifting them from 0°C to 37°C, live-cell fluorescence signal was detected in a time-dependent manner. We observed a significantly increased integrated fluorescence signal in SW620/sh MACC1 cells after 180 min as compared to SW480/MACC1 cells, indicating a pHrodo-Tf accumulation into degradative and low pH compartments (Fig. 29, A).

Moreover, the fluorescence signal was observed after 180 min of assay in SW620/sh MACC1 cells as compared to the control (Fig. 29, B-2). To conclude, our findings show that MACC1 KD leads to the accumulation of pHrodo-Tf-TfR complex in low pH and degradative compartments over time (Fig. 29, A and B-2).

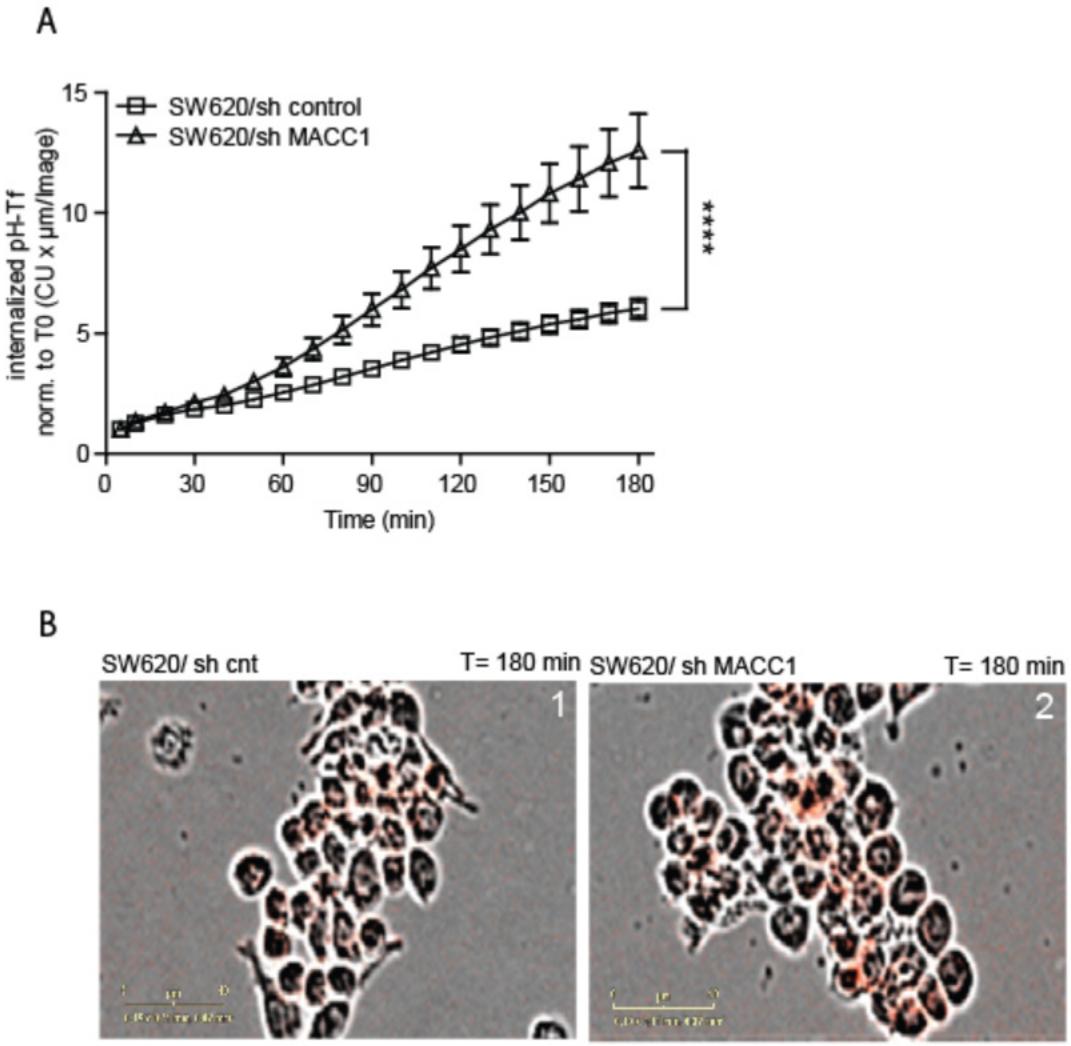

Figure 29 MACC1 knockdown targets TfR to the degradative compartments. Cells were seeded ($1x10^4$) in a 96-well plate and after starvation, were fed with pHrodo-Tf (50 ug/ml), and the integrated fluorescence signal was observed in a time-dependent manner. (A) Integrated pH-sensitive signal intensities of internalized pHrodo-Tf over time. Results are shown as means ± SEM of four independent experiments. ****p < 0.0001. (B) Representative pictures from the IncuCyte live imaging system of MACC1 SW620/sh cnt (1) and SW620/ sh MACC1 cells (2) and the pHrodo-Tf compound after 3 h of endocytic assay.

4.2.8 MACC1 knockdown leads TfR to degradation following specific internalization stimuli

Our results show increased TfR trafficking into low pH and degradative compartments in SW620/sh MACC1 cells as compared to the control cell line (Fig. 29, A-B). Therefore, to confirm the MACC1-mediated effect on TfR targeted traffic to degradative compartments, we measured the TfR total protein level after ligand-stimulated CME.

After seeding and starving cells, TfR internalization was specifically stimulated with h-Tf. Cells were lysed after 10 or 20 min of stimulation and the total TfR protein was measured by SDS-PAGE and WB. In line with previous data (Fig.29), MACC1 KD increases TfR degradation after 20 min of h-Tf stimulation (Fig. 30, A-B). Hence, to check whether the MACC1-dependent degradation could be reverted, cells were pre-treated with Bafilomycin A1, an inhibitor of lysosomal degradation.

Stimulation of TfR internalization for 10 and 20 minutes with h-Tf after Bafilomycin A1 leads to an accumulation of the TfR total protein in both cell lines (Fig. 30, C-D). We therefore conclude that MACC1 KD leads to TfR degradation via degradative compartments, while inhibition of lysosomal degradation results in a TfR protein accumulation in SW620 sh MACC1 cells, similarly to SW620/sh control.

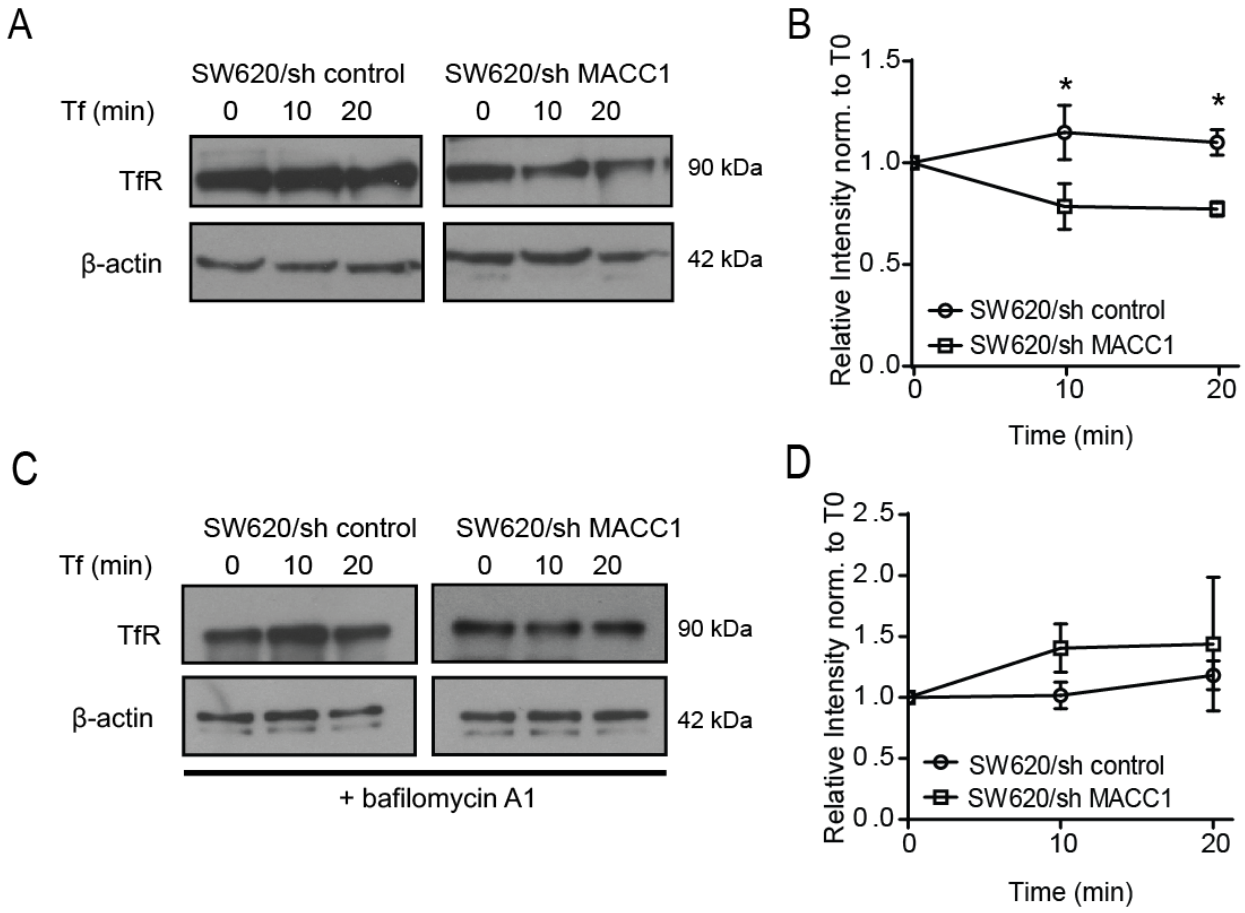

Figure 30 MACC1 knockdown leads to TfR degradation following specific internalization stimuli. (A, C) TfR degradation was studied after seeding and starvation (with or without pre-treatment with bafilomycin A1 for 4 h), cells ($3x10^5$) were fed with h-Tf (50 ug/ml) for 10 and 20 min and total protein changes were checked over time. Representative blot of three independent experiments. (B, D) Quantification of TfR/β-actin ratio upon h-Tf stimulation, after quantification of WB signal intensities and normalization to t = 0 min.; *p < 0.05

4.2.9 Endogenously overexpressed MACC1 increases the endocytic traffic of TfR in SW620 cells compared to SW480 cells, virtually non-expressing MACC1

To understand the general MACC1-dependent effect on TfR endocytic traffic we analyzed it from another point of view. A reported correlation between Dukes cancer staging and altered TfR expression and distribution in patients tissue raised the question as to whether we could detect an altered TfR surface distribution and internalization in CRC cell lines employed in this thesis, i.e. SW480 cells (Duke B, low MACC1 expression) and SW620 cells (Duke C, high MACC1 expression), originating from the primary tumor and a lymph node metastasis respectively, from the same patient[177].

Gene expression of MACC1, SH3BP4, and TfR in both cell lines were analyzed via gene specific qRT-PCR and WB. Altered expression levels of MACC1 and TfR were observed (Fig. 23, E-F). Thus, to find out the MACC1 overall effect on TfR endocytic routing, we studied the surface distribution of TfR as well as TfR internalization by indirectly labeling extracellular TfR with Tf-647 at 0°C, and for the time resolved uptake of the receptor-ligand-complex at 37°C (Fig. 31, A-B), observing the surface and internalized signal via FACS.

As expected, our data show increased PM-bound Tf-647 in SW620 cells in accordance with previous data (Fig. 23, E-F). On the other hand, increased TfR internalization was also observed in SW620 highly expressing MACC1, we speculate it might depend from the increased TfR expression and surface distribution in SW620 (Figure 31, A).

Next, we used the IncuCyte® Live-imaging system to elucidate the overall effect of the endogenously high expression of MACC1 on the TfR traffic, taking into consideration the MACC1-dependent fast recycling of TfR (Figure 26, A). The overall effect, as expected, shows a sustained endocytic traffic of TfR in SW620 cells towards low pH compartments (Fig. 31, C-D).

To conclude, SW620 cells show increased PM distribution of TfR, indirectly measured. Depending on the PM distribution, the internalized TfR-Tf-647 complex is increased in SW620 compared to SW480 low-MACC1 expressing cells. We conclude that MACC1 is regulating both TfR internalization and recycling. In SW620 cells this overall increases in the endocytic rate of TfR traffic in low pH compartments, might depend on the TfR higher expression together with MACC1 increased effect on TfR recycling.

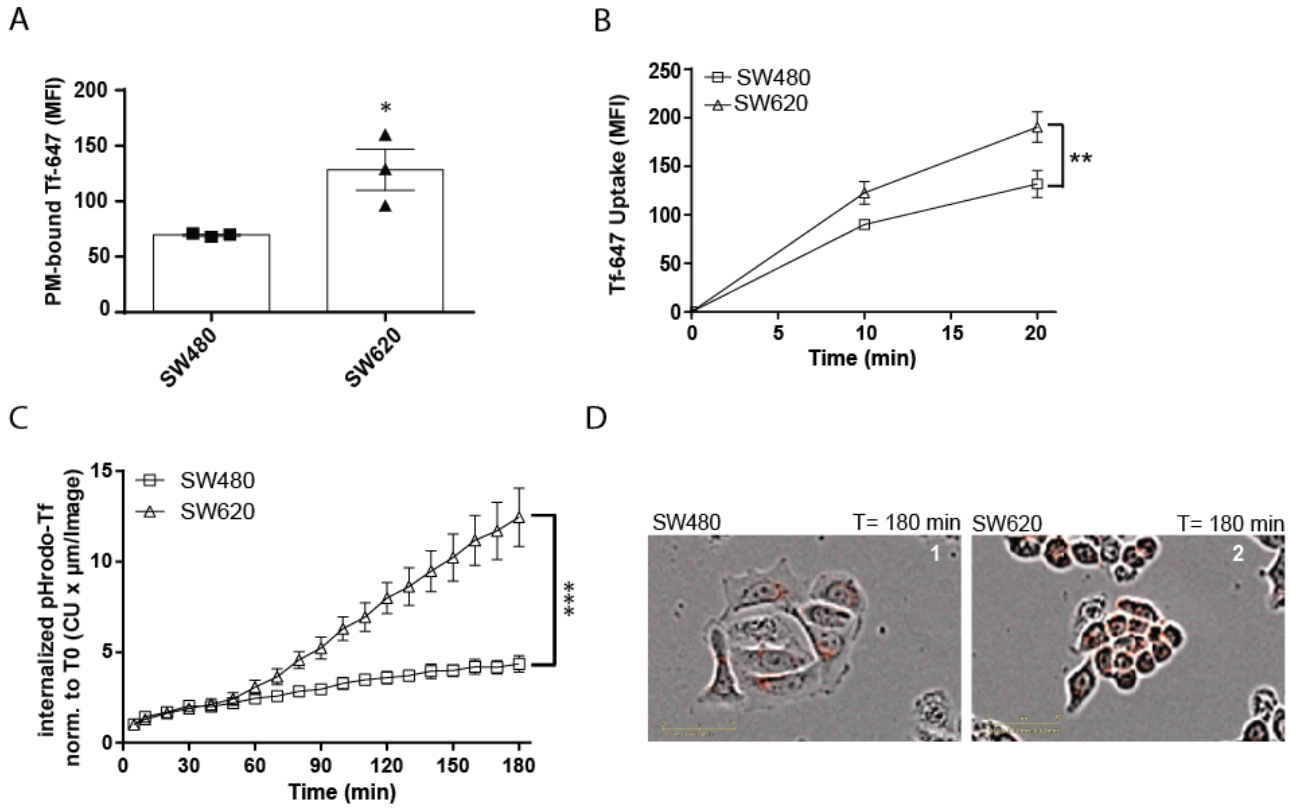

Figure 31 Endogenously overexpressed MACC1 increases the endocytic traffic of TfR in SW620 compared to SW480, virtually non-expressing MACC1. After cell seeding ($1x10^6$) and starvation, cells were harvested and marked with Tf-647 (25 µg/ml) at 0°C and then shifted to 37°C (see Material and Methods for details) (A) Surface staining of TfR marked with Tf-647 of SW620 and SW480 cell lines is represented. Total surface Tf-647 signal intensities were determined by FACS. Results are shown as means ± SEM of three independent experiments. (B) Internalized Tf-647 signal intensities after temperature shift for subsequent time points. (C) Cells were seeded ($1x10^4$) in a 96-well plate and after starvation, were fed with pHrodo-Tf (50 ug/ml) and the red fluorescence signal was observed in a time-dependent manner. Integrated pH-sensitive signal intensities of internalized pHrodo-Tf over time are reported. Results are shown as means ± SEM of four independent experiments. (D) Representative pictures from the IncuCyte® live imaging system of SW620 (1) and SW480 (2) cells and the pHrodo-Tf compound (in red) after 3 h of endocytic assay. *$p < 0.05$, **$p < 0.01$, ***$p< 0.001$.

4.3 Characterization of the impact of MACC1 CME domains

4.3.1 Generation and characterization of the MACC1 mutants

After observing the MACC1-dependent effect on TfR internalization and routing into later compartments, we decided to define the contribution of MACC1 CME domains (Fig.19, A) in order to dissect their impact and relevance during TfR CME. The *in silico* analysis of MACC1 amino acid sequence, focusing on putative structural domains and linear protein interaction motifs, revealed several N-terminally located interaction motifs for CME factors, and the SH3 domain.

We thereby generated the MACC1ΔNT-GFP construct by deleting all putative N-terminal interaction sites for CME factors (clathrin box, NPFs, DPF, Fig. 19 A) in a CMV-promoter-driven-MACC1-GFP fusion construct. Similarly, the SH3 domain was deleted, generating the MACC1ΔSH3-GFP construct, and a combination of both deletions were structurally converged, generating the MACC1ΔNTΔSH3-GFP mutant.

Structures of the deleted cassettes and the generated constructs are schematically represented (Fig. 32, A). Expression levels of the mutated constructs of MACC1, as well as SH3BP4 and TfR were determined by qRT-PCR and WB (Fig. 32, B-C), to exclude again any MACC1-dependent effect at the mRNA and protein level. All MACC1-constructs presented increased expression as expected, and we did not observe any change in mRNA and protein expression of the indicated genes, compared to SW480/GFP.

Globally, data show that the establishment of SW480/MACC1ΔNT-GFP, SW480/MACC1ΔSH3-GFP and SW480/MACC1ΔNTΔSH3-GFP cell lines for our further purposes was successful, and overexpression of MACC1 deleted versions in the cell lines was not influencing mRNA and protein expression of both TfR and SH3BP4.

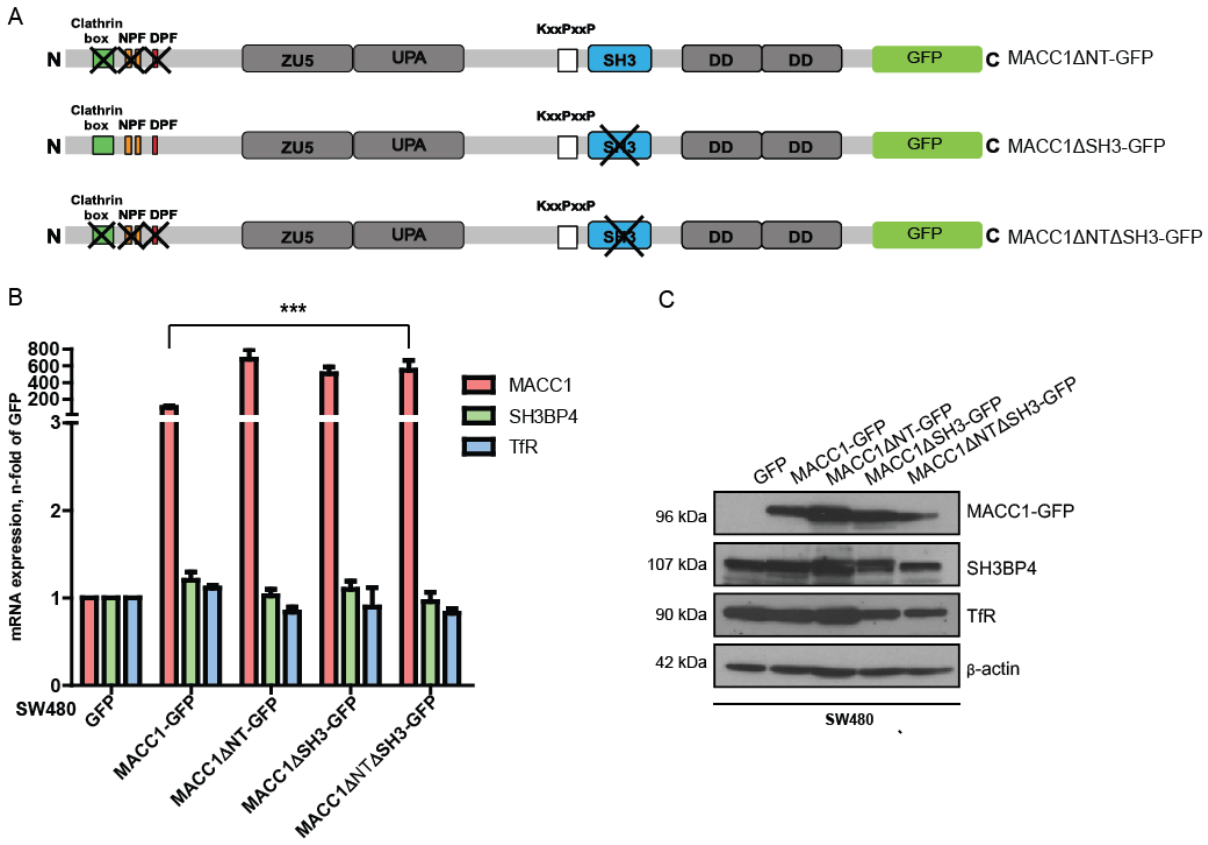

Figure 32 Generation and characterization of the MACC1 mutants. (A) Schematic overview of MACC1 mutants with deleted N-terminal CME-related interaction motifs (MACC1ΔNT, top), deleted SH3 domain (MACC1ΔSH3, middle), and a combination of both deletions (MACC1ΔNTΔSH3, bottom), C-terminally tagged with GFP. MACC1, TfR and SH3BP4 mRNA and protein expression were checked in all cells harboring the MACC1 deleted versions. (B) Thus, after seeding cells ($3x10^5$), total RNA was extracted, reverse transcribed and quantified by real time PCR. Results are first normalized to GADPH and then represented as n-fold of the control cell line with respect to the gene of interest. Results are shown as means ± SEM of three independent experiments. (C) For the MACC1, TfR and SH3PB4 protein expression analysis, after seeding cells ($3x10^5$), cells were harvested, lysed in RIPA lysis buffer (see Material and Method for details). Proteins of the cell lysates were quantified and each sample was immunoblotted on nitrocellulose membranes, for MACC1, TfR, SH3BP4 and β-actin as loading control. A representative blot of three independent experiments is shown. NPF – interaction motif for EPS15-homology domains; DPF - interaction motif for adapter-protein 2 complex; ZU5 – domain present in zona occludens 1 and uncoordinated-5; UPA – domain found in uncoordinated-5, p53-induced death domain protein 1 and ankyrins; SH3 – Src homology domain 3; DD – death domain. ***$p < 0.001$

4.3.2 The SH3 domain is pivotal for MACC1 distribution at PM and relevant for the binding with TfR

To clarify the importance of MACC1 CME domains, and their role in the protein distribution, MACC1 localization was analysed via confocal microscopy (Figure 33, A). As shown, the full-length MACC1-GFP protein is distributed and accumulated at PM, as well as the in the MACC1ΔNT-GFP mutant cell line (second panel from left).

Strikingly, MACC1 distribution at PM is completely lost when the MACC1 SH3 domain is deleted, resulting in a dispersed MACC1 localization throughout the cytoplasm (third panel, Figure 33). Moreover, a dispersed localization of MACC1 in the cytoplasm was noticed not only in SW480/MACC1ΔSH3-GFP but also SW480/MACC1ΔNTΔSH3-GFP cells.

Our findings show that MACC1 SH3 domain determines its distribution and accumulation at PM, suggesting a stronger and predominant role for SH3 domain in the TfR endocytic traffic. To define the relevance of MACC1's CME-domains in the interactions with CLTC, DNM2 and TfR, we studied the loss of binding between MACC1 and these proteins in the MACC1 deleted mutant cell lines (Figure 33, B-D). MACC1 binding to CLTC and DNM2 was lost in all deleted mutant (Figure 33, B-C). Also, MACC1 binding with TfR was completely lost in the SH3-deleted cell line while was still observed in the NT-deleted cell line (Figure 33, D).

Together, these findings confirm a strong and predominant role of the SH3 domain for the MACC1 localization at the PM in SW480/MACC1-GFP cells. Moreover, our results confirm the involvement of both the MACC1 CME domains (at the N-terminus) and the SH3 domain in the binding with CLTC and DNM2. Also, our observations point out that MACC1/TfR interaction is mediated by the SH3 domain but it might be linked to the endocytic machinery via the N-terminal interaction motifs.

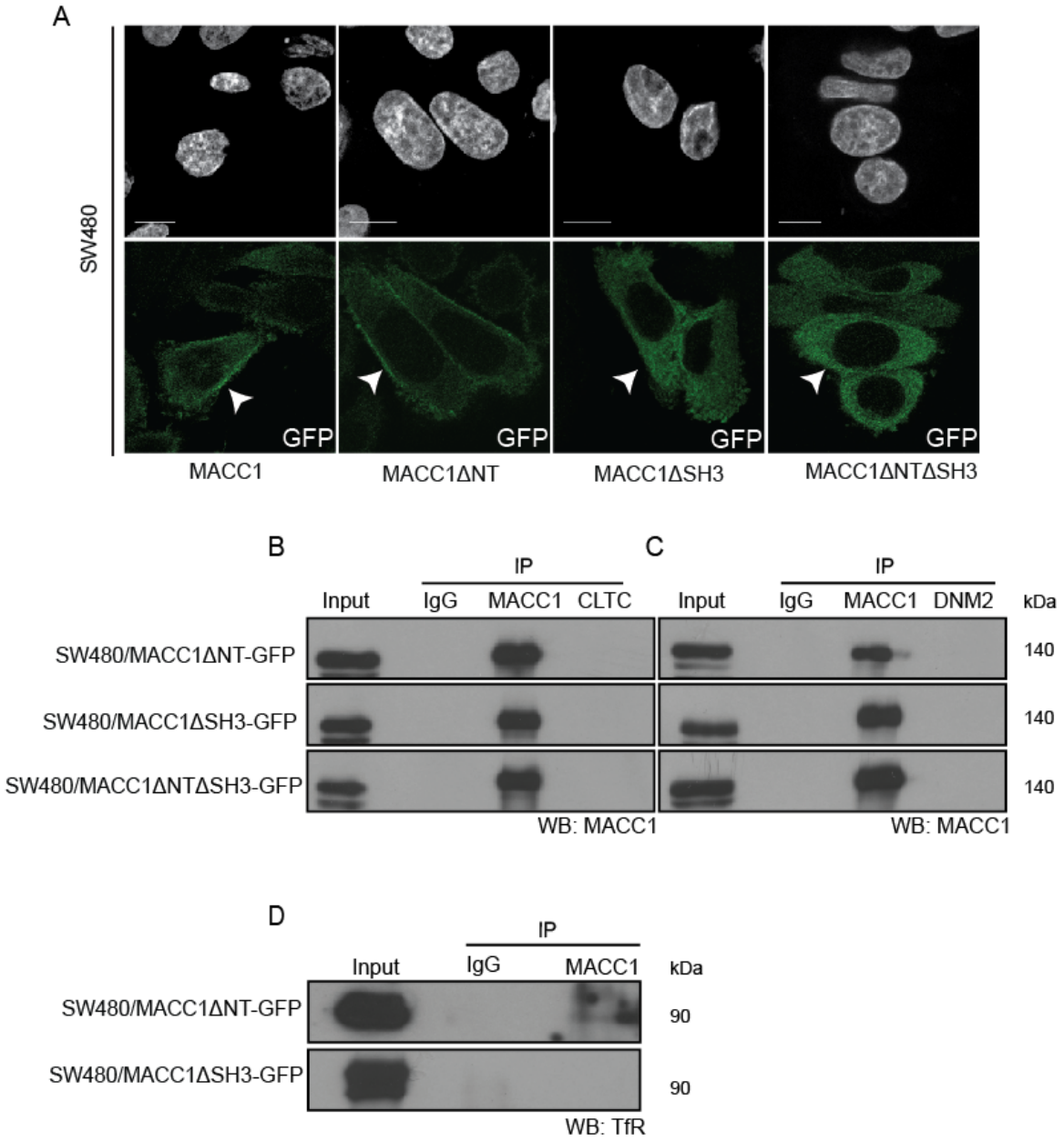

Figure 33 MACC1 SH3 domain is pivotal for its distribution at PM the binding with TfR. A confluent monolayer of MACC1 CME deleted mutant cells ($1x10^4$) was seeded. (A) Cellular localization of MACC1-GFP and all deleted mutants were assessed by confocal microscopy. Arrows indicate the loss of the MACC1-GFP localization at the PM. Nuclei were stained with DAPI. Scale bar=10µm (B-D) Pull-down of MACC1 deletion variants with CLTC, DNM2 and MACC1 antibodies and immunostaining for MACC1 (B and C) or TfR (D).

4.3.3 CME-related domains of MACC1 regulate the TfR distribution at the PM and the first steps of TfR CME

To understand how the MACC1 deleted cassettes were impacting the TfR endocytic traffic, we employed the previously introduced methods for the following experiments. Surface located TfR was indirectly marked with fluorescence-labeled transferrin (Tf-647, at 0°C) in MACC1 mutated cell lines, and quantified by FACS analysis as already introduced for previous experiments. Our findings show, that the SH3-domain deletion on MACC1 caused accumulation of TfR at PM (Fig. 34, A) compared to the overexpressing MACC1-GFP full-length cell line.

Accordingly, to understand whether the loss of MACC1 SH3-domain was also impacting the TfR uptake, surface-marked mutant cells were shifted from 0°C to 37°C, and TfR uptake displayed a significant and progressive decrease in all deleted mutant cell lines as compared to the full-length SW480/MACC1 and the control cells (Figure 34, B).

Furthermore, we verified via confocal microscopy the SH3-deletion-dependent impairment during TfR-Tf-647 uptake. For this purpose, the full-length MACC1-GFP and the SH3-deleted mutant cell lines were fed with Tf-647 for 15 min and stained for EEA1. As shown (Fig. 34, C), SW480/MACC1-GFP shows not only a prominent MACC1 PM distribution as compared to the SH3 deleted construct (in line with previous data in Figure 33, A), but also overlaps with Tf-647 at the PM (shown in cyan in Figure 34, C). These data were confirmed by measuring the Tf-647 integrated intensity in both the cell lines (Figure 34, D).

Furthermore, we used pHrodo-Tf to study the endocytic fate of the receptor. After feeding the cells with the pH sensitive compound, the TfR fate was monitored for 180 min. As a result, we observed increased internalized fluorescence signal in the control SW480/GFP cells, and decreased but still detectable signal in SW480/MACC1-GFP cells (Figure 34, E). Only weak increase of the signal was detected for the SW480/MACC1ΔNT-GFP mutant cell line and no increase in signal could be detected for the SW480/MACC1ΔSH3-GFP and SW480/MACC1ΔNTΔSH3-GFP cell lines (Fig. 34, B).

To conclude, our data show that the SH3 deletion of MACC1 is dominantly causing an excess of TfR at the PM. Moreover, the MACC1 SH3 deletion impairs strikingly the TfR uptake compared to full-length MACC1 and the ΔNT-GFP deletion construct. These data suggest that the SH3 domain of MACC1 is pivotal in the TfR-Tf-647 complex uptake.

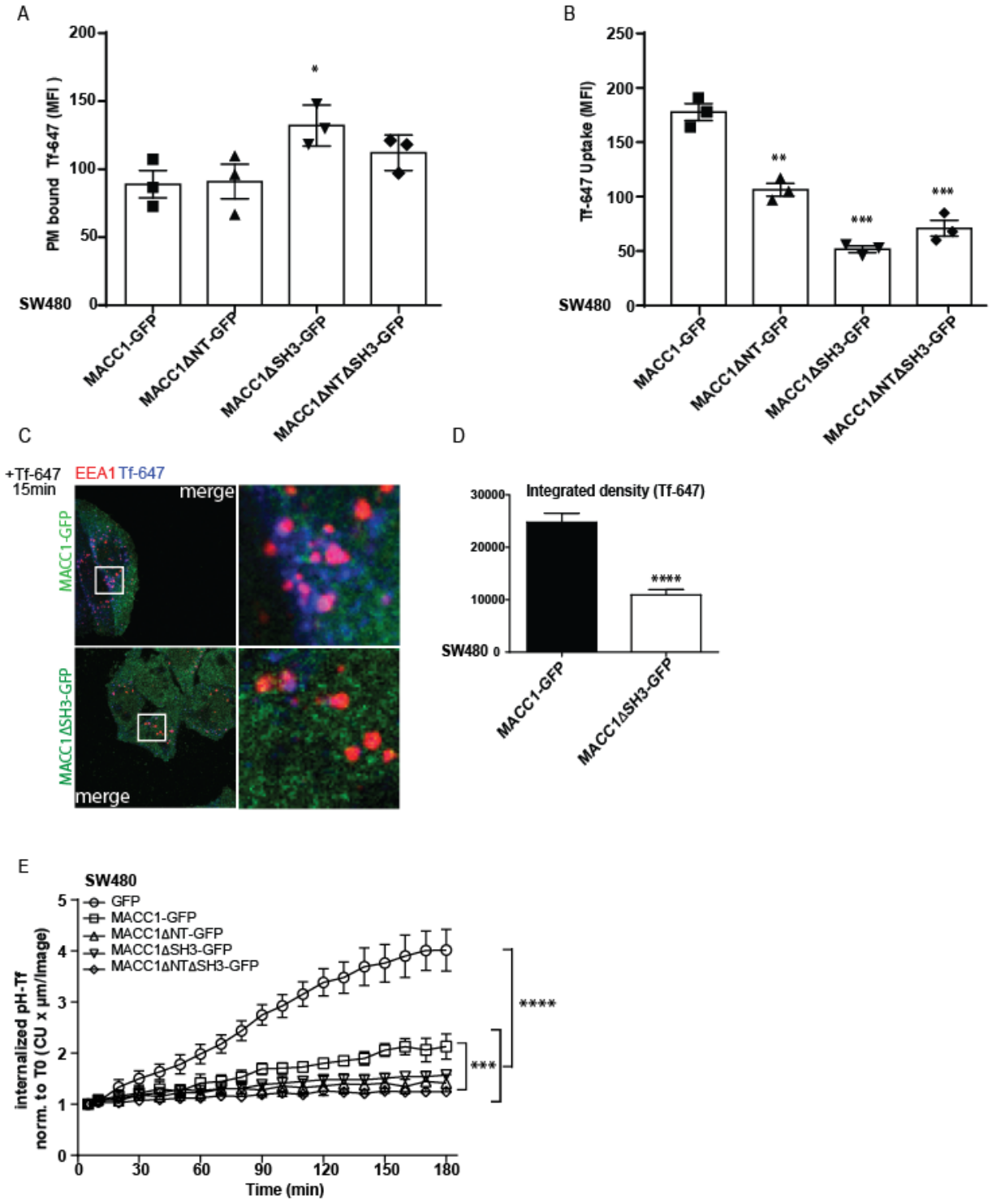

Figure 34 CME-related domains of MACC1 regulate the TfR distribution at the PM and the first steps of TfR endocytosis. (A) After cell seeding ($1x10^6$) and starvation, cells were harvested and marked with Tf-647 (25 µg/ml) at 0°C for 1 h (see Material and Methods for details). Surface staining of TfR indirectly marked with Tf-647 of MACC1 CME mutants is represented. Total surface Tf-647 signal intensities were determined by FACS. Data represent mean ± SEM of three independent experiment (B) Internalized Tf-647 signal intensities after temperature shift for 20 min. Data represent mean ± SEM of three independent experiment (C) A confluent monolayer of SW480/MACC1 cells ($1x10^4$) has been seeded, serum starved and treated for 15 min with Tf-647 (25 ug/ml) to measure by immunofluorescence (SP5, Leica) sensible changes in the colocalization with endocytic markers (EEA1, in particular) after TfR specific stimulated internalization. Single channel images are provided in Supplementary Figure 5 for EEA1, Tf-647 in SW480/MACC1-GFP and SW480/MACC1ΔSH3-GFP cells.

Scale bar = 10 µm. Indicated regions are displayed enlarged (10x). (D) Integrated intensity of the internalized Tf-647 is reported for SW480/MACC1-GFP and SW480/MACC1ΔSH3-GFP cells (E) Cells were seeded ($1x10^4$) in a 96-well plate and after starvation, were fed with pHrodo-Tf (50 ug/ml). The red fluorescence signal was observed in a time-dependent manner. Integrated pH-sensitive signal intensities of internalized pHrodo-Tf over time are represented. Data represent mean ± SEM of three independent experiment *p < 0.05, **p < 0.01, ***p < 0.001, ****p < 0.0001

4.4 Characterization of MACC1 impact on RTKs endocytic traffic

4.4.1 Investigating MACC1 impact on other RTKs: MACC1 binds both EGFR and MET

After we validated MACC1 interactions with proteins involved in CME and with TfR (Fig. 20, B-D), we asked whether other CME-dependent tyrosine kinase receptors were also affected in a MACC1-driven manner. Therefore, to validate other receptor-MACC1 interactions we coimmunoprecipitated the EGFR and MET receptors, and we searched for the MACC1 binding in SW620, SW480/MACC1 and SW480/MACC1-GFP (as previously shown in Fig.2 B-E). Both receptors show an interaction with MACC1 screened as a band on the immunoblot (Fig.35, A-B). Our data confirm that MACC1 binds directly or indirectly to these two RTKs.

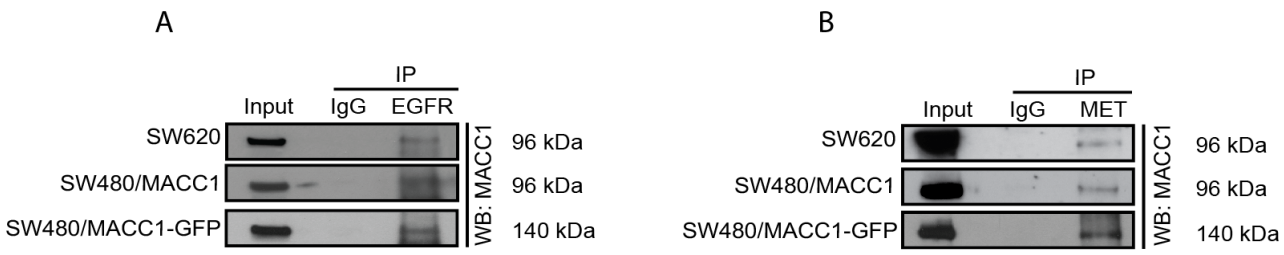

Figure 35 Investigating other cancer-related cargoes: new insights, new cargoes and a long way to go. (A-B) The validation of MACC1 binding to RTKs was carried out via coIP and immunoblot, in different CRC cell lines (SW620, SW480/MACC1 and SW480/MACC1-GFP). After seeding ($4x10^6$), cells were harvested after 48 h, lysed in coIP lysis buffer and the cell lysates were pulled down with EGFR (A) and MET (B) antibodies and immunoblotted for MACC1. IgG control was used as a negative control.

4.4.2 MACC1 overexpression determines EGFR and TfR associated cargo selection in CCV, upon EGFR-stimulated internalization

After confirming MACC1's role during TfR endocytosis (see, Chapter 4.2), we investigated its function during RTK endocytosis. On the one hand, it is known that TTP is behaving as endocytic adaptor for TfR via its SH3 domain collaborating predominately with DNM's PRD domain[121]. On the other hand, SH3BP4 endocytic role has been dissected during FGFR endocytosis, concluding that SH3BP4 regulates FGFR fate by directing it towards recycling or degradative routes depending on the p-85/SH3BP4 complex recruitment at FGFR tail, after ligand-induced CME[122].

Also, it is known that TTP selectively joins TfR-marked CCV, depending on the cargo, but did not interact with the oncogenic driver EGFR[198]. Considering the difference between these two receptors (TfR and EGFR), it was speculated that inclusion or exclusion of RTKs from TfR-marked vesicles would depend on the phosphorylation of TTP or dynamin[121]. Nevertheless, literature search revealed that TfR and EGFR cooperate in non-small lung cancer (NSLC)[187]. In particular, the kinase activity of EGFR controls TfR distribution at PM.

Considering what we found so far, our next step was to determine whether MACC1 could also mediate the inclusion/exclusion of EGFR from TfR-marked CCV, upon specific stimulation of the receptor in CRC cell lines. To address this issue, we used a concentration of EGF (20 ng/ml) that allowed us to exclude any NCE[130] and checked whether in the absence or presence of MACC1 we could find EGFR in TfR-marked CCV.

We treated SW480/e.v. and SW480/MACC1 cells with EGF for 8 min and we searched for colocalization of the three proteins respectively, MACC1, EGFR and TfR. As shown the colocalization between EGFR, TfR and CLTC was found (represented in white spots) in SW480/MACC1 EGF-stimulated cells, while it was not found in control cells (SW480/e.v.) (Fig. 36, lower left panels).

As control for the induced EGF-internalization, both cell lines were previously treated with dynasore, which prevents dynamin GTPase activity while pinching off CCV into cytoplasm, creating an accumulation of vesicles at PM (with "long neck" shape as shown in Fig. 36, lower right panels). Concluding, our findings show that EGFR colocalization into TfR-marked vesicle is MACC1 dependent. Moreover, we assumed that, likewise SH3BP4 (for TfR and FGFR), MACC1 might selectively choose cargoes to be included in TfR-marked CCV vesicles, following them in the first endocytic steps.

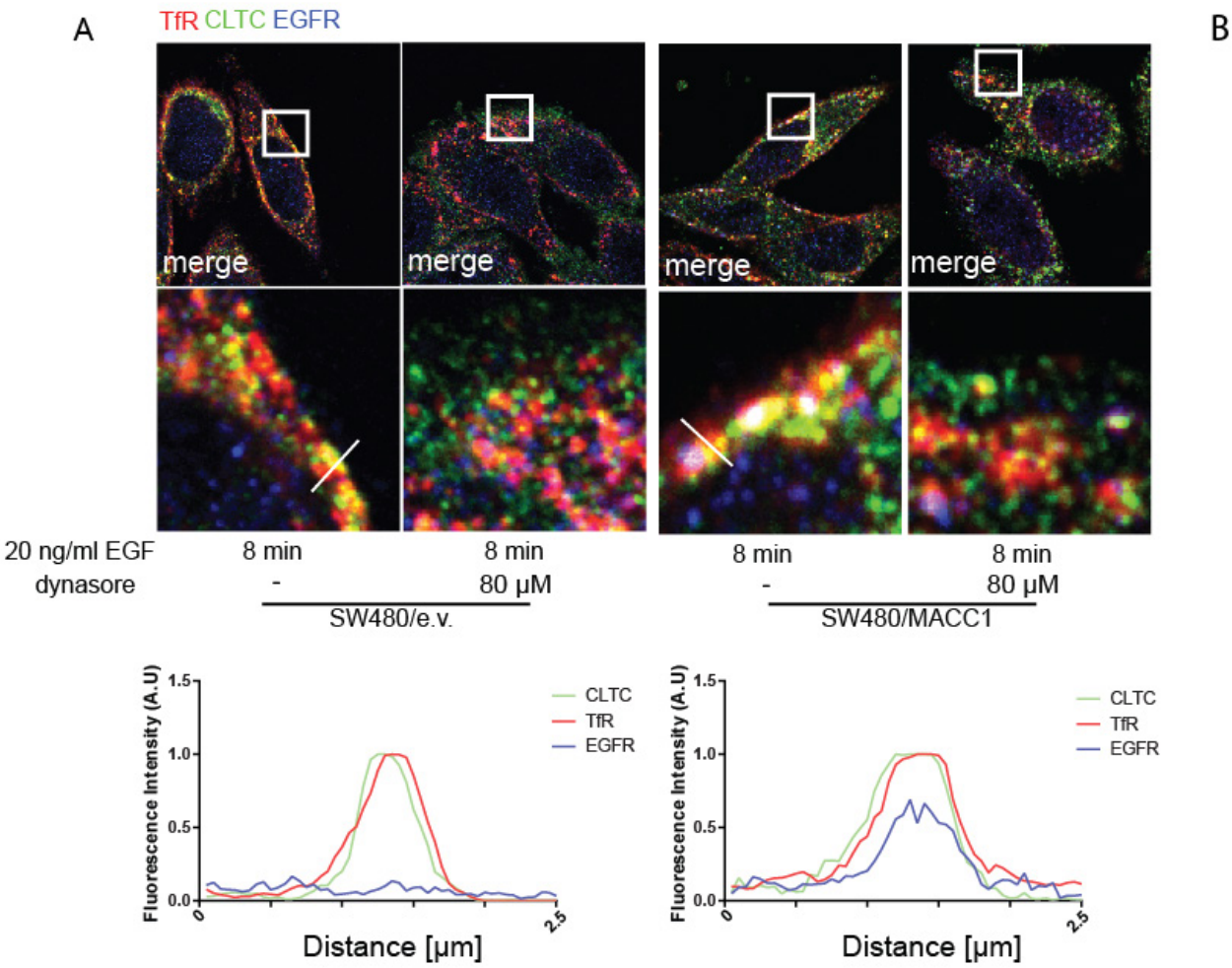

Figure 36 MACC1 overexpression determines EGFR and TfR associated cargo selection in CCV, upon receptor-stimulated internalization. A confluent monolayer of SW480/e.v. and SW480/MACC1 ($1x10^4$) has been seeded, serum starved and treated for 8 minutes with 20 ng/ml EGF in presence or absence of the dynasore inhibitor pretreatment (80 µM). The three fluorescence signals from CLTC, EGFR and TfR, were measured by immunofluorescence (SP5, Leica) to observe changes. (A) Colocalization of EGFR, TfR and CLTC after triple-staining of SW480/e.v. cells treated (left panel) and untreated (right panel) respectively with 8 min with EGF with or without pretreatment with dynasore (80 µM). (B) Colocalization of EGFR, TfR and CLTC after triple-staining of SW480/MACC1 cells treated (left panel) and untreated (right panel) respectively with 8 min with EGF or 8 min with EGF after pretreatment with dynasore (80 µM). Indicated regions are displayed enlarged 10x, and histograms show the spatial distribution of the signal intensities across indicated sections. Representative pictures of three independent experiments. All panels show merged images. Single channel images are provided in Supplementary Figure 6. Scale bar = 10 µm

4.4.3 MACC1 overexpression increases the presence of EGF in low pH compartments

Our previous results demonstrate the MACC1-dependent selection of the EGFR into TfR-marked vesicles (Fig.36, A-B). For this reason, we choose to further study the EGFR in order to deepen our knowledge with respect to MACC1´s impact on CME of RTKs receptors. In our previous studies, we found that in EGF-stimulated SW480/MACC1 cells TfR and EGFR were colocalizing with TfR-marked CCVs, which was not the case in SW480/e.v. cells (Fig. 36, A-B). Thus, to understand whether MACC1 might regulate EGFR internalization we used pHrodo-EGF and measured the integrated fluorescent signal as shown in the experiments before, and using the IncuCyte® system[199–202]. pHrodo-EGF allows to measure the release of the compound into acidic pH compartments in case of recycling[200,203] or the progressively increased fluorescence in case of degradation of the receptor[203,204], depending on different pH and compartments.

Considering this, we expected the fluorescence signal weaker or stronger dependent on the pH of endosomes and ERC204,205 (pH 6.5-6.0) or MVBs and lysosomes (pH 5-4.5) hence, revealing the sorting route of EGFR/pH-EGF complexes to different endocytic pathways. To determine whether MACC1 might also influence EGFR endocytic traffic, we detected the integrated fluorescence intensity of pHrodo-EGF in a time-dependent manner. Our data revealed an enhanced internalization of pHrodo-EGF-EGFR complexes in SW480/MACC1-GFP cells as compared to SW480/GFP control cells, relevant only after 3h of compound accumulation in acidic compartments (Fig. 37).

As controls for the correct uptake of the pHrodo-EGF-EGFR complex and delivery towards endocytic compartments, SW480/e.v. and SW480/MACC1 cells were also pre-treated with the endocytic inhibitors dynasore and bafilomycin A1. As shown, the dynasore and bafilomycin pre-treatments decrease strongly the integrated fluorescence signals. Therefore, we concluded that pHrodo-EGF, is endocytosed in a dynamin-dependent manner, and it is correctly targeted to low/acid pH compartments (Figure 37).

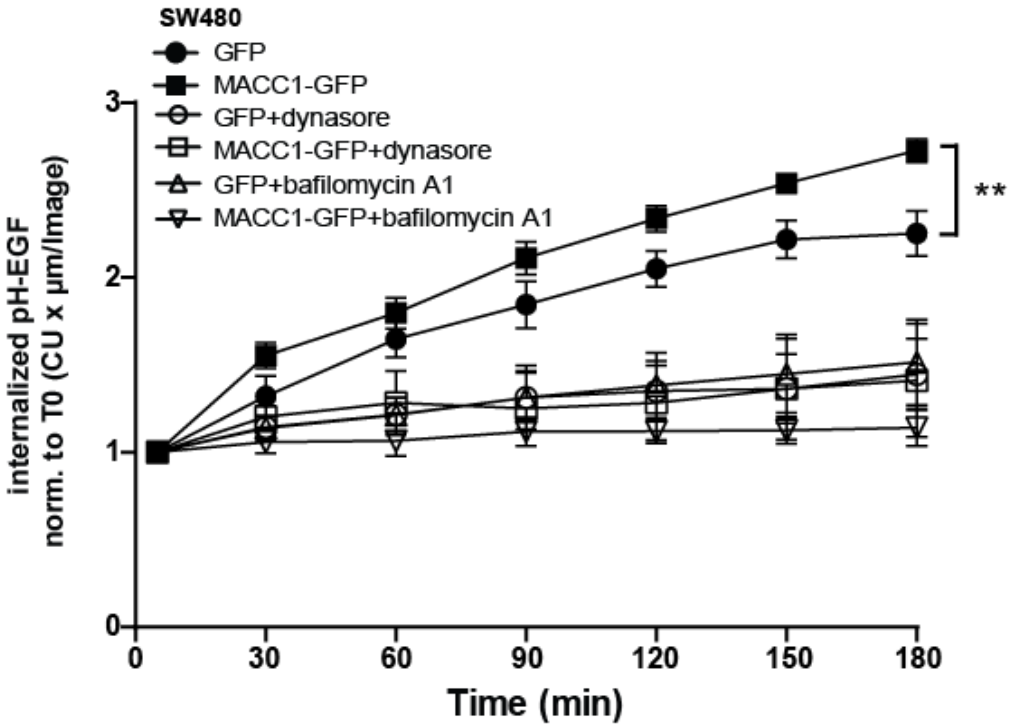

Figure 37 MACC1 overexpression increases the presence of EGF in low pH compartments. Cells were seeded ($1x10^4$) in a 96-well plate and after starvation, were fed with pHrodo-EGF (5 ug/ml) and the integrated fluorescence signal was observed in a time-dependent manner for 180 min. Integrated pH-sensitive signal intensities of internalized pHrodo-EGF over time are represented here for SW480/GFP and SW480/MACC1-GFP cells, pre-treated for 4 h or not with Dynasore (80 µM) and Bafilomycin A1 (100 nM). Results are shown as means ± SEM of three independent experiments. **$p < 0.01$.

4.3.4 MACC1 overexpression increases the recycling pool of EGFR at PM thereby targeting slow and fast recycling pathways

Our results so far revealed that the overexpression of MACC1 enhances the presence of pHrodo-EGF in acidic compartments, which in our case might result in the accumulation of pHrodo-EGF within endosomes, recycling endosomes and lysosomes (Fig. 37). EGFR is normally targeted for degradation, but the EGF remains bound to the receptor when reaching very low-pH compartments[183,205]. Moreover, the latest EGFR endocytic model shows that EGFR releases the bound EGF in recycling endosomes (pH 6.5) while it is disassembled in order to be recycled back to the PM[182,183,205].

Therefore, to clarify the mechanism behind MACC1-mediated increase in pHrodo-EGF within acidic compartments (Fig. 37), we indirectly measured via FACS the effect of MACC1 overexpression on the receptor recycling back to PM. The EGFR pool available at the PM (surface signal at time point 0) was indirectly marked with EGF-647 of HCT116/GFP and HCT116/MACC1-GFP cells, as well as SW480/e.v. and SW480/MACC1 cells, at 0°C. To quantify the recycled pool present at the PM after ligand-induced internalization via CME, the receptor pool at PM was indirectly measured by re-probing the surface with EGF-647 at 0°C after 30 min of EGF-stimulated internalization (20 ng/ml)[130] (Figure 38, A-B and D). SW480/MACC1 cells but not HCT116/MACC1-GFP cells showed a decreased surface distribution of EGFR as compared to the respective control cell line SW480/e.v. Interestingly after 30 min of EGF-stimulated internalization, the EGFR recycled pool available at PM is significantly increased in HCT116/MACC1-GFP and in SW480/MACC1 cells (Figure 38, A-D). These data confirm the MACC1-mediated increase on recycling rate of EGFR to PM.

In order to understand whether the increased pool of EGFR at PM was caused by the MACC1-mediated effect on internalization and recycling, we repeated the previous assay, and we pre-treated the cells with monensin, an inhibitor of both the fast (RAB4) and slow (RAB11) routes of recycling for EGFR[206]. As shown (Fig. 38, B) the EGFR recycled pool at PM after EGF-stimulated-CME endocytosis, is significantly decreased in the monensin-treated HCT116/MACC1-GFP cells compared to HCT116/GFP cells (Fig. 38, B).

These findings confirm that MACC1 overexpression in HCT116 cells mediates the faster EGFR recycling to PM, via both the recycling routes (slow and fast). The absence of changes of the EGFR recycled pool at the PM in HCT116/GFP still remains unclear, but we assumed a slower/decreased response to EGF-stimulated CME in this cell line, compared to SW480. This observation might be further confirmed considering the complete absence of change in the EGFR pool at PM before and after EGF-stimulated CME (Figure 38, B). To conclude, our findings show that MACC1 overexpression

enhances the EGFR available pool at the PM via MACC1-mediated CME and by targeting EGFR to PM via slow and fast recycling routes.

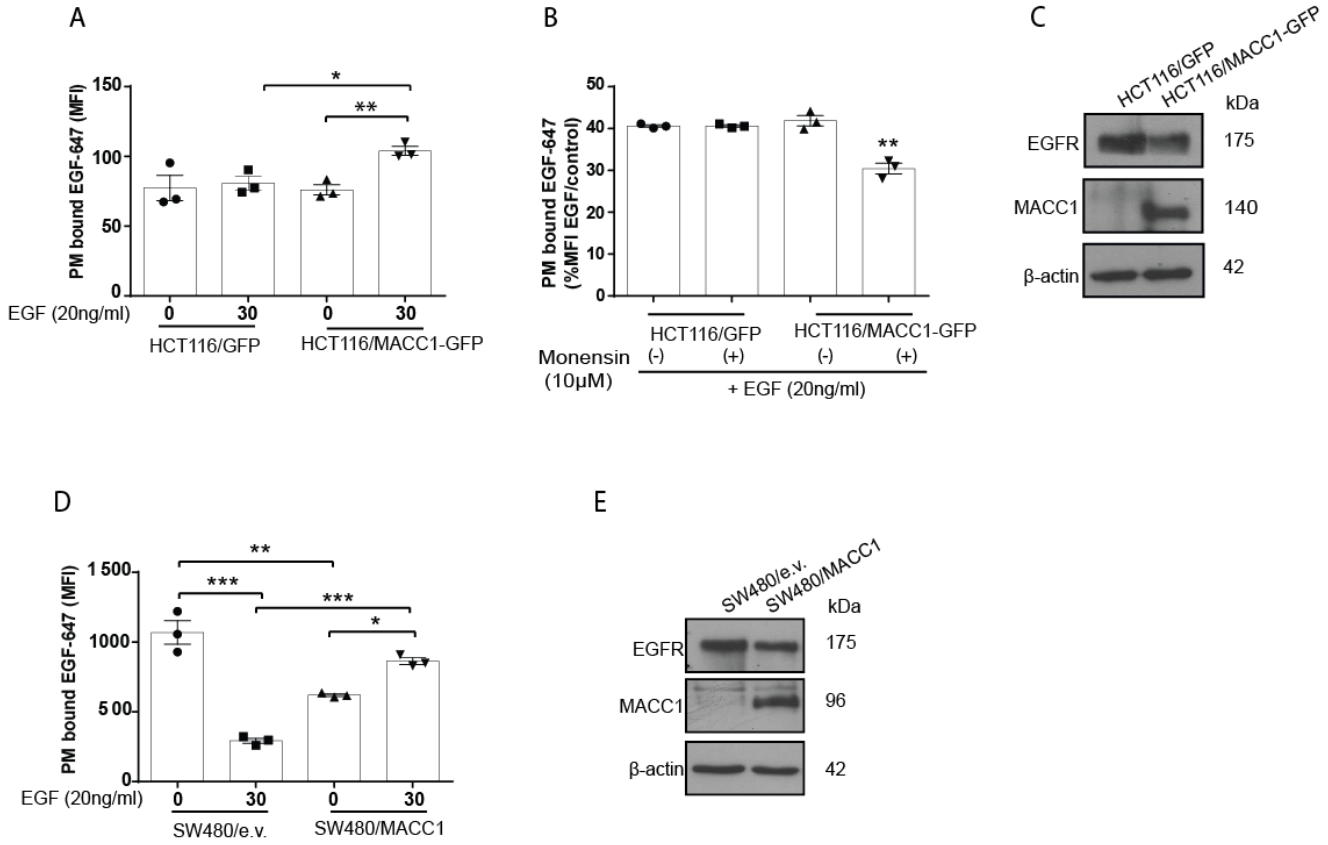

Figure 38 MACC1 overexpression increases the EGFR recycling pool at the PM in two different cell lines via targeting both the recycling slow and fast pathways. (A, D) After cell seeding (1-3x10^5) and starvation, cells were harvested and marked with EGF-647 (2.5 µg/ml) at 0°C for 1 h, without (for the surface EGFR pool) or with (for the recycled EGFR pool) ligand-stimulated CME for 30 min with 20 ng/ml EGF. After staining and fixation, the indirect surface fluorescence signal of EGFR of HCT116-derived (A) and SW480-derived (D) cell lines is represented. Total surface EGF-647 signal intensities were determined by FACS. Data represent mean ± SEM of three independent experiments. (B) After cell seeding (1-3x10^5) and starvation, cells were harvested and marked with EGF-647 (2.5 µg/ml) at 0°C for 1 h after 30 min of EGFR specific CME, stimulated with 20 ng/ml EGF, in presence or absence of Monensin pre-treatment (10 µM) of 4 h. After staining and fixation, the indirect surface fluorescence signal of EGFR of HCT116-derived cell lines is represented. Total surface EGF-647 signal intensities were determined by FACS and normalized to the initial surface signal beforehand. Data represent mean ± SEM of three independent experiments. (C, E) For the steady state MACC1 and EGFR protein expression analysis in the considered cell lines, after cells were seeded (3x10^5), harvested, and lysed in RIPA lysis buffer. Proteins in cell lysates were quantified and each sample was immunoblotted on nitrocellulose membranes for MACC1, EGFR and β-actin as loading control. A representative blot of three independent experiments is shown.

4.3.5 MACC1-mediated CME sustains EGFR routing into recycling compartments and it is dependent on its SH3 domain

After we showed increased uptake of the pHrodo-EGF-EGFR complexes in SW480/MACC1-GFP cells compared to SW480/GFP cells (Fig. 37), we were curious to understand whether MACC1 was also regulating the PM distribution and uptake of EGFR as for TfR (Fig.39, A-B) with its CME cassettes. Therefore, as previously shown, we stained the surface of cells expressing MACC1-deleted constructs with EGF-647 to test indirectly the EGFR distribution at PM. A progressive accumulation of EGFR at the PM is observed in MACC1-CME deleted mutants cell lines. In particular, the EGFR accumulation at PM is increased in SW480/MACC1ΔSH3-GFP as compared to SW480/MACC1-GFP cells (Fig. 39, A). Furthermore, a decreased EGFR PM distribution was observed in SW480/MACC1-GFP as compared to the control cell line SW480/GFP, coherently with previous results (Fig.34, A-B).

After we observing a progressive deletion-dependent accumulation of EGFR at PM, our next step was understanding whether MACC1 CME mutant cells were differing in EGFR uptake, comparing them also to our previous results. Indeed (Fig. 39, B-D), the MACC1 CME deleted MACC1 cell lines showed increased integrated fluorescence signal, statistically relevant for the SH3-deleted and the double-deleted mutant cell lines compared to the full-length SW480/MACC1. As control, we also pre-treated the MACC1 mutant cell lines with dynasore and compared to the untreated mutants, observing no internalization of EGFR-pHrodo-EGF complexes (Fig. 39, C).

These data show that MACC1 SH3 domain is likely regulating not only EGFR distribution at the PM, but also mediates the dynamin-dependent EGFR endocytic delivery of the EGFR-EGF-pHrodo compound into later endocytic compartments after internalization. Comparing the difference in signal intensity between the cell lines (Fig. 39, D), the MACC1-mediated EGFR distribution at PM and routing into degradative compartments is SH3-domain regulated and dependent.

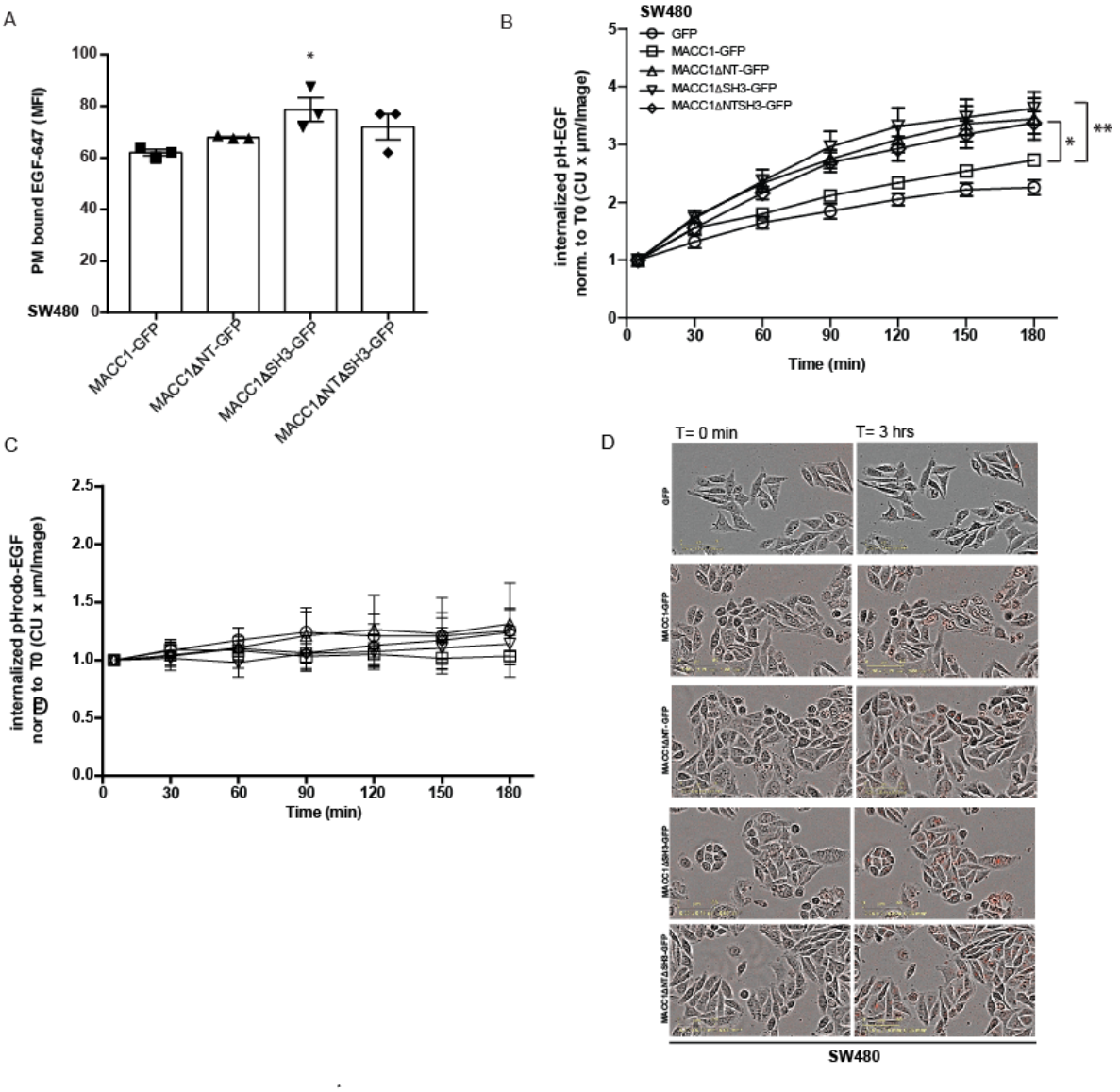

Figure 39 MACC1-mediated CME sustains EGFR routing into recycling compartments and it is dependent on its SH3 domain. (A) After cell seeding ($1x10^6$) and starvation, cells were harvested and marked with EGF-647 (2.5 µg/ml) at 0°C for 1 h, (see Material and Methods for details). Surface staining of EGFR indirectly marked with EGF-647 of MACC1 CME mutants is represented. Total surface EGF-647 signal intensities were determined by FACS. Data represents mean ± SEM of three independent experiments (B) Cells were seeded ($1x10^4$) in a 96-well plate and after starvation, were fed with pHrodo-EGF (5 ug/ml) and the red fluorescence signal was observed in a time-dependent manner. Integrated pH-sensitive signal intensities of internalized pHrodo-EGF over time are represented. Results are shown as means ± SEM of four independent experiments. *$p < 0.05$, **$p < 0.01$, ***$p < 0.001$. (C) Cells were seeded ($1x10^4$) in 96-well plate and after starvation, were pre-treated for 4 h with dynasore to impede dynamin scission of the vesicle into the cytoplasm (80 µM), then fed with pHrodo-EGF (5 ug/ml) and the fluorescence signal was observed in a time-dependent manner. Integrated pH-sensitive signal intensities of internalized pHrodo-EGF over time are represented. Results are shown as means ± SEM of four independent experiments. *$p < 0.05$, **$p < 0.01$, ***$p < 0.001$. (D) Representative pictures of the MACC1 CME mutant cells before and after 3 h of pHrodo-EGF endocytic traffic assay.

4.3.6 EGFR transphosphorylation upon EGF-stimulated CME and downstream signaling cascade is regulated by MACC1 CME cassettes

Receptor internalization, recycling and degradation can differentially affect the strength and duration of signalling[36]. In particular, increased receptor recycling sustains and prolongs the signaling[122]. Besides SH3BP4, several other selective cargo proteins are known to prolong signaling [122]. Thus, after we elucidated MACC1's role in EGFR recycling, we decided to investigate the impact of MACC1 CME cassettes on different signaling cascades. Therefore, we induced the EGFR CME by specifically treating serum-starved MACC1 CME mutant cells with low concentrations of EGF (20 ng/ml) for different time intervals (0-90 min).

In order to check the activation, signal prolongation and transphosphorylation of EGFR after ligand-induced CME stimulation, we studied the phosphorylation of tyrosine 1068 (Y1068) located on the cytoplasmic tail of EGFR. As expected, (Fig. 40, A, C) SW480/GFP cells, show EGFR activation (pY1068) progressively increasing after EGF-stimulation, while SW480/MACC1 cells show a sustained activation and transphosphorylation (pY1068) after 8 and 30 min of stimulation.

Regarding the downstream targets of the ligand-activated EGFR, MACC1 overexpression increased and sustained ERK1/2 and AKT phosphorylation (Fig. 40, A, C, D) until 90 min after stimulation. The impact of MACC1 overexpression EGFR downstream targets was also compared between the full-length MACC1 overexpressing cell line and the MACC1-deleted mutant cell lines (Fig. 40, B). As shown, the loss of MACC1 N-terminal CME domains as well as the SH3 domain strongly impairs the EGFR activation after EGF-stimulation, comparable to the GFP control (Fig. 40, B, C).

Also, in both the SH3-deleted mutant and the double mutant cell lines we observed a weak EGFR activation as compared to SW480/MACC1-GFP, which, however, was stronger compared to SW480/MACC1ΔNT-GFP and the GFP control cell line.

Looking into the AKT-downstream cascade, SW480/MACC1 cells show increased phosphorylation of AKT compared to the control cell line at any time point (SW480/MACC1-GFP). In contrast, both SW480/MACC1ΔSH3-GFP and SW480/MACC1ΔNTΔSH3-GFP show a sustained AKT phosphorylation still 90 min after EGFR ligand-stimulated CME. SW480/MACC1ΔNT-GFP cell line show similar downstream activation of AKT to the GFP control. The AKT downstream activation is overall impaired compared to the full-length MACC1 expressing cell lines (Figure 40, B, D).

Regarding the ERK1/2- phosphorylation profile, SW480/MACC1-GFP, SW480/MACC1ΔNT-GFP show a similar ERK1/2 activation to GFP. On the contrary, downstream activation of ERK 1/2 in

SW480/MACC1ΔSH3-GFP and SW480/MACC1ΔNTΔSH3-GFP is strikingly impaired, compared to the full-length MACC1 (Fig. 40, B, E). These data suggest that MACC1 CME cassettes are important for downstream activation of ERK1/2

To understand the functional relevance of the MACC1 CME cassettes loss, we studied the mutants cell lines proliferation in presence of low EGF concentrations (20 ng/ml) continuously for 72 h. The different activation patterns of EGFR (pY1068) in SW480/mutant-MACC1 cell lines are preserved in the proliferation assay.

The full-length MACC1 overexpression in SW480 cells significantly increased the cell confluence after 3 days of ligand-stimulated proliferation (Fig. 40, F). In addition, the SW480/MACC1ΔSH3-GFP and the double mutant cell lines consistently show a similar proliferation rate to SW480/GFP.

Our findings show new insights on MACC1 as endocytic protein. Our data suggest that MACC1 has a role during the EGFR activation via its SH3-domain as we observed by monitoring the docking-site (pY1068) transactivation during the EGF stimulated CME.

Although downstream phosphorylation of ERK1/2 and AKT diverge in MACC1-mutant cell lines compared to control and the full-length cell line, only the MACC1 wild type overexpression in SW480 guarantees the efficiency of ERK 1/2 and AKT-signalling cascades resulting in increased proliferation. These results were also confirmed by the decreased proliferation observed in SW480/MACC1ΔSH3-GFP and SW480/MACC1ΔNTΔSH3-GFP cell lines.

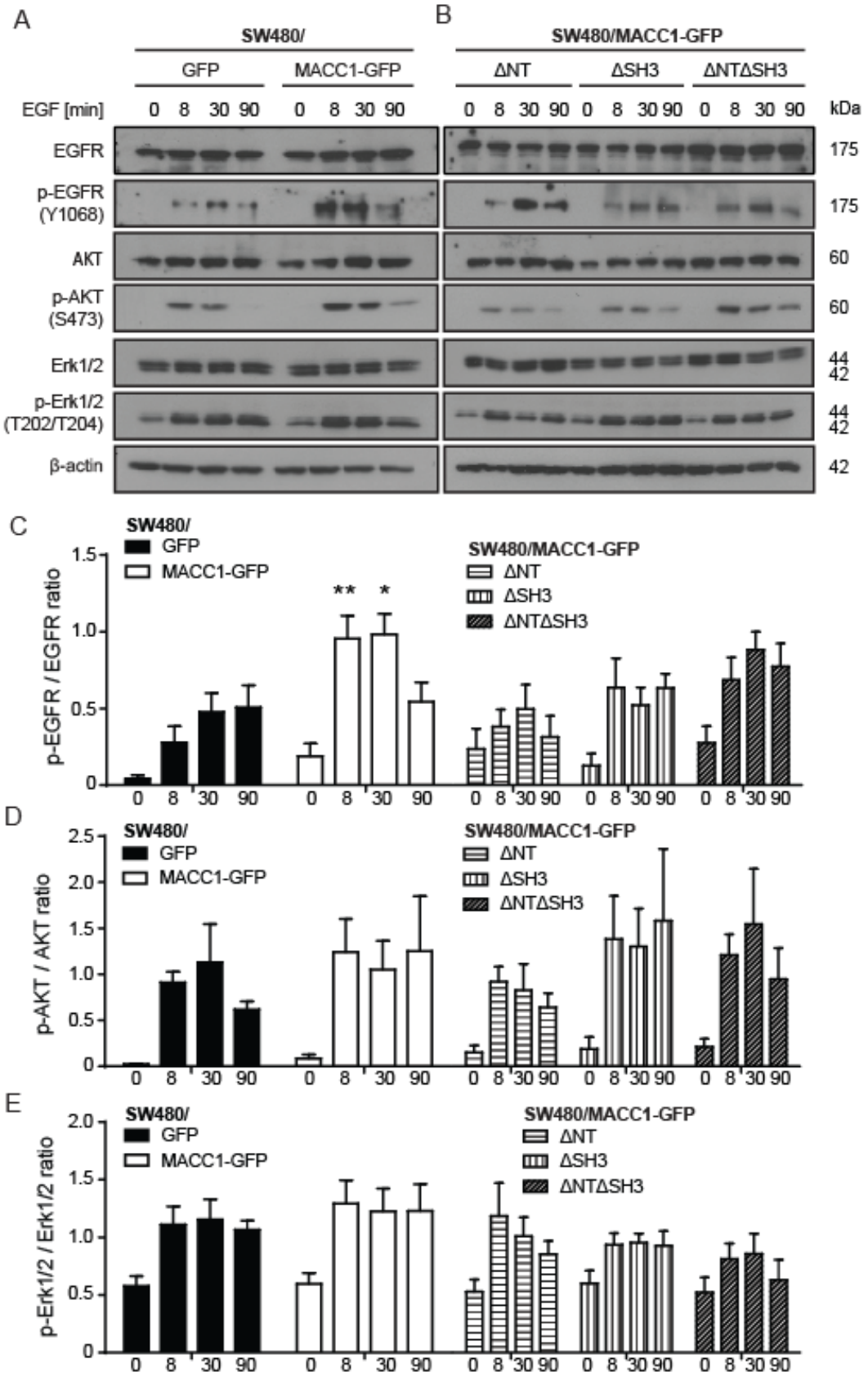
A
SW480/
GFP
MACC1-GFP
EGF [min]
0 8 30 90 0 8 30 90
EGFR
p-EGFR (Y1068)
AKT
p-AKT (S473)
Erk1/2
p-Erk1/2 (T202/T204)
β-actin
B
SW480/MACC1-GFP
ΔNT
ΔSH3
ΔNTΔSH3
0 8 30 90 0 8 30 90 0 8 30 90
kDa
175
175
60
60
44
42
44
42
42
C
SW480/
GFP
MACC1-GFP
SW480/MACC1-GFP
ΔNT
ΔSH3
ΔNTΔSH3
p-EGFR / EGFR ratio
1.5
1.0
0.5
0
**
*
0 8 30 90 0 8 30 90 0 8 30 90 0 8 30 90 0 8 30 90
D
SW480/
GFP
MACC1-GFP
SW480/MACC1-GFP
ΔNT
ΔSH3
ΔNTΔSH3
p-AKT / AKT ratio
2.5
2.0
1.5
1.0
0.5
0
0 8 30 90 0 8 30 90 0 8 30 90 0 8 30 90 0 8 30 90
E
SW480/
GFP
MACC1-GFP
SW480/MACC1-GFP
ΔNT
ΔSH3
ΔNTΔSH3
p-Erk1/2 / Erk1/2 ratio
2.0
1.5
1.0
0.5
0
0 8 30 90 0 8 30 90 0 8 30 90 0 8 30 90 0 8 30 90

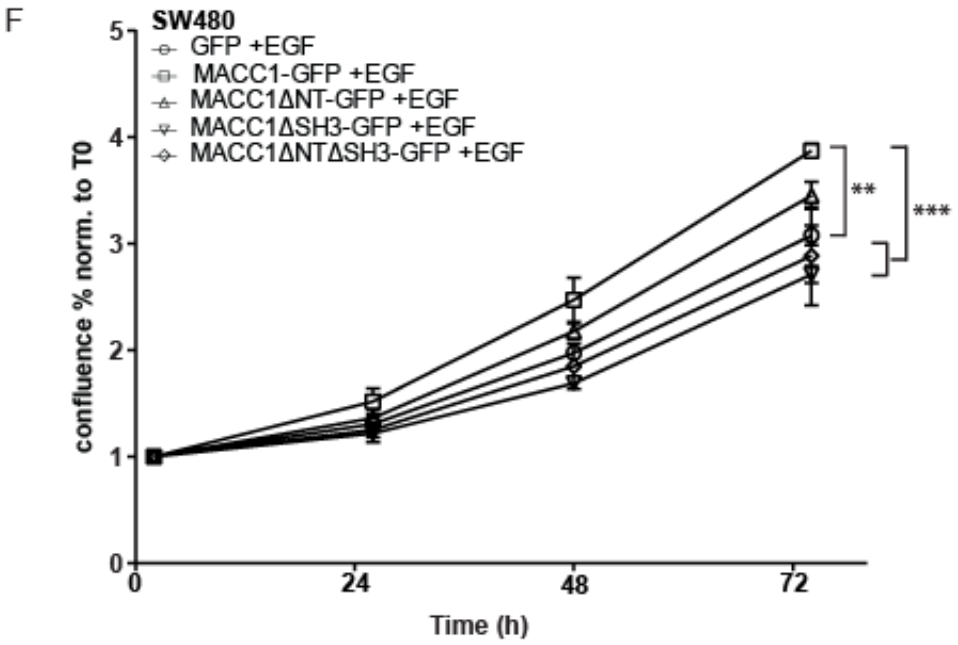

Figure 40 EGFR activation and downstream cascade is regulated by MACC1 CME cassettes. (A-B) After seeding ($3x10^5$) and serum-free starvation, MACC1 mutants were stimulated with low concentration of EGF (20 ng/ml) for an interval 0-90 min, to induce EGFR-specific internalization. After stimulation, cells were harvested and lysed in RIPA lysis buffer (see Material and Method for details). Proteins of the cell lysates were quantified and each sample was immunoblotted for different cascade antibodies and β-actin as loading control. A representative blot of four independent experiments is shown. Western blot analysis of EGFR, activated and phosphorylated EGFR (Tyr1068), ERK 1/2 and phosphorylated ERK (Thr202/Tyr204), AKT and phosphorylated AKT (Ser473) was performed in SW480 overexpressing MACC1 deletion constructs. (C-E) Quantification of pEGFR/EGFR, pAKT/AKT, pERK/ERK ratio upon EGF (20ng/ml) stimulation, after quantification of WB signal intensities; *p < 0.05, **p < 0.01, ***p < 0.001 (F) Proliferation of the SW480 cell line overexpressing MACC1 deletion construct was measured for 72 h in presence of continuous EGF treatment (20 ng/ml) in RPMI 2% FBS. The data shown are the mean ± SEM of four independent experiments. *p<0.05, **p<0.01, *** p<0.001

4.5 Supplementary Figures and Tables

ID	Gene Name	Species	CHROMOSOME	CYTOBAND	ENSEMBL_GENE_ID	ENTREZ_GENE_ID
IPI00217354	ADP-ribosylation factor GTPase activating protein 1	Homo sapiens	20	20q13.33,	ENSG00000101199,	55738
IPI00017184	EH-domain containing 1	Homo sapiens	11	11q13,	ENSG00000110047,	10938
IPI00100980	EH-domain containing 2	Homo sapiens	19	19q13.3,	ENSG00000024422,	30846
IPI00514400	G protein-coupled receptor kinase 5	Homo sapiens	10	10q24-qter,	ENSG00000198873,	2869
IPI00429190	RAB11A, member RAS oncogene family	Homo sapiens	15	15q21.3-q22.31,	ENSG00000103769,	8766
IPI00017344	RAB5B, member RAS oncogene family	Homo sapiens	12	12q13,	ENSG00000111540,	5869
IPI00019169	SH3-domain GRB2-like 1	Homo sapiens	19	19p13.3,	ENSG00000141985,	6455
IPI00294962	SH3-domain kinase binding protein 1	Homo sapiens	22	Xp22.1-p21.3,	ENSG00000147010,	30011
IPI00304577	adaptor-related protein complex 2, alpha 1 subunit	Homo sapiens	19	19q13.33,	ENSG00000196961,	160
IPI00016621	adaptor-related protein complex 2, alpha 2 subunit	Homo sapiens	11	11p15.5,	ENSG00000183020,	161
IPI00784366	adaptor-related protein complex 2, beta 1 subunit	Homo sapiens	17	17q11.2-q12,	ENSG00000006125,	163
IPI00909772	adaptor-related protein complex 2, mu 1 subunit	Homo sapiens	3	3q28,	ENSG00000161203,	1173
IPI00025974	chromatin modifying protein 4B	Homo sapiens	20	20q11.22,	ENSG00000101421,	128866
IPI00024067	clathrin, heavy chain (Hc)	Homo sapiens	17	17q11-qter,	ENSG00000141367,	1213
IPI00014589	clathrin, light chain (Lcb)	Homo sapiens	5	4q2-q3,4q2-q3|5q35,	ENSG00000175416,	1212
IPI00179438	disabled homolog 2, mitogen-responsive phosphoprotein (Drosophila)	Homo sapiens	5	5p13,	ENSG00000153071,	1601
IPI00514550	dynamin 2	Homo sapiens	19	19p13.2,	ENSG00000079805,	1785
IPI00845319	epsin 3	Homo sapiens	17	17q21.33,	ENSG00000049283,	55040
IPI00003865	heat shock 70kDa protein 8	Homo sapiens	11	11q24.1,	ENSG00000109971,	3312
IPI00006176	hepatocyte growth factor-regulated tyrosine kinase substrate	Homo sapiens	17	17q25,	ENSG00000185359,	9146
IPI00941170	neural precursor cell expressed, developmentally down-regulated 4-like	Homo sapiens	18	18q21,	ENSG00000049759,	23327
IPI00938079	programmed cell death 6 interacting protein	Homo sapiens	3	3p22.3,	ENSG00000170248,	10015
IPI00022462	transferrin receptor (p90, CD71)	Homo sapiens	3	3q29,	ENSG00000072274,	7037
IPI00182728	vacuolar protein sorting 4 homolog B (S. cerevisiae)	Homo sapiens	18	18q21.32-q21.33,	ENSG00000119541,	9525

Supplementary Figure 1. List of the involved proteins in CME, found by KEGG Pathway Analysis. After analysing our IPI_IDs from the MS list with DAVID bioinformatic tool, we also extracted a representative figure of the involved pathway, in our case “Endocytosis”. Together with the representative positions (red stars, on Figure 1) of MACC1 potential interactors in the endocytic pathway, the KEGG analysis also provides a list of the involved proteins, including ENSEML and ENTREZ gene ID, represented above (for the graphical screen, see supplementary figure 10).

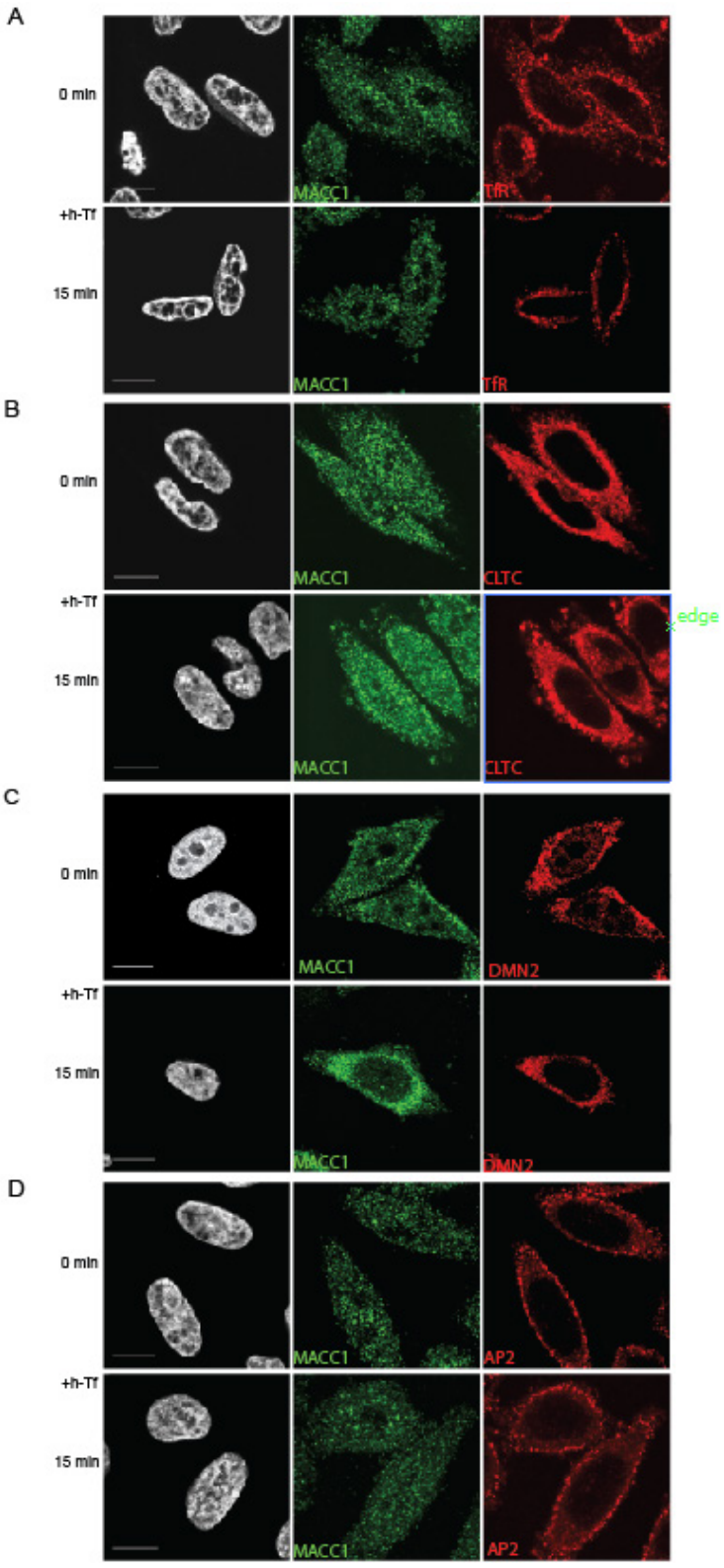

Supplementary Figure 2. MACC1 changes colocalization with validated CME interactors upon ligand-stimulated TfR CME. A confluent monolayer of SW480/MACC1 ($1x10^4$) has been seeded, serum starved and treated for 15 min with an excess of h-Tf (250 µg/ml) in order to measure by immunofluorescence (SP5, Leica) changes in the protein distribution and correlation at steady state and after TfR specific stimulated internalization. (A-D) Single channel images of the colocalization studies of MACC1 and TfR (A), CLTC (B), DNM2 (C) and AP2 (D) in SW480/MACC1 cells before (upper panel) and after (lower panel) 15 min stimulation of TfR internalization with h-Tf. Scale bar = 10 µm.

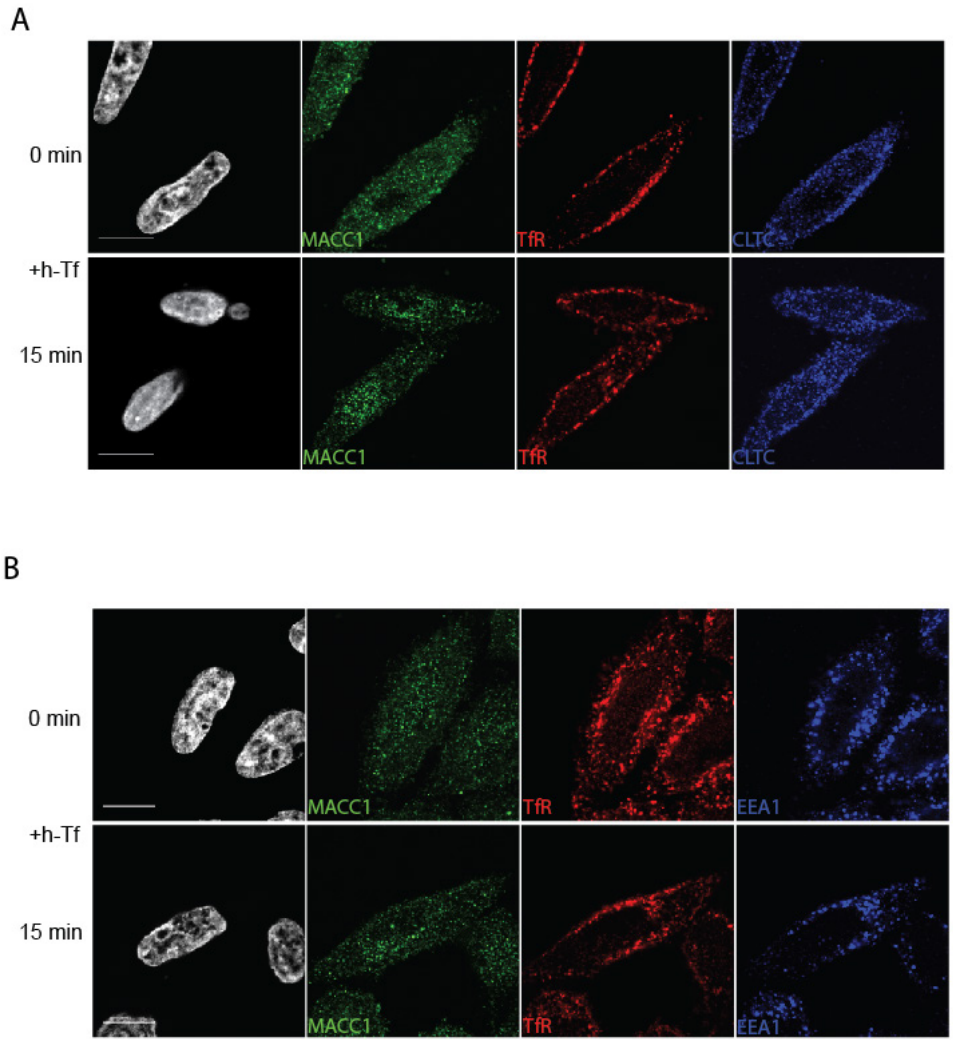

Supplementary Figure 3. MACC1 marks TfR-containing vesicles and TfR-containing endosomes, upon h-Tf triggered TfR CME internalization. A confluent monolayer of SW480/MACC1 cells ($1x10^4$) has been seeded, serum starved (1 hr) and treated for 15 min with h-Tf (250 µg/ml) in order to measure by immunofluorescence (SP5, Leica) changes in the protein distribution and correlation at steady state and after TfR specific stimulated internalization. (A-B) Single channel images of the colocalization of MACC1, TfR and CLTC (A) or EEA1 (B) after triple-staining of SW480/MACC1 cells before (upper panel) and after (lower panel) 15 min stimulation of TfR internalization with h-Tf. Scale bar = 10 µm.

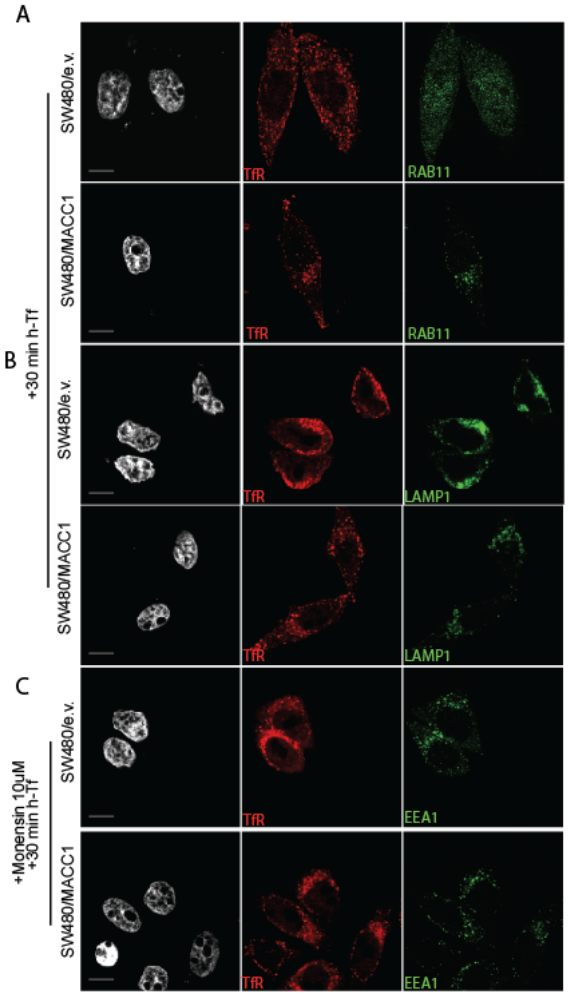

Supplementary Figure 4. MACC1 recruitment during TfR-stimulated CME increases the TfR receptor colocalization in RAB11-marked compartments and a decrease of TfR in LAMP1-marked degradative compartments. A confluent monolayer of SW480/e.v. and SW480/MACC1 cells ($1x10^4$) has been seeded, serum starved and treated for 15 min with h-Tf (50 µg/ml) in order to measure by immunofluorescence (SP5, Leica) changes in the protein distribution and correlation with different endocytic compartments. (A-C) Colocalization of MACC1 and RAB11 (A), LAMP1 (B), EEA1 (C) in SW480/e.v. and SW480/MACC1 cells after 15 min stimulation of TfR internalization with h-Tf. Scale bar = 10 µm. Indicated regions are displayed enlarged (10x).

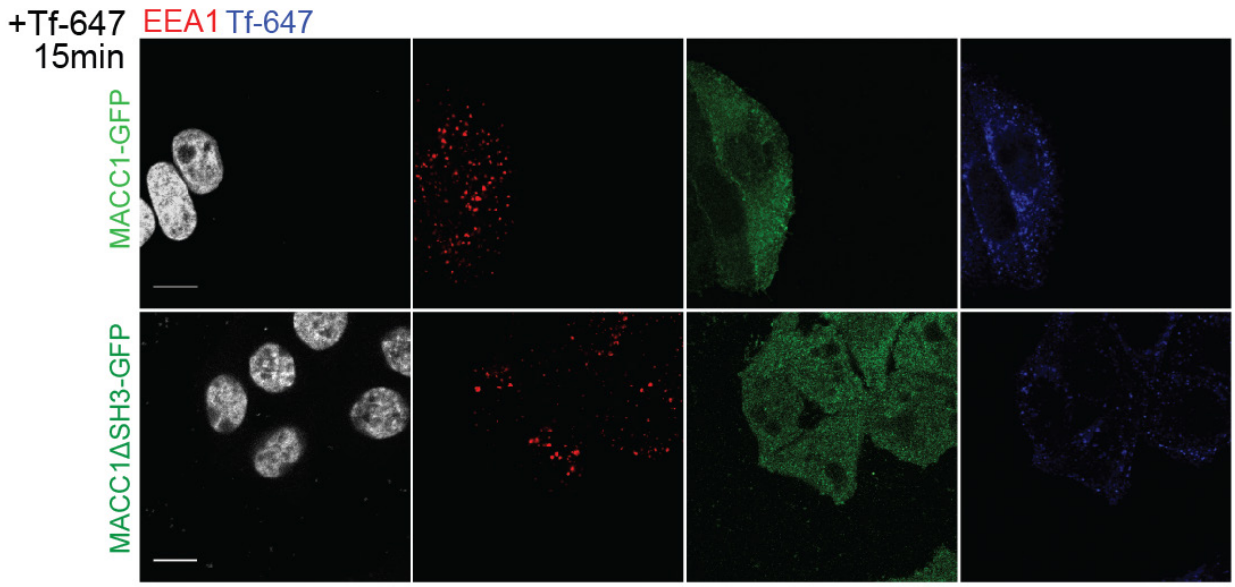

Supplementary Figure 5. CME-related domains of MACC1 mutants regulate the TfR distribution at the PM and the first steps of TfR endocytosis. A confluent monolayer of SW480/MACC1-GFP and SW480/MACC1ΔSH3-GFP cells ($1x10^4$) has been seeded, serum starved and treated for 15 min with Tf-647 (25 µg/ml) in order to measure by immunofluorescence (SP5, Leica) changes in the protein distribution within the cell and in endosomal compartments (EEA1-maked, in particular). Scale bar = 10 µm. Indicated regions are displayed enlarged (10x).

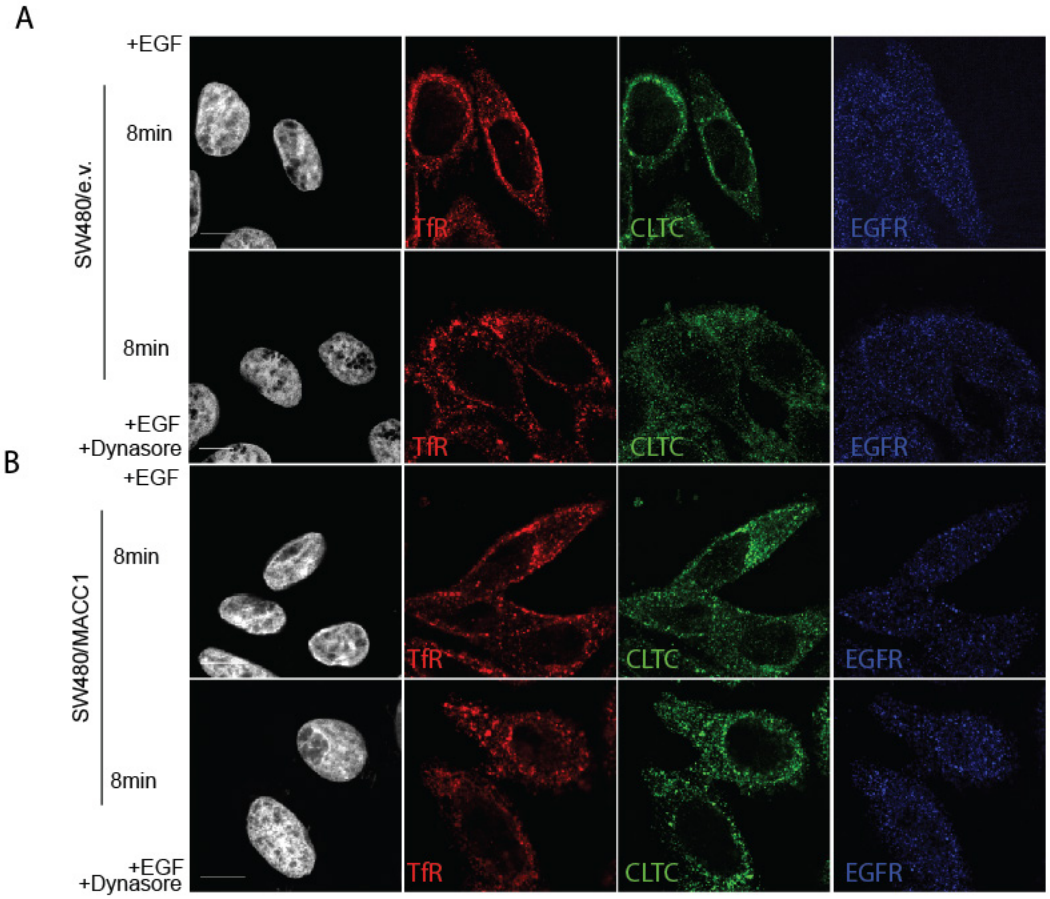

Supplementary Figure 6. MACC1 overexpression determines EGFR and TfR associated cargo selection in CCV, upon receptor-stimulated internalization. Single channel images are provided. A confluent monolayer of SW480/e.v. and SW480/MACC1 cells ($1x10^4$) has been seeded, serum starved and treated for 8 min with 20 ng/ml EGF in presence or absence of the dynasore inhibitor (80 µM). The three fluorescent signals from CLTC, EGFR and TfR were measured by immunofluorescence distribution and detection (SP5, Leica). (A) Colocalization of EGFR, TfR and CLTC after triple-staining of SW480/e.v. cells treated (left panel) and untreated (right panel) respectively with EGF for 8 min or with EGF for 8 min after pretreatment with dynasore (80 µM). (B) Colocalization of EGFR, TfR and CLTC after triple-staining of SW480/MACC1 cells treated (left panel) and untreated (right panel) respectively with EGF for 8 min or with EGF for 8 min after pretreatment with dynasore (80 µM). Single channel images are provided. Scale bar = 10 µm.

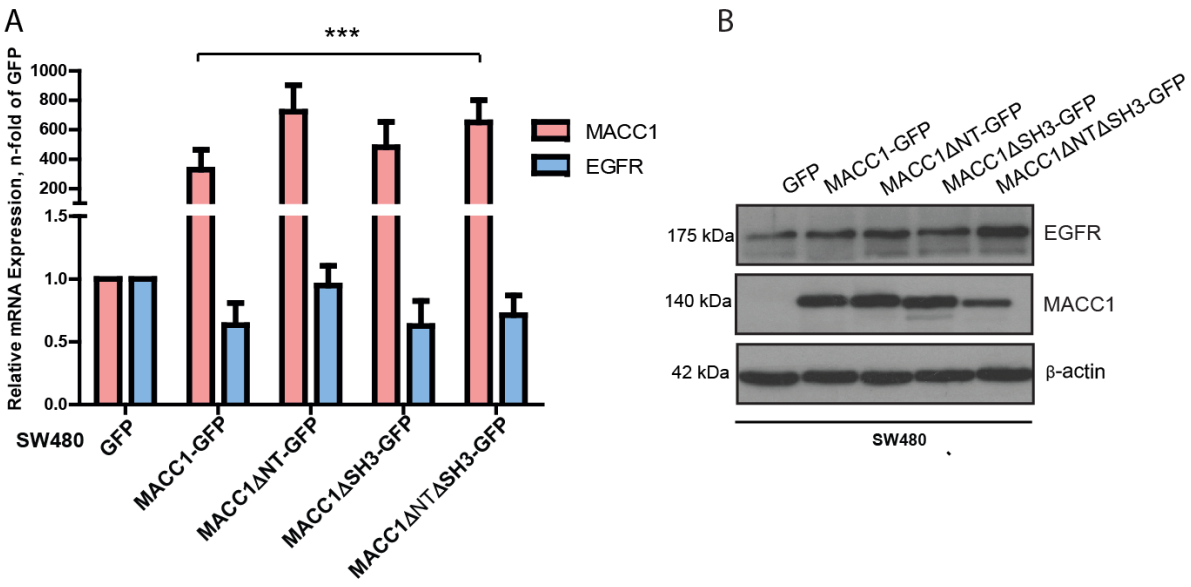

Supplementary Figure 7. Assessment of MACC1 and EGFR expression in MACC1 CME mutants. (A) MACC1 and EGFR mRNA and protein expression were determined in all the MACC1-mutant cells. Thus, 48 h after seeding cells ($3x10^5$), total RNA was extracted, reverse transcribed and quantified by real time PCR. Results are first normalized to GADPH and then represented as n-fold of the control cell line with respect to the gene of interest. Results are shown as means ± SEM of three independent experiments. *$p < 0.05$, **$p < 0.01$, ***$p < 0.001$ (B) For the MACC1 and EGFR protein expression analysis, 48 h after seeding cells ($3x10^5$), cells were harvest and lysed in RIPA lysis buffer (See Material and Method for details). Proteins of cell lysates were quantified and each sample was immunoblotted on nitrocellulose membrane, for MACC1, EGFR and β-actin as loading control. A representative blot of three independent experiments is shown.

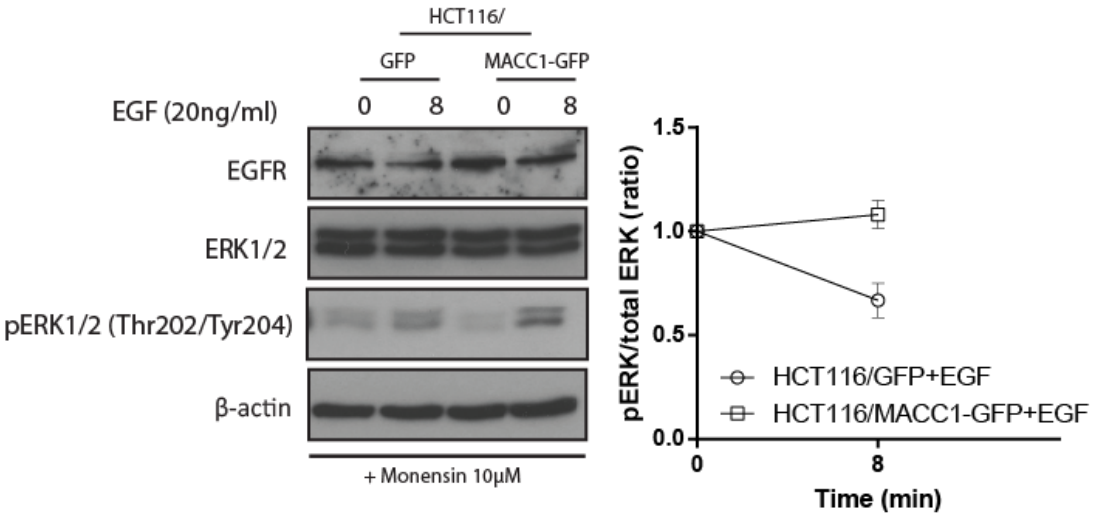

Supplementary Figure 8. MACC1 overexpression retains a sustained downstream ERK 1/2 signaling upon EGF stimulation and accumulation at endosomes. After cell seeding ($3x10^5$), serum-free starvation and treatment with Monensin (10 μM), HCT116-derived cell lines were stimulated with low concentration (20 ng/ml) of EGF for 0, 8 min, to induce EGFR-specific internalization. After stimulation, cells were harvested and lysed in RIPA lysis buffer (see Material and Method for details). Proteins of cell lysates were quantified and each sample was immunoblotted on nitrocellulose membrane, for ERK1/2 cascade antibodies and β-actin as loading control. A representative blot of three independent experiments is shown. Western blot quantification represents the ratio of the phosphorylated ERK1/2 / total protein.

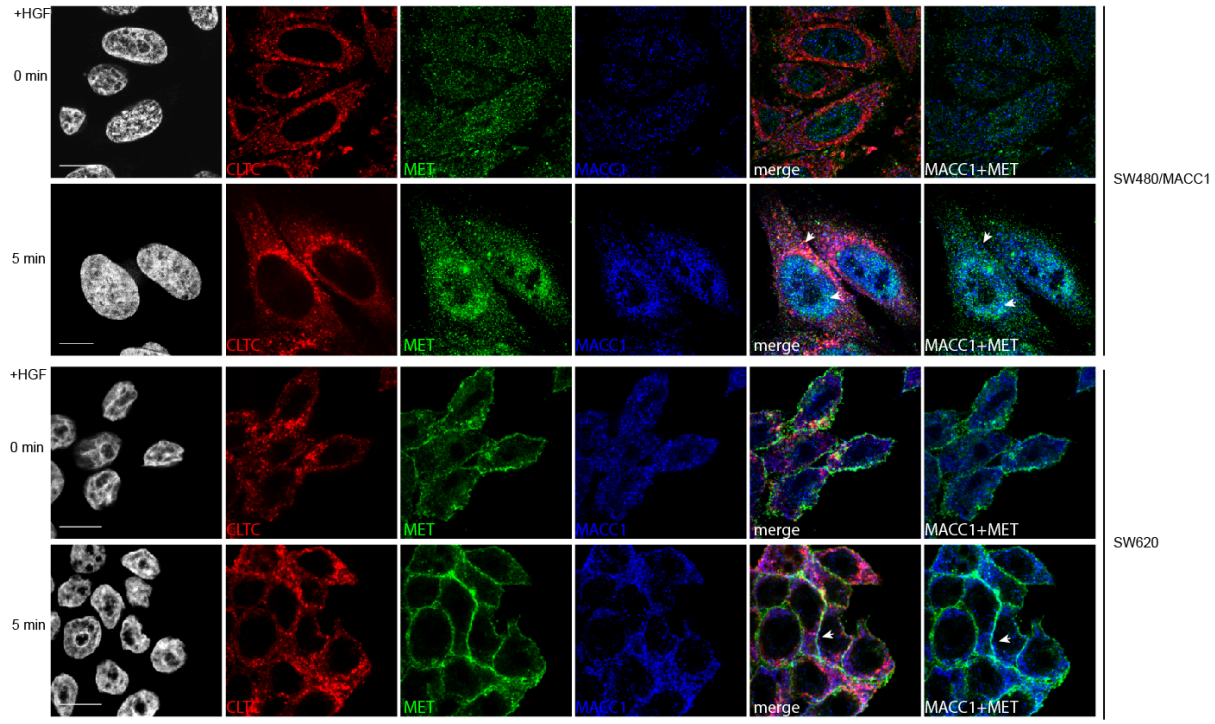

Supplementary Figure 9. MACC1 migrates into SW480/MACC1 nucleus and at the PM in SW620 cells after HGF stimulation. A confluent monolayer of SW480/MACC1 and SW620 cells ($1x10^4$) has been seeded, serum starved and treated for 5 min with 2 ng/ml HGF. The three fluorescence signals from CLTC, MET and MACC1 were measured by immunofluorescence distribution and detection (SP5, Leica). Colocalization of MACC1, MET and CLTC triple-staining of cells untreated (A, B upper panel) and treated (A, B lower panel) respectively. Representative pictures of three independent experiments. All panels show merged images. Scale bar = 10 µm.

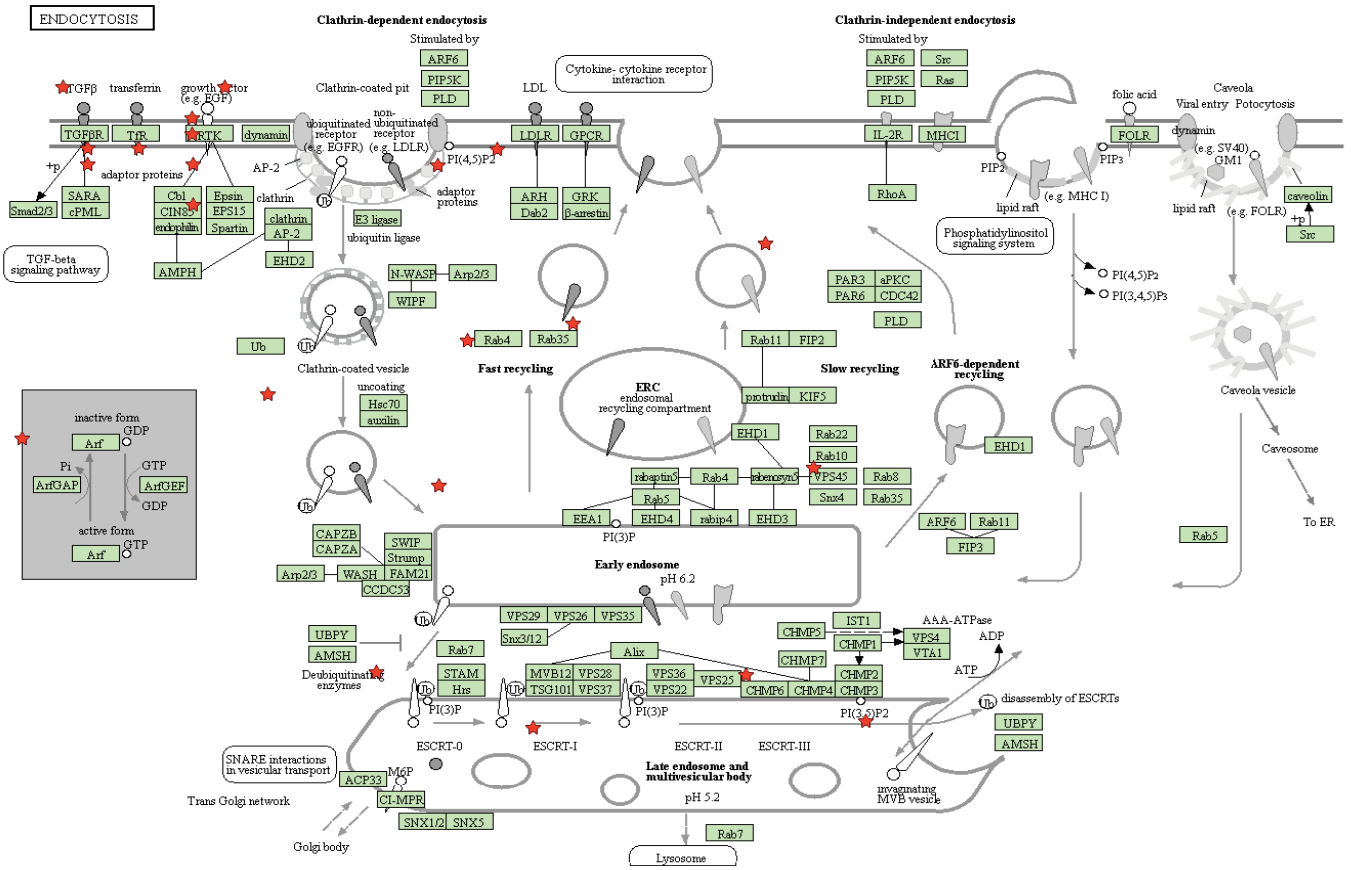

Supplementary Figure 10. KEGG pathway analysis via DAVID is screened, endocytosis interactors of MACC1 are indicated by red stars, useful to understand at which level of endocytic processes, MACC1 might be involved and have putative interactors (the complete list is the Supplementary Figure 1).

5. Discussion

In 2018, CRC is still one of the heaviest and deadliest burdens for society[207]. The development of CRC is complex, due to a gradual accumulation of genetic and epigenetic changes and to environmental factors. If CRC progresses until the late stages this predicts, a poor outcome, while at early stages the disease is often curable. A key to preventing deaths and improving the survival of patients in later stages of CRC will surely be to gain an understanding of the molecular mechanisms associated with crucial steps in the genetic development of the disease. Identifying new prognostic markers to predict CRC development and progression is an important milestone toward personalizing treatments.

The gene MACC1 was identified in 2009 as a new marker in early stages of CRC that proved prognostic for the development of metastases. MACC1 has been linked to a number of signaling pathways, but its physiological functions have remained elusive. In this thesis we identified a complete new biological role for MACC1 during CME.

Our data shed new light on the impact of MACC1-mediated CME on two distinct receptors, TfR and EGFR. In particular, MACC1 shows a clear involvement during internalization and increases TfR recycling during CME. MACC1 binds CLTC, DNM2 and TfR via all the predicted CME domains. Moreover, MACC1's N-terminus CME domains and the SH3 domain are differently involved and influence both TfR and EGFR during CME. Our data show a predominant role for the SH3 domain. Surprisingly, after we observed an increased colocalization of TfR and EGFR in CCVs in MACC1 overexpressing cells during EGF-stimulated CME, we hypothesized a MACC1-mediated increased recycling of EGFR. This thesis not only confirms our mechanistic hypothesis on the increase MACC1-mediated recycling of EGFR but also characterize the functional impact of MACC1 CME domains on EGFR-mediated proliferation. Our functional studies also indicate that if MACC1 lacks its endocytic cassettes, both EGFR transactivation and downstream ERK/MAPK and PI3K/AKT signaling are deregulated.

In summary, this work exposes a novel biological role for MACC1, that might lead in future to exploitation in the development of targeted treatments against metastasis and the progression of CRC.

5.1 MACC1 and its homology with SH3BP4: protein structure, localization and interaction

The first insights into MACC1 functions were hypothesized from its homology to SH3BP4; they share 43.7% homology in their amino acid sequence and predicted structural features. Both exhibit an SH3 domain[91], in the C-terminus of the protein structure. These similarities suggested a role during CME (Fig. 19). In this thesis I first showed that MACC1's interaction partners include a well-defined known set of proteins involved in CME. MACC1 shows interesting new dynamics with CME interactors including CLTC, AP-2, DMN2 and TfR (Fig.2-3). Our data reveal slight differences between the interactomes of MACC1 and SH3BP4[12289] but both proteins share interactions with proteins involved in endocytosis, as established through GO terms enrichment, which is highly indicative for a role in regulating CME[122] (Fig.1).

Among the overlap in the proteins' interactomes, MACC1 predicted interactions with CLTC, DNM2, AP-2α and TfR were validated (Fig. 20, B-E). These validations suggest that MACC1 is part of the endocytic machinery and is probably involved in the process of CCV formation. In terms of cellular distribution, reports have placed SH3BP4 in punctate structures in the cytoplasm and at the periphery of the cells, and has also been detected in the nucleus[121]. In 2009, MACC1 was characterized for its distribution and shuttling from the nucleus to cytoplasm. Until the present work, however, neither its punctual distribution with CME proteins in the cytoplasm nor dynamic, stimulus-dependent changes in localization had been observed.[89]

Our colocalization studies reveal a distribution of MACC1 within CCV and the TfR (Fig. 21, A-B). This increases over time, after a specific stimulation that leads to TfR internalization. In contrast to CLTC and TfR, the colocalization of MACC1 and DNM2 decreases after TfR-specific stimulation (Fig. 21, C). This tendency toward an inverse correlation of MACC1 and DMN2, compared to TfR or CLTC, indicates that MACC1 associates in distinct ways with proteins that are involved in early and late stages of the CCV machinery.

We speculate that MACC1 might play a role in the sequential recruitment of these endocytic proteins. Upon stimulation of TfR, MACC1's CME binding domains might regulate a decisive and limiting step of cargo-containing vesicle excision from PM[208–210]. Our results also suggest that the interaction of MACC1 and AP-2α is indirect and probably mediated by CLTC or TfR, which form the main hub of the CCV (Fig. 21, D). Interestingly, SH3BP4 exhibited no codistribution with the endocytic markers RAB11 and EEA1, although a triple colocalization was found with TfR and CLTC[121]. In contrast, our data show that upon TfR-stimulated CME, MACC1 was found colocalizing with the TfR and CLTC or the endosomal marker EEA1 (Fig. 22). Since MACC1 was observed to colocalize with these two endocytic markers, we speculate that it might shuttle from the PM to the endosomes via TfR-loaded CCVs.

In summary, the interactomes of MACC1 and SH3BP4 present similar endocytic protein signatures. Their common interactions with CME proteins and significant homology suggest similar functions. On the other hand, their distinctive traits are likely to give them different roles during CME. MACC1 appears to be involved in the endocytic machinery at the steady state and after specific-receptor trigger confirmed by our observations in its dynamic changes in the distribution with endocytic proteins. Also, our data confirm MACC1 presence in TfR-marked vesicles and endosomes after CME initiation. These conclusions and preliminary results suggested that we should investigate a new aspect of MACC1, as a key player in endocytosis.

5.2 MACC1 overexpression effect and the TfR endocytic cycle

The present work shows a novel role for MACC1 in the process of CME. Our preliminary screen of MACC1 interactors suggested a role in endocytic trafficking (Fig. 19-22). To test this hypothesis, we studied the internalization of TfR in MACC1-overexpressing and -knockdown conditions. Differently from SH3BP4, which shows an accumulation of TfR at PM dependent on its interference during TfR internalization, upon overexpression, MACC1 does not mediated an accumulation of TfR at the PM instead, the TfR surface distribution decreases in MACC1 overexpressing cell lines (Fig. 24, A). Similar results and effect on TfR PM distribution were also obtained in SW480/SH3BP4 (Fig. 24, A)[121]. Overexpression of either SH3BP4 or MACC1 interferes with the internalization of Tf-647 compared to control cell lines (Fig. 24, B). These findings suggest that MACC1 is not only part of the endocytic machinery during the first steps of TfR internalization, but might regulate it. Regarding SH3BP4, its knowing role during TfR internalization and in the endocytic machinery, was used to compare MACC1 behaviour and as a positive control.

In contrast, our findings also show an unusual block in the endocytic trafficking of pHrodo-Tf (Fig. 25, A-B). This pH-sensitive compound was unable to progress towards and accumulate in strongly acidic and degradative compartments, exhibiting a decrease in its fluorescent signal that stayed stably at low levels, compared to the control (Fig. 25, A-B). A convincing clarification of the mechanism came through the recycling assay, where the overexpression of MACC1 caused a faster loss of the Tf-647 signal compared to control cell line (Fig. 26, A-B). In line with previous data SH3BP4 is not showing any effect on TfR recycling. These data suggested a dual and distinct role for MACC1 during the internalization and the recycling of TfR. The colocalization of TfR within RAB11-marked recycling compartments and decreased colocalization of TfR in LAMP1-marked degradative compartments in SW480/MACC1, compared to the control cell line, provided further evidence (Fig. 27, A-B). We concluded that the faster recycling of TfR toward RAB11-positive compartments might depend only

on the recruitment of MACC1 to the tail of the TfR during CME, since TfR the tail does not contains docking sites for signaling adaptors.[211] An alternative possibility is that the increase in recycling mediated by MACC1 might also depend on its interactions with TfR at the endosomal level with RAB11, or through a specific targeting of the receptor to ERC or TGN via interaction with ESCRT machinery (Supplementary Fig. 1 and Fig. 19). Our data reveal that MACC1 has a dual effect: on TfR distribution at the PM and internalization, and on the increased TfR recycling. Differently from SH3BP4's previous data, which show an accumulation of TfR at PM and no effect on recycling, we concluded backwards that SW480/MACC1 cells might not need a rich pool of TfR on the PM, considering its increased effect on TfR recycling. That, might be an explanation of the altered the TfR amount at PM at steady state in SW480/MACC1.

MACC1's role in increasing the RAB11-recycling route for TfR is a key step in understanding its endocytic functions. MACC1 overexpression decreases the presence of the TfR into degradative compartments compared to the control cell line (Fig. 25-27). Thus, MACC1 has an impact at several steps of TfR endocytic trafficking, as shown from our data. Still needs to be clarified how MACC1 directs the TfR receptor towards recycling or degradative routes.

A similar situation has been observed for the Rab11 family-interacting protein Rip11/FIP5. This protein also enriches the endocytic recycling compartments and mediates the transport of TfR from endosomes to RAB11-marked compartments. In contrast to MACC1, a knockdown of Rip11/FIP5 increases the uptake, recycling, and PM distribution of TfR[212] .In contrast, MACC1 overexpression interferes with TfR uptake and blocks pHrodo-Tf trafficking towards late and degradative endocytic routes, but does not mediate and accumulation of TfR at PM.

These observations suggest that MACC1 might act mainly at the endosomal or recycling compartments, after it has mediated the sorting of TfR at the PM through direct or indirect recruitment at the endocytic machinery. As a predicted RAB11-interacting protein, MACC1, might mediate the directional targeting of TfR through their association en route at the endosomes and by recruiting/excluding specific RABs.

MACC1 blocks the targeting of pHrodo-Tf to degradative and late compartments (Fig. 25), thereby suggesting that its recruitment to the TfR-endocytic complex might exclude RAB12 or RAB7, which were not detected in the MACC1 interactome (Suppl. Fig. 1). The differential recruitment of RAB12 or RAB7 at the endosomal compartment has an important effect, by targeting TfR to the degradative pathway instead of along the recycling route, as happens with RAB11 (slow recycling route from ERC) or RAB4 (fast recycling route from endosomes).

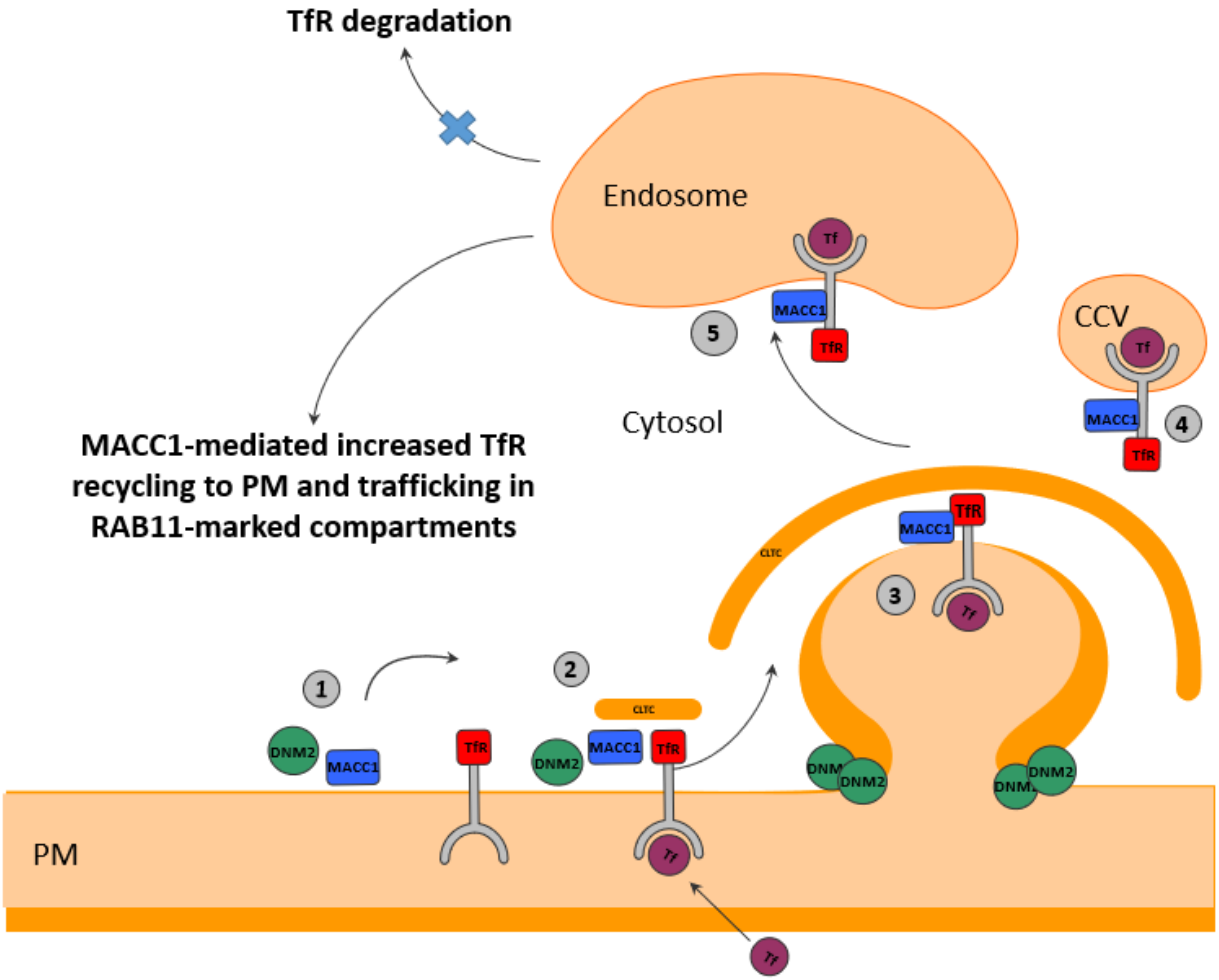

Figure 41 Investigating MACC1's role in the TfR endocytic traffic. (1) MACC1 was found colocalizing with DNM2 at PM before TfR-triggered internalization. (2) Upon TfR stimulated CME, its colocalization increases with CLTC and TfR. (3) After the endocytic machinery has loaded TfR on CLTC-marked vesicles, MACC1 travels (4) together with TfR from PM to endosomes. (5) Probably, at the endosomal compartment MACC1 might mediates the TfR sorting into recycling compartments, by increasing the TfR targeting to RAB11-compartments, instead of LAMP1-marked compartments or degradative routes.

5.3 MACC1 knockdown effect and the TfR endocytic cycle

The present work assigns an endocytic role to MACC1. We previously showed how MACC1 overexpression blocks the trafficking of TfR into degradative compartments, and how this influences the most commonly used model of TfR-CME (Fig. 41) Our next step was to dissect the effects of MACC1 knockdown (KD) on TfR endocytic trafficking. Interestingly, this does not alter the PM distribution of TfR from the situation seen in the overexpression studies (Fig. 28, A), but it alters equally the TfR internalization process, confirming MACC1 as a regulator of the TfR internalization (Fig.28, B).

These data, coupled with the results from the MACC1 overexpression experiments (Fig.25-27), suggested that the distribution of TfR on the PM might depend on downstream endocytic events such as endosomal sorting and TfR recycling in SW620 cells overexpressing MACC1 KD. We cannot exclude a connection between the activity of MACC1 and SH3BP4 during the TfR internalization and sorting phase, which might influence our results in this context. Our conclusion was that interference of MACC1 KD on TfR uptake confirms its endocytic role during the TfR internalization process. The effects of MACC1 KD on TfR routing and its accumulation in recycling or degradative compartments in SW620 cell lines were interesting and bear further investigation (Fig. 29, A-B)

After 3 h of pHrodo-Tf trafficking, we observed that MACC1 KD clearly triggers and strengthens the accumulation of TfR in degradative and low pH compartments compared to the control (Fig. 29, B). This effect was visualized via live imaging as a red-fluorescent accumulation in SW620 cells (Fig.29, 1 and 2) both panels). We could also confirm a MACC1-dependent effect of TfR routing into degradative compartments by measuring the decrease of total TfR protein level after 20 min of h-Tf stimulation (Fig. 30, A). Additionally, bafilomycin A1 caused a block of the degradative compartments, leading to a visible accumulation of the TfR receptor resembling that of the control (Fig. 30, B), as expected. We conclude that in contrast to SH3BP4, MACC1 is an endocytic protein both involved in the internalization and the recycling of the TfR. Still unclear but very intriguing is whether the MACC1-dependent effect on TfR sorting into recycling compartments is dependent on specific recruitments orchestrated by MACC1. Our data could not clarify whether such events take place during TfR internalization or at the endosomal compartment at the sorting machinery through an inclusion or exclusion of specific trafficking proteins.

5.4 Biological impact of MACC1-mediated endocytic trafficking of TfR

It has recently been shown that there is a relationship between TfR expression and the stages of colorectal carcinoma (Dukes A, B, C, D). In particular, differentiated colorectal carcinoma cells (Dukes A and B) present high expression of TfR while poorly differentiated cells (Dukes C and D)[177] exhibit only weak TfR expression. This may be related to changes in the metabolic requirements of cancer cells at different stages of their development. Here, iron plays a role as a fundamental biological nutrient and cellular entity. It has particular importance in regulating DNA synthesis over the cell cycle. Iron depletion generally blocks the cell in G1/S phase and causes apoptosis[213]. Modulating iron transport and balancing cellular quantities are crucial in maintaining a healthy relationship between nutrients and cell growth[213]. Any deregulation in these processes can lead to unbalanced and aggressive proliferation, particularly in neoplasia[214]. Thus, by modulating TfR, MACC1 has a potential

to profoundly alter cell metabolism in ways that may be either supportive or detrimental to the progression of cancer.

To define the MACC1 general impact on internalization and recycling of TfR we used SW480 (Dukes B) cell lines derived from the primary tumor and SW620 (Dukes C) from a lymph node metastasis from the same CRC patient. The aim was to assess the biological impact of MACC1 on iron uptake in primary tumours and in distant metastasis. MACC1 is endogenously overexpressed in SW620; in SW480 there is virtually no expression. Interestingly, the mRNA expression of TfR in SW480 and SW620 cells do not reflect the mentioned TfR mRNA expression. The expression of TfR mRNA is 2-fold higher in SW620 cells than in SW480 (Fig. 23, E-F).

We confirmed a higher indirect membrane distribution for TfR/Tf-647 complexes in SW620 than in SW480 cells (Fig.13, A). We also confirmed that MACC1 weakly interferes with TfR uptake in SW620 cells (Fig. 13, C). But we also showed that the endogenous expression of MACC1 in these cells causes TfR to accumulate in acidic compartments in a time-dependent manner (Fig. 13, D-E). We speculate that this effect depends not only on the increased distribution of TfR at the PM but also on enhanced MACC1-mediated endocytic recycling of TfR and consequent increase of TfR delivery to degradative compartments. In summary, these data suggest that in highly TfR expressing cells (SW620), MACC1 mediates the regulation of TfR transport, ultimately leading to an increase in iron metabolism and we speculate, to subsequent cell proliferation.

5.5 A role for TfR in novel approaches to CRC therapies

Ultimately, the metastatic progression of CRC is the principal cause of deaths from the disease[215]. This makes preventing the formation of metastases in the early stages of tumours a key therapeutic goal. TfR is an expression marker for many cancer types, including CRC[166,167,170], and is linked to the availability of iron, a nutrient crucial for cell growth and proliferation[216]. Here we present strong evidence that MACC1 has an impact on both TfR internalization and recycling. It has been shown that the progression to CRC is driven by an increased expression of iron import proteins which subsequently sustain increased proliferation[178]. Our data show that SW620 cells, which highly express MACC1 and increased TfR compared to SW480, (Fig. 23, E-F) exhibit an increase in TfR endocytic traffic through recycling compared to SW480 cells, which express virtually no MACC1. Overall, this leads to an increase in the import of TfR (Fig. 31, C-D).

MACC1 has been indicated as a prognostic factor for many cancer types[105,217–222], and our research sheds new lights on the MACC1 role during physiological processes. Our data reveal MACC1 as a

decisive driver of the switch of TfR fate from degradation to recycling. This suggests a potential handle for treatments.
Because increased iron import is a prerequisite for highly proliferative cancer cells, a number of novel therapies are targeting this process. Very recently, TfR has become an attractive target for these approaches because it is upregulated in many drug-resistant and metastatic cancer entities in a highly specific way. Moreover, TfR is already being efficiently used to deliver therapeutic compounds and molecules into malignant cells[173,223,224]. Despite the fact that TfR is the most known and characterized receptor able to recycle to the PM after internalization[171], a mechanistic involvement of MACC1 in its distribution had not been shown.

Here we show that MACC1 has a striking impact on TfR's distribution on the PM. MACC1 increases of TfR endocytic traffic towards recycling instead of degradation potentially makes it a potent player in the development of efficient therapies. Tf-conjugated/targeted compounds might be used in future for primary tumors and metastases, particularly aiming to develop highly selective cytotoxic strategies to target highly proliferative cancer cells.

5.6 Impact of MACC1 CME domains during TfR trafficking

Endocytosis is essential in mediating the transport of nutrients and molecules from the extracellular environment to the cell interior, integrates cellular signaling and regulates the composition of the PM[225]. CME regulates signal attenuation and the fates of receptors at the PM by internalizing them. Relatively disruptions of CME have been identified as drivers of cancer. Numerous proteins that act as endocytic modulators of receptor recycling enhance cancer-related cell signaling, which can lead to malignant progression[122,226–228]. Here we identify MACC1 as a new endocytic protein with a dual impact on TfR trafficking. As for many endocytic proteins, MACC1 exhibits predicted CME interacting domains at its N-Terminus and also contains a predicted interacting SH3 domain at the C-Terminus. To dissect the impact of MACC1 CME domains on endocytic traffic, we deleted them and observed the effects on distinct endocytic-limiting steps. Interestingly, we also found that deleting the SH3 domain predominantly causes an accumulation of the indirectly stained TfR at the PM (Fig. 34, A) and also strongly impairs pH-Tf internalization (Fig 34, E). This led us to speculate on a stronger SH3-dependent impact on MACC1-mediated TfR internalization compared to the ΔNT mutant MACC1 protein. We observed a SH3 domain-dependent MACC1-mediated uptake of the TfR/Tf-647 complex using also confocal microscopy (Fig. 34, C). By quantifying the integrated density of fluorescence, we could confirm that the lack of the SH3 domain strikingly inhibits Tf-647 uptake into the cell (Fig. 34, C-D). We also found that the MACC1 SH3 domain predominantly determines MACC1 distribution and

accumulation at the PM (Fig. 33, A), compared to the mutant harbouring the ΔNT deletions. The deleted cassettes (ΔNT and ΔSH3) caused the loss of the interaction between MACC1 and CLTC and DNM2 (Fig. 33, B-C).

Moreover, MACC1 binding to TfR is SH3 domain-dependent and is lost when the SH3 domain is deleted (Fig. 33, D). TfR binds to MACC1 when the N-Terminus cassettes are deleted, suggesting that the MACC1/TfR complex might be mediated indirectly by other endocytic proteins such as CLTC after TfR-stimulated internalization (Fig. 33, D). We conclude that the impact of the SH3 domain of MACC1 is clearly dominant over the N-Terminal interaction motifs and necessary for the uptake of TfR, as it is strikingly impaired in the ΔSH3 mutant compared to the ΔNT mutant cell lines. The MACC1 N-Terminus CME cassettes and the SH3 domain might show synergistic effects during the process of TfR-stimulated internalization, but the TfR/Tf-647 accumulation at PM (Fig.33, A) clearly suggests that the MACC1 SH3 domain is involved in the rate-limiting step of the vesicle scission and TfR internalization.

In contrast to all the other correlations between MACC1 and endocytic proteins we tested, MACC1 exhibits a high inverse correlation with DNM2 (Fig. 21, A-D) before CME is triggered by h-Tf stimulation. In contrast to the MACC1/CLTC correlation, MACC1/DNM2 decreases after TfR stimulation. We speculate that MACC1 might bind to DNM2 before h-Tf triggers TfR. Alternatively, MACC1 might sequentially bind first to DNM2 and then TfR during the internalization step, and the two binding partners might compete for MACC1 SH3 domain during this process.

In summary, MACC1 has an impact on the CME-based internalization and recycling of TfR. It is known that dynamin binds and initiates its GTPase activity after self-assembly via PRD/SH3 domain interactions and this regulates the rate-liming steps of CCV scission[209,229–232]. MACC1 seems to be involved in the first steps of this process. Further investigation will be needed to clarify whether the MACC1-dynamin interaction might also affect the budding of endosomal-derived recycling vesicles, a process which targets receptors to the PM[233]. We speculate that MACC1 might act in the manner of the “vesicle loading model” (Fig. 8, introduction), and mutually work with DNM2 to guarantee the correct sequential recruitment of endocytic proteins together with the receptor. This would hierarchically orchestrate their inclusion or exclusion from vesicles, predominantly via the MACC1 SH3 domain.

5.7 Discovery of the MACC1 impact on receptor tyrosine kinase endocytic traffic

Since MACC1 was identified in our lab in 2009[89], it has been characterized as a driver oncogene for metastasis in several other types of cancer[105,234–238]. So far biological evidence for a MACC1-dependent mechanism of enforced signaling has not been presented. Here, for the first time, we introduce evidence for a role for MACC1 as an endocytic protein that can increase TfR recycling. Endocytic recycling has only recently been identified as a leading cause of sustained signaling for many receptors[122,228,239].

Our KEGG pathway analysis of the MACC1 interactome, predicted interactions with RTKs (Fig. 19, C), so we decided to validate MACC1's binding with MET (Fig. 35, B). Mainly out of curiosity, we also examined whether MACC1 binds to EGFR, a well-known prognostic marker for CRC[240]. Unexpectedly, we confirmed their interaction (Fig. 35, A). In CRC, ligand-stimulated EGFR dimerizes and trans-autophosphorylates specific tyrosine sites on its cytoplasmic tail. This enables numerous docking sites for signalosome adaptors (GRB2, GAB1, etc.) and activates signaling pathways such as PI3K/AKT, Jak/STAT, Src, and MAPK[241]. Furthermore, ligand-induced kinase activity of EGFR and subsequent tyrosines phosphorylation of SH3BP4 or dynamin during the internalization process prevent their interaction and probably mediates the exclusion of SH3BP4 from EGFR-containing CCP[121].

In contrast, a cooperation of TfR and EGFR in the cytoplasm has been found in lung cancer, and it is dependent on EGFR kinase activity that generates an increase of TfR membrane distribution[187]. Based on this finding from the literature, we tested whether MACC1 overexpression might have influenced the inclusion or exclusion of EGFR from TfR-marked CCVs upon its ligand-stimulated internalization and trans-autophosphorylation. In SW480/MACC1 cells, we could not confirm that EGFR is excluded from TfR-marked CCPs or CCVs (Fig. 36), but when dynamin was inhibited with dynasore, the two receptors could not be found in CCVs and CCPs. Taking this into account, we concluded that in CRC cell lines which overexpress MACC1, it does not mediate an exclusion of EGFR from CCPs and CCV upon EGFR kinase activation. This suggested that EGFR and TfR follow the same early endocytic pathway, as they are found in TfR-marked vesicles. Observing this we then speculated that TfR and EGFR could have been sorted after internalization to the recycling route and transported back to the PM.

5.8 The impact of MACC1 on EGFR endocytic traffic

MACC1's role during CME was identified first by studying its impact on the endocytic trafficking of TfR. Our research shows two MACC1-mediated effects: the ligand-stimulated internalization of TfR and the faster release of the TfR-Tf-647 complex from the endosome to PM via RAB11-marked compartments. We further observed MACC1 binding to EGFR in three different cell lines (Fig. 35, A)

and showed that MACC1 overexpression includes EGFR in TfR-marked vesicles upon EGF stimulation. Our next step was to understand the impact of MACC1 during ligand-stimulated EGFR internalization. In SW480 cells, MACC1 overexpression mediates a significant increase of dynamin-mediated endocytic traffic of pH-EGF into acidic compartments after 3 h (Fig. 37).

It has recently been shown that EGFR is targeted to degradative or recycling compartments in a ligand-concentration-dependent manner. At low EGF concentrations, ligand-stimulated EGFR is recycled back to the PM and only one-third of the pool is destined for degradation, which sustains EGFR signaling. At high EGF concentrations, with an involvement of both NCE and CME, the receptor is targeted preferentially to degradative compartments (40% cases). This has a differential impact on the EGFR signaling by decreasing its intensity[130]. In the most recent model of EGFR (Fig. 16, introduction), the recycled receptor needs to release the EGF-ligand in mild endocytic compartments such as endosomes/recycling endosomes before being disassembled. In turn it is transported back to the PM, increasing its availability and sustaining signaling[182,183,242].

Our data show that MACC1 overexpression causes an increased endocytic trafficking of the pH-sensitive compound to low pH/acidic compartments in SW480 cells (Fig. 37). We cannot exclude that a sizable proportion of the receptor is destined to degradation, considering the high EGF concentration used (5 µg/ml), nor that the increased accumulation depends on the pH-EGF released in endosomes/recycling endosomes, which allows EGFR to be recycled[182,183]. In accordance with our data, the sequential deletion of MACC1 CME cassettes strongly increased endocytic traffic of pH-EGF/EGFR complexes into low pH compartments in mutant cell lines. Together, these data suggest that the endocytic features of MACC1 are important to correctly ensure EGFR routing into CME, maintaining the balance of EGFR between recycling and degradation. To conclude, we speculate that the deletion of MACC1 CME domains might be the leading cause of the destabilization of the pH-EGF/EGFR complex and its direct targeting into low pH and degradative compartments, compared to the full-length MACC1 and the control cell lines

5.9 MACC1 overexpression increases EGFR recycling to the PM

After focusing on the way by which MACC1 influences TfR recycling we were curious to investigated its impact on endocytic traffic of RTK receptors. Without evidence for one receptor over another, we first validated the indirect or direct binding of MACC1 to MET and EGFR (Fig. 35). Interestingly, the kinase activity of EGFR promotes Tf-internalization and increases the distribution of TfR at the PM in NLSC. Also, both EGFR and TfR colocalized in the cytoplasm after EGF-stimulated internalization[187].

Considering this and our previous results into account (Fig. 36), and the MACC1-mediated increase of TfR recycling, we decided to test whether MACC1 overexpression could also affect EGFR recycling. At a low CME-inducing concentration of EGF (20 ng/ml), we found that MACC1 overexpression increases the pool of EGFR available on the surface after ligand-specific stimulation in two different expressing cell lines (Fig. 38, A, E). This finding suggests a first physiological role for MACC1 during EGF-stimulated endocytic traffic leading us to hypothesized a MACC1-mediated in sustained signaling upon EGF-stimulated CME, dependent from its CME domains.

5.10 EGFR activation and trans-autophosphorylation is sustained by MACC1 overexpression and affects two distinct downstream signaling cascades

The structure of EGFR includes the extracellular region responsible for EGF ligand recognition and binding. EGFR also possesses the intracellular region including the juxtamembrane regulatory region, the kinase domain, and the intracellular C-terminal regulatory tail containing tyrosine residues which become phosphorylated upon EGF binding[243]. The binding of EGF, stabilizes EGFR monomers and induces EGFR dimerization. This, in turn, causes structural changes in the cytoplasmic domain, leading to the allosteric activation of the EGFR kinase domain[244]. In the active dimer, specific tyrosine residues in the cytoplasmic regions of each monomer trans-autophosphorylate, acting as a docking station for proteins and triggering the signaling cascade.

To be recycled back to the PM, EGFR needs to effectively reach endosomes and must be routed into RE. There it disassembles into monomeric units and is targeted back to the PM, making it available for another round of transphosphorylation upon EGF binding[183]. Our data show that in line with the increased recycled EGFR pool, MACC1 overexpression in SW480 cells causes sustained trans-autophosphorylation of the receptor at Y1068 for 30 min after stimulation. This confirms that MACC1-mediated increased recycling of EGFR sustains the activation of the receptor and its trans-autophosphorylation. The effectiveness of this process depends on the MACC1 CME cassettes. Any MACC1 deregulation by deletion results in different effects on EGFR trans-autophosphorylation of Y-1068; a decreased EGFR transphosphorylation as observed in the ΔNT mutant cell line, or decreased and prolonged transphosphorylation until 90 min after stimulation in the ΔSH3 and ΔNTΔSH3 mutant cell lines.

Since its discovery in 2009, MACC1 has been implicated in driving sustained signaling in diverse molecular cascades including the HGF/c-Met[245,246,76] pathway, the PI3K/AKT cascade[98,247], and the Wnt/β-catenin[248,]and ERK/MAPK[249] pathways. As previously shown for many cancer entities, the overexpression of MACC1 also drives sustained downstream signaling of ERK1/2 cascade (Fig. 40, A-B). In contrast, in the ΔNT mutant cell line downstream ERK1/2 phosphorylation is weakly decreased while ΔSH3 and ΔNTΔSH3 mutant cell lines show a stronger decrease of ERK1/2 phosphorylation compared to the ΔNT mutant cell line. All the mutant cell lines harbouring MACC1 deleted versions show a general decrease of ERK1/2 phosphorylation compared to the full-length. Regarding the downstream activation of AKT, we observed some differences. MACC1 overexpression shows a mild increase AKT downstream phosphorylation compared to the control cell line. When we observed the MACC1 deletions effect on AKT phosphorylation we noticed an impairment in the signaling cascade in the ΔNT-deleted mutant cell line compared to the MACC1 full-length cell line. And indeed, we

observed an increase AKT downstream signaling for both ΔSH3 and ΔNTΔSH3 mutant cell lines. These data suggest that if the SH3 domain deletion causes a loss of MACC1 biological functions, in this context MACC1 might be temporarily replaced at PM by another protein (eg.SH3BP4). SH3BP4 may rescue the downstream activation of AKT. We further speculate that since SH3BP4 sustains AKT signaling during FGFR stimulation by interacting with the catalytic subunit (p85) of PI3K and promoting receptor recycling[122], the SH3BP4 effect might overlap with MACC1 when studying AKT downstream phosphorylation.

Considering these data, we suggest that MACC1 acts as an endocytic protein which is involved in physiological processes not only as an enhancer of receptor recycling, but also as a modulator of the process via its CME domains, which are necessary for effective downstream signaling.

5.11 MACC1 CME domains ensure and efficient cell proliferation upon EGF stimulation

Our current understanding of endocytosis has moved beyond seeing its functions in terminating ligand-induced signaling and the biological availability of surface receptors due to new insights and discoveries[250]. A deregulation of signaling is inherently connected to the development of cancer; sustained signaling in particular, is typical for RTKs during enforced recycling and is a major contributor to the continuous and uncontrolled growth of cancer cells. Since 2009, MACC1 has been identified as a prognostic marker for many solid entities, and as a key regulator of sustained proliferation[76,236,247,251,252]. MACC1 transcriptionally regulates the HGF receptor c-MET and promotes the HGF/c-MET axis as proliferative boost via ERK/MAPK and PI3K/AKT[245]. In this thesis, we identified a new role for MACC1 in relation to the EGFR-stimulated downstream pathways ERK/MAPK and PI3K/AKT. Data show that MACC1 participates during TfR endocytosis via its endocytic domains and substantially influences it, as seen in particular through the dominant effects of SH3 domain deletion. Conversely, any studied deletion of the MACC1 protein structure impairs the trans-autophosphorylation of the EGFR receptor and the downstream signaling of both ERK/MAPK and PI3K/AKT pathways, but differently. This pattern of impairment was functionally confirmed by testing all the MACC1 cell lines harbouring CME-deleted domains (Fig. 40, F). The proliferation of cell lines containing these mutations only increased in the wild-type MACC1 cell line, compared to control and all the deletions. In conclusion, our data show a completely new biological role for MACC1 through its clear impact on CME, on EGFR downstream signaling and functionally on MACC1-mediated proliferation upon EGF stimulation.

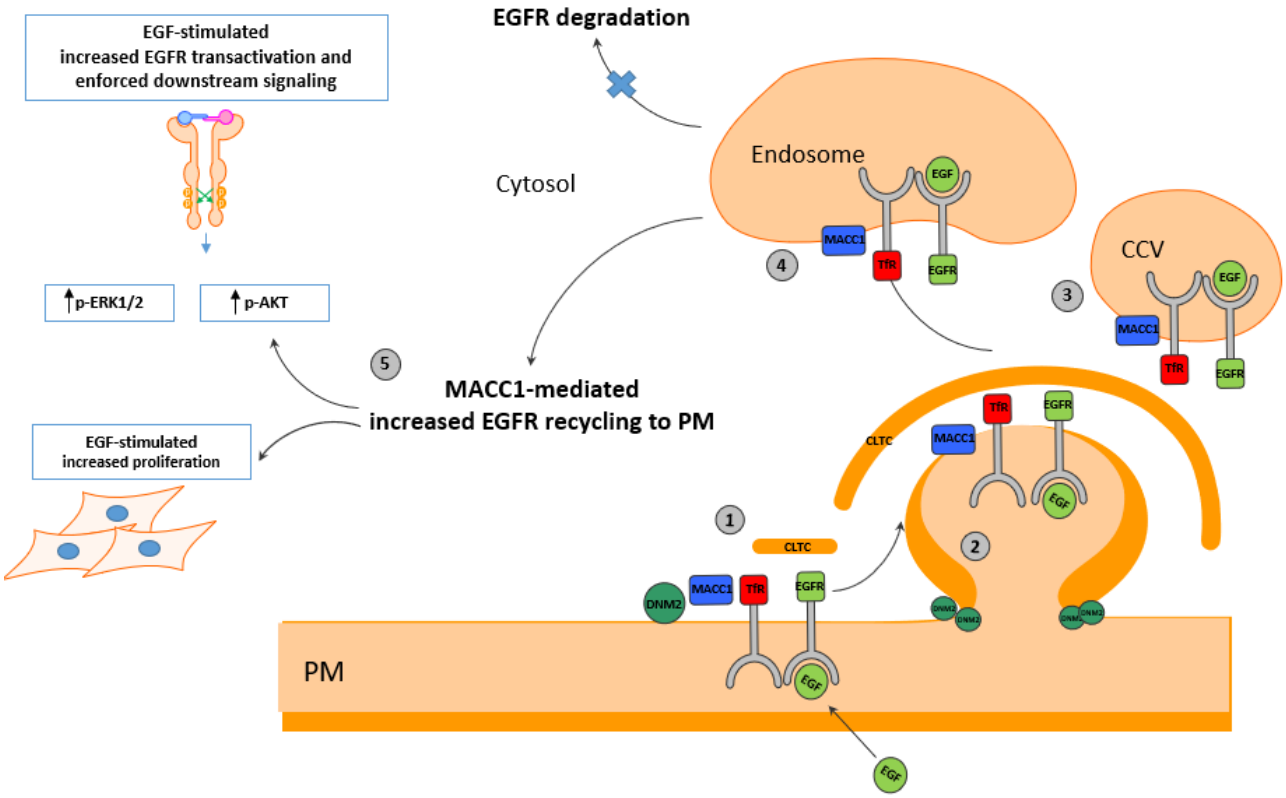

Figure 42 Investigating MACC1's role during EGFR endocytic traffic. (1) After EGF-triggered EGFR internalization, EGFR and TFR were found colocalizing in MACC1 overexpressing cell in CCPs and CCVs, (3-4) we speculate that MACC1 might travel together with the receptors after stimulation, probably via its interaction with TfR (established in the previous model) and its suggested shuttling in CCV-TfR marked vesicles and TfR-marked endosomes. (4) Probably MACC1 recruitment to the TfR-EGFR multicomplex mediates a faster recycling of EGFR to PM after stimulated internalization. Further studies are needed to dissect where and how, MACC1 intervenes during EGFR internalization to increase EGFR recycling to PM, probably decreasing its degradation (5) As result, MACC1 overexpression prolongs EGFR transphosphorylation for 30 minutes after EGF-stimulated internalization. Furthermore, MACC1 increases AKT downstream activation and mildly also ERK1/2 downstream activation, globally resulting in increased EGF-stimulated proliferation.

5.12 Future outlook

SH3BP4 has been characterized as taking part in TfR internalization and switching the fate of FGFR between degradation and recycling upon ligand-specific stimulation[121,122]. MACC1 is involved in CME and was found to regulate TfR internalization and recycling. We also found that in the presence of MACC1, EGF stimulation causes TfR and EGFR to follow the same early endocytic pathway, revealing an increased delivery of EGF to acidic compartments. We clarified that the overexpression of MACC1 is able to increase the recycling of EGFR, which partially explains this increase in the delivery of EGF. More interestingly, MACC1 overexpression increases the transactivation of EGFR upon ligand stimulation and leads to sustained EGF-mediated proliferation (Fig. 40). MACC1 KD downregulates EGFR gene expression in SW620/sh MACC1 compared to SW620/sh control. We also detected (Supplementary Fig. 9) MACC1 and MET colocalizing at the PM after triggering the receptor with HGF for 5 min. MACC1's regulation of the HGF/c-MET axis was first identified in our lab, and constitutes the key regulator of the prognostic and metastatic driving feature of MACC1. With our preliminary evidence on MACC1's regulative role of TfR and EGFR, CME constitutes a new first line of investigation for the future, with a focus on the role of MACC1 during MET CME. Studying MACC1's role in MET's endocytic trafficking opens a potential field of research for new compounds and therapeutic strategies to intervene and target on MACC1-mediated endocytic signaling enforcement. Recycling in CME by coupling MACC1-targeted therapeutic strategies with those aiming to impair cancer-associated signaling may open an effective path toward improving the overall survival of CRC patients.

Bibliography

1. Ferlay, J. *et al.* Estimating the global cancer incidence and mortality in 2018: GLOBOCAN sources and methods. *Int. J. Cancer* ijc.31937 (2018). doi:10.1002/ijc.31937

2. American Cancer Society. Cancer Facts & Figures. *Cancer Journal for Clinicians* (2018). Available at: https://www.cancer.org/content/dam/cancer-org/research/cancer-facts-and-statistics/annual-cancer-facts-and-figures/2018/cancer-facts-and-figures-2018.pdf. (Toegang verkry: 12th Februarie 2019)

3. Torre, L. A. *et al.* Global cancer statistics, 2012. *CA. Cancer J. Clin.* **65,** 87–108 (2015).

4. Lessons from Hereditary Review Colorectal Cancer.

5. Migliore, L., Migheli, F., Spisni, R. & Copped, F. Genetics, cytogenetics, and epigenetics of colorectal cancer. *J. Biomed. Biotechnol.* **2011,** (2011).

6. Ma, H. *et al.* Pathology and genetics of hereditary colorectal cancer. *Pathology* **50,** 49–59 (2018).

7. Markowitz, S. D. & Bertagnolli, M. M. *Molecular Basis of Colorectal Cancer*.

8. Gamage, S. M. K., Dissabandara, L., Lam, A. K.-Y. & Gopalan, V. The role of heme iron molecules derived from red and processed meat in the pathogenesis of colorectal carcinoma. *Crit. Rev. Oncol. Hematol.* **126,** 121–128 (2018).

9. Kruger, C. & Zhou, Y. Red meat and colon cancer: A review of mechanistic evidence for heme in the context of risk assessment methodology. *Food Chem. Toxicol.* **118,** 131–153 (2018).

10. Bastide, N. M., Pierre, F. H. F. & Corpet, D. E. Heme Iron from Meat and Risk of Colorectal Cancer: A Meta-analysis and a Review of the Mechanisms Involved. *Cancer Prev. Res.* **4,** 177–184 (2011).

11. Markowitz, S. DNA repair defects inactivate tumor suppressor genes and induce hereditary and sporadic colon cancers. *J. Clin. Oncol.* **18,** 75S–80S (2000).

12. Perucho, M. Tumors with microsatellite instability: many mutations, targets and paradoxes. *Oncogene 2003 2215* (2003).

13. Fearnhead, N. S., Wilding, J. L. & Bodmer, W. F. Genetics of colorectal cancer: Hereditary aspects and overview of colorectal tumorigenesis. *Br. Med. Bull.* **64,** 27–43 (2002).

14. Groden, J. *et al.* Identification and characterization of the familial adenomatous polyposis coli gene. *Cell* **66,** 589–600 (1991).

15. Bodmer, W. F. *et al.* Localization of the gene for familial adenomatous polyposis on chromosome 5. *Nature* **328,** 614–616 (1987).

16. Munemitsu, S., Albert, I., Souza, B., Rubinfeld, B. & Polakis, P. Regulation of intracellular beta-catenin levels by the adenomatous polyposis coli (APC) tumor-suppressor protein. *Proc. Natl. Acad. Sci. U. S. A.* **92,** 3046–50 (1995).

17. Aberle, H., Bauer, A., Stappert, J., Kispert, A. & Kemler, R. beta-catenin is a target for the ubiquitin-proteasome pathway. *EMBO J.* **16,** 3797–804 (1997).

18. Schuijers, J., Mokry, M., Hatzis, P., Cuppen, E. & Clevers, H. Wnt-induced transcriptional activation is exclusively mediated by TCF/LEF. *EMBO J.* **33,** 146–156 (2014).

19. Walther, A. *et al.* Genetic prognostic and predictive markers in colorectal cancer. *Nat. Rev. Cancer* **9,** 489–99 (2009).

20. Valtorta, E. *et al.* KRAS gene amplification in colorectal cancer and impact on response to EGFR-targeted therapy. *Int. J. Cancer* **133,** 1259–1265 (2013).

21. Sundaram, M. RTK/Ras/MAPK signaling. *WormBook* 1–19 (2006). doi:10.1895/wormbook.1.80.1

22. Caldieri, G., Malabarba, M. G., Di Fiore, P. P. & Sigismund, S. EGFR Trafficking in Physiology and Cancer. in 235–272 (2018). doi:10.1007/978-3-319-96704-2_9

23. Hubbard, S. R. EGF Receptor Activation: Push Comes to Shove. *Cell* **125,** 1029–1031 (2006).

24. Walther, A. *et al.* Genetic prognostic and predictive markers in colorectal cancer. *Nat. Rev. Cancer* **9,** 489–499 (2009).

25. Haigis, K. M. *et al.* Differential effects of oncogenic K-Ras and N-Ras on proliferation, differentiation and tumor progression in the colon. *Nat. Genet.* **40,** 600–608 (2008).

26. Bos, J. L. *et al.* Prevalence of ras gene mutations in human colorectal cancers. *Nature* **327,** 293–297 (1987).

27. Li, W. *et al.* Colorectal carcinomas with KRAS codon 12 mutation are associated with more advanced tumor stages. *BMC Cancer* **15,** 340 (2015).

28. Valentini, A. M., Cavalcanti, E., Di Maggio, M. & Caruso, M. L. RAS-expanded Mutations and

HER2 Expression in Metastatic Colorectal Cancer. *Appl. Immunohistochem. Mol. Morphol.* **26,** 1 (2017).

29. Akiyoshi, K. *et al.* A Prospective, Multicenter Phase II Study of the Efficacy and Feasibility of 15-minute Panitumumab Infusion Plus Irinotecan for Oxaliplatin- and Irinotecan-refractory, KRAS Wild-type Metastatic Colorectal Cancer (Short Infusion of Panitumumab Trial). *Clin. Colorectal Cancer* **17,** e83–e89 (2018).

30. Wojas-Krawczyk, K. *et al.* Analysis of KRAS, NRAS, BRAF, and PIK3CA mutations could predict metastases in colorectal cancer: A preliminary study. *Adv. Clin. Exp. Med.* (2018). doi:10.17219/acem/76162

31. Amado, R. G. *et al.* Wild-Type *KRAS* Is Required for Panitumumab Efficacy in Patients With Metastatic Colorectal Cancer. *J. Clin. Oncol.* **26,** 1626–1634 (2008).

32. De Roock, W. *et al.* Association of KRAS p.G13D Mutation With Outcome in Patients With Chemotherapy-Refractory Metastatic Colorectal Cancer Treated With Cetuximab. *JAMA* **304,** 1812 (2010).

33. Koch, C. *et al.* Anti-EGF Receptor-Based Conversion Chemotherapy in RAS Wild-Type Colorectal Cancer Patients: Impact on Survival and Resection Rates. *Digestion* **98,** 263–269 (2018).

34. Marcel, V., Nguyen Van Long, F. & Diaz, J.-J. 40 Years of Research Put p53 in Translation. *Cancers (Basel).* **10,** 152 (2018).

35. Fischer, M. Census and evaluation of p53 target genes. *Oncogene* **36,** 3943–3956 (2017).

36. Zilfou, J. T. & Lowe, S. W. Tumor suppressive functions of p53. *Cold Spring Harb. Perspect. Biol.* **1,** a001883 (2009).

37. Baugh, E. H., Ke, H., Levine, A. J., Bonneau, R. A. & Chan, C. S. Why are there hotspot mutations in the TP53 gene in human cancers? *Cell Death Differ.* **25,** 154–160 (2018).

38. Salvador, J. M., Brown-Clay, J. D. & Fornace, A. J. Gadd45 in Stress Signaling, Cell Cycle Control, and Apoptosis. in 1–19 (Springer, New York, NY, 2013). doi:10.1007/978-1-4614-8289-5_1

39. Taylor, W. R. & Stark, G. R. Regulation of the G2/M transition by p53. *Oncogene* **20,** 1803–1815 (2001).

40. Li, X.-L., Zhou, J., Chen, Z.-R. & Chng, W.-J. *p53* mutations in colorectal cancer- molecular

pathogenesis and pharmacological reactivation. *World J. Gastroenterol.* **21,** 84 (2015).

41. Vogelstein, B. *et al.* Genetic Alterations during Colorectal-Tumor Development. *N. Engl. J. Med.* **319,** 525–532 (1988).

42. Popat, S. & Houlston, R. S. A systematic review and meta-analysis of the relationship between chromosome 18q genotype, DCC status and colorectal cancer prognosis. *Eur. J. Cancer* **41,** 2060–2070 (2005).

43. Fleming, N. I. *et al.* SMAD2, SMAD3 and SMAD4 Mutations in Colorectal Cancer. *Cancer Res.* **73,** 725–735 (2013).

44. Heldin, C.-H., Miyazono, K. & ten Dijke, P. TGF-β signalling from cell membrane to nucleus through SMAD proteins. *Nature* **390,** 465–471 (1997).

45. Villalba, M., Evans, S. R., Vidal-Vanaclocha, F. & Calvo, A. Role of TGF-β in metastatic colon cancer: it is finally time for targeted therapy. doi:10.1007/s00441-017-2633-9

46. Derynck, R. & Zhang, Y. E. *Smad-dependent and Smad-independent pathways in TGF-b family signalling*. (2003).

47. Xie, W., Rimm, D. L., Lin, Y., Shih, W. J. & Reiss, M. Loss of Smad signaling in human colorectal cancer is associated with advanced disease and poor prognosis. *Cancer J.* **9,** 302–12

48. Todosi, A.-M., Gavrilescu, M.-M., Aniţei, G.-M., Filip, B. & Scripcariu, V. Colon cancer at the molecular level--usefulness of epithelial-mesenchymal transition analysis. *Rev. Med. Chir. Soc. Med. Nat. Iasi* **116,** 1106–11

49. McKeown, E. *et al.* Current approaches and challenges for monitoring treatment response in colon and rectal cancer. *J. Cancer* **5,** 31–43 (2014).

50. Quirke, P., Risio, M., Lambert, R., von Karsa, L. & Vieth, M. Quality assurance in pathology in colorectal cancer screening and diagnosis—European recommendations. *Virchows Arch.* **458,** 1–19 (2011).

51. Haggar, F. A. & Boushey, R. P. Colorectal Cancer Epidemiology: Incidence, Mortality, Survival, and Risk Factors. doi:10.1055/s-0029-1242458

52. American Cancer Society. Cancer Facts & Figures, 2014. *Am. Cancer Soc.* (2014).

53. Hanahan, D. & Weinberg, R. A. Hallmarks of cancer: the next generation. *Cell* **144,** 646–74 (2011).

54. Aguirre-Ghiso, J. A. Models, mechanisms and clinical evidence for cancer dormancy. *Nat. Rev. Cancer* **7,** 834–46 (2007).

55. Jin K1, Gao W, Lu Y, Lan H, Teng L, C. F. Mechanisms regulating colorectal cancer cell metastasis into liver. doi:10.3892/ol.2011.432

56. Lamouille, S., Xu, J. & Derynck, R. Molecular mechanisms of epithelial–mesenchymal transition. *Nat. Rev. Mol. Cell Biol.* **15,** 178–196 (2014).

57. Huang, R. Y.-J., Guilford, P. & Thiery, J. P. Early events in cell adhesion and polarity during epithelial-mesenchymal transition. *J. Cell Sci.* **125,** 4417–4422 (2012).

58. Nisticò, P., Bissell, M. J. & Radisky, D. C. Epithelial-mesenchymal transition: general principles and pathological relevance with special emphasis on the role of matrix metalloproteinases. *Cold Spring Harb. Perspect. Biol.* **4,** a011908–a011908 (2012).

59. Yang, X., Pursell, B., Lu, S., Chang, T.-K. & Mercurio, A. M. Regulation of 4-integrin expression by epigenetic modifications in the mammary gland and during the epithelial-to-mesenchymal transition. *J. Cell Sci.* **122,** 2473–2480 (2009).

60. Makrodouli, E. *et al.* BRAF and RAS oncogenes regulate Rho GTPase pathways to mediate migration and invasion properties in human colon cancer cells: a comparative study. *Mol. Cancer* **10,** 118 (2011).

61. Lo, H.-W. *et al.* Epidermal Growth Factor Receptor Cooperates with Signal Transducer and Activator of Transcription 3 to Induce Epithelial-Mesenchymal Transition in Cancer Cells via Up-regulation of *TWIST* Gene Expression. *Cancer Res.* **67,** 9066–9076 (2007).

62. Lu, Z., Ghosh, S., Wang, Z. & Hunter, T. Downregulation of caveolin-1 function by EGF leads to the loss of E-cadherin, increased transcriptional activity of β-catenin, and enhanced tumor cell invasion. *Cancer Cell* **4,** 499–515 (2003).

63. TNM | UICC. Available at: https://www.uicc.org/resources/tnm. (Toegang verkry: 24th Januarie 2019)

64. Edge, S. B. & Compton, C. C. The American Joint Committee on Cancer: the 7th Edition of the AJCC Cancer Staging Manual and the Future of TNM. *Ann. Surg. Oncol.* **17,** 1471–1474 (2010).

65. Meyerhardt, J. A. & Mayer, R. J. Systemic Therapy for Colorectal Cancer. *N. Engl. J. Med.* **352,** 476–487 (2005).

66. Saltz, L. B. *et al.* Bevacizumab in Combination With Oxaliplatin-Based Chemotherapy As First-

Line Therapy in Metastatic Colorectal Cancer: A Randomized Phase III Study. *J Clin Oncol* **26,** 2013–2019

67. Hurwitz, H. *et al.* Bevacizumab plus Irinotecan, Fluorouracil, and Leucovorin for Metastatic Colorectal Cancer. *N. Engl. J. Med.* **350,** 2335–2342 (2004).

68. Lockhart, C. & Berlin, J. D. The epidermal growth factor receptor as a target for colorectal cancer therapy. *Semin. Oncol.* **32,** 52–60 (2005).

69. Krens, L. L., Baas, J. M., Gelderblom, H. & Guchelaar, H.-J. Therapeutic modulation of k-ras signaling in colorectal cancer. *Drug Discov. Today* **15,** 502–16 (2010).

70. Misale, S. *et al.* Emergence of KRAS mutations and acquired resistance to anti-EGFR therapy in colorectal cancer. *Nature* **486,** (2012).

71. Stein, U. MACC1 - a novel target for solid cancers. *Expert Opin. Ther. Targets* **17,** 1039–52 (2013).

72. Meng, F. *et al.* MACC1 Down-Regulation Inhibits Proliferation and Tumourigenicity of Nasopharyngeal Carcinoma Cells through Akt/β-Catenin Signaling Pathway. *PLoS One* **8,** e60821 (2013).

73. Hu, H. *et al.* Metastasis-Associated in Colon Cancer 1 Is a Novel Survival-Related Biomarker for Human Patients with Renal Pelvis Carcinoma. *PLoS One* **9,** e100161 (2014).

74. Zhou, X. *et al.* Metastasis-Associated in Colon Cancer-1 Associates With Poor Prognosis and Promotes Cell Invasion and Angiogenesis in Human Cervical Cancer. *Int. J. Gynecol. Cancer* **25,** 1353–1363 (2015).

75. Wang, L. *et al.* Metastasis-associated in colon cancer-1 upregulation predicts a poor prognosis of gastric cancer, and promotes tumor cell proliferation and invasion. *Int. J. Cancer* **133,** 1419–1430 (2013).

76. Li, H. *et al.* Overexpression of MACC1 and the association with hepatocyte growth factor/c-Met in epithelial ovarian cancer. *Oncol. Lett.* **9,** 1989–1996 (2015).

77. Zhu, M. *et al.* Overexpression of Metastasis-Associated in Colon Cancer-1 Associated with Poor Prognosis in Patients with Esophageal Cancer. *Pathol. Oncol. Res.* **19,** 749–753 (2013).

78. Ma, J., Ma, J., Meng, Q., Zhao, Z.-S. & Xu, W.-J. Prognostic Value and Clinical Pathology of MACC-1 and c-MET Expression in Gastric Carcinoma. *Pathol. Oncol. Res.* **19,** 821–832 (2013).

79. Huang, N. *et al.* MiR-338-3p inhibits epithelial-mesenchymal transition in gastric cancer cells

by targeting ZEB2 and MACC1/Met/Akt signaling. *Oncotarget* **6,** 15222–15234 (2015).

80. Mudduluru, G., Ilm, K., Dahlmann, M. & Stein, U. MACC1, a Novel Player in Solid Cancer Carcinogenesis. in *Mechanisms of Molecular Carcinogenesis – Volume 1* 11–38 (Springer International Publishing, 2017). doi:10.1007/978-3-319-53659-0_2

81. Pichorner, A. *et al.* In vivo imaging of colorectal cancer growth and metastasis by targeting MACC1 with shRNA in xenografted mice. *Clin. Exp. Metastasis* **29,** 573–83 (2012).

82. Wang, G., Gu, J. & Gao, Y. MicroRNA target for MACC1 and CYR61 to inhibit tumor growth in mice with colorectal cancer. *Tumour Biol.* **37,** 13983–13993 (2016).

83. Lemos, C. *et al.* MACC1 Induces Tumor Progression in Transgenic Mice and Colorectal Cancer Patients via Increased Pluripotency Markers Nanog and Oct4. *Clin. Cancer Res.* **22,** 2812–24 (2016).

84. Chen, Z. M., Shi, H. R., Li, X., Deng, Y. X. & Zhang, R. T. Downregulation of MACC1 expression enhances cisplatin sensitivity in SKOV-3/DDP cells. *funpecrp.com.br Genet. Mol. Res. Genet. Mol. Res* **14,** 17134–17144 (2015).

85. Wang, C. *et al.* MACC1 mediates chemotherapy sensitivity of 5-FU and cisplatin via regulating MCT1 expression in gastric cancer. *Biochem. Biophys. Res. Commun.* **485,** 665–671 (2017).

86. ZHANG, R. *et al.* Knockdown of MACC1 expression increases cisplatin sensitivity in cisplatin-resistant epithelial ovarian cancer cells. *Oncol. Rep.* **35,** 2466–2472 (2016).

87. Li, H.-F. *et al.* Downregulation of MACC1 inhibits invasion, migration and proliferation, attenuates cisplatin resistance and induces apoptosis in tongue squamous cell carcinoma. *Oncol. Rep.* **33,** 561–660 (2015).

88. Juneja, M. *et al.* Statin and rottlerin small-molecule inhibitors restrict colon cancer progression and metastasis via MACC1. *PLoS Biol.* **15,** e2000784 (2017).

89. Stein, U. *et al.* MACC1, a newly identified key regulator of HGF-MET signaling, predicts colon cancer metastasis. *Nat. Med.* **15,** 59–67 (2009).

90. Kokoszyńska, K., Kryński, J., Rychlewski, L. & Wyrwicz, L. S. Unexpected domain composition of MACC1 links MET signaling and apoptosis. *Acta Biochim. Pol.* **56,** 317–324 (2009).

91. Stein, U., Dahlmann, M. & Walther, W. MACC1 - more than metastasis? Facts and predictions about a novel gene. *J. Mol. Med. (Berl).* **88,** 11–8 (2010).

92. Wang, Z. *et al.* Requirement for the adapter protein GRB2 in EGF receptor endocytosis.

Science **272,** 1935–9 (1996).

93. Seedorf, K. *et al.* Dynamin binds to SH3 domains of phospholipase C gamma and GRB-2. *J. Biol. Chem.* **269,** 16009–16014 (1994).

94. Wang, L. *et al.* Metastasis-associated in colon cancer-1 promotes vasculogenic mimicry in gastric cancer by upregulating TWIST1/2. *Oncotarget* **6,** 11492–11506 (2015).

95. Wang, L. *et al.* MACC-1 Promotes Endothelium-Dependent Angiogenesis in Gastric Cancer by Activating TWIST1/VEGF-A Signal Pathway. *PLoS One* **11,** e0157137 (2016).

96. Zhen, T. *et al.* MACC1 promotes carcinogenesis of colorectal cancer via β-catenin signaling pathway. **5,** (2014).

97. Zhou, W. *et al.* Combination of Endothelial-Monocyte-Activating Polypeptide-II with Temozolomide Suppress Malignant Biological Behaviors of Human Glioblastoma Stem Cells via miR-590-3p/MACC1 Inhibiting PI3K/AKT/mTOR Signal Pathway. *Front. Mol. Neurosci.* **10,** 68 (2017).

98. Liu, J. *et al.* A new mechanism of trastuzumab resistance in gastric cancer: MACC1 promotes the Warburg effect via activation of the PI3K/AKT signaling pathway. *J. Hematol. Oncol.* **9,** 76 (2016).

99. Migliore, C. *et al.* MiR-1 downregulation cooperates with MACC1 in promoting MET overexpression in human colon cancer. *Clin. Cancer Res.* **18,** 737–47 (2012).

100. Wang, G. *et al. MACC1: A potential molecule associated with pancreatic cancer metastasis and chemoresistance*. *Oncology Letters* **4,** ([Spandidos Publications], 2012).

101. Li, S., Zhu, J., Li, J., Li, S. & Li, B. MicroRNA-141 inhibits proliferation of gastric cardia adenocarcinoma by targeting MACC1. *Arch. Med. Sci.* **13,** (2017).

102. Kim, G.-E., Lee, J. S., Park, M. H. & Yoon, J. H. Metastasis associated in colon cancer 1 predicts poor outcomes in patients with breast cancer. *Anal. Quant. Cytopathol. Histopathol.* **37,** 96–104 (2015).

103. Shirahata, A. *et al.* MACC 1 as a marker for vascular invasive hepatocellular carcinoma. *Anticancer Res.* **31,** 777–80 (2011).

104. Li, H. *et al.* The expression of MACC1 and its role in the proliferation and apoptosis of salivary adenoid cystic carcinoma. *J. Oral Pathol. Med.* **44,** 810–817 (2015).

105. Jin, Z. *et al.* Increased expression of metastasis-associated in colon cancer-1 in renal cell

carcinoma is associated with poor prognosis. *Int J Clin Exp Pathol* **8,** 3857–3863 (2015).

106. Guo, L., Lu, W., Zhang, X., Luo, D. & Zhang, H. Metastasis-associated colon cancer-1 is a novel prognostic marker for cervical cancer. *Int. J. Clin. Exp. Pathol.* **7,** 4150–5 (2014).

107. Jian Wu Dawei Zhang Jun Li Xin Deng Guannan Liang Yang Long Xuemei He Tianyang Dai Delian Ren *et al. MACC1 induces autophagy to regulate proliferation, apoptosis, migration and invasion of squamous cell carcinoma*. *Oncology Reports* **38,** ([National Hellenic Research Foundation], 1994).

108. Acunzo, M., Romano, G., Wernicke, D. & Croce, C. M. MicroRNA and cancer – A brief overview. *Adv. Biol. Regul.* **57,** 1–9 (2015).

109. Pan, T. *et al.* miR-944 inhibits metastasis of gastric cancer by preventing the epithelial-mesenchymal transition via MACC1/Met/AKT signaling. *FEBS Open Bio* **7,** 905–914 (2017).

110. Li, J., Mao, X., Wang, X., Miao, G. & Li, J. miR-433 reduces cell viability and promotes cell apoptosis by regulating MACC1 in colorectal cancer. *Oncol. Lett.* **13,** 81–88 (2016).

111. Cui, Z., Tang, J., Chen, J. & Wang, Z. Hsa-miR-574-5p negatively regulates MACC-1 expression to suppress colorectal cancer liver metastasis. *Cancer Cell Int.* **14,** 47 (2014).

112. Shang, C., Hong, Y., Guo, Y. & Xue, Y. Mir-338-3p Inhibits Malignant Biological Behaviors of Glioma Cells by Targeting MACC1 Gene. *Med. Sci. Monit.* **22,** 710–6 (2016).

113. Zhang, T. *et al.* Down-regulation of microRNA-338-3p promoted angiogenesis in hepatocellular carcinoma. *Biomed. Pharmacother.* **84,** 583–591 (2016).

114. Dunlevy, J. R., Berryhill, B. L., Vergnes, J.-P., Sundarraj, N. & Hassell, J. R. Cloning, Chromosomal Localization, and Characterization of cDNA from a Novel Gene, SH3BP4, Expressed by Human Corneal Fibroblasts.

115. Dunlevy, J. R., Berryhill, B. L., Vergnes, J. P., SundarRaj, N. & Hassell, J. R. Cloning, chromosomal localization, and characterization of cDNA from a novel gene, SH3BP4, expressed by human corneal fibroblasts. *Genomics* **62,** 519–24 (1999).

116. Association for Research in Vision and Ophthalmology., K., Tesluk, L., Kolberg, J. B. & Dunlevy, J. R. The Subcellular Localization of SH3BP4 in Human Retinal Pigment Epithelial and COS-7 Cell Lines. in *Investigative Ophthalmology & Visual Science* **44,** 4544–4544 (C.V. Mosby Co, 1977).

117. Association for Research in Vision and Ophthalmology., J. R., Koppelman, E. D. & Kolberg, J. B.

The Expression of a SH3BP4–Related Protein in Retinal Cells. in *Investigative Ophthalmology & Visual Science* **46,** 2996–2996 (C.V. Mosby Co, 1977).

118. Association for Research in Vision and Ophthalmology., E. D., Kolberg, J. B. & Dunlevy, J. R. Characterization of the Novel Protein SH3BP4 Death Domain during Oxidant-induced Apoptosis in Human Pigment Epithelial (ARPE-19) Cells. in *Investigative Ophthalmology & Visual Science* **44,** 4545–4545 (C.V. Mosby Co, 1977).

119. Fu, H., Subramanian, R. R. & Masters, S. C. 14-3-3 Proteins: Structure, Function, and Regulation. *Annu. Rev. Pharmacol. Toxicol.* **40,** 617–647 (2000).

120. Kornnika Khanobdee,1,2 Jon B. Kolberg, 1 & Jane R. Dunlevy1. Nuclear and plasma membrane localization of SH3BP4 in retinal pigment epithelial cells. *Mol. Vis.* **10,** 933–42 (2004).

121. Tosoni, D. *et al.* TTP specifically regulates the internalization of the transferrin receptor. *Cell* **123,** 875–888 (2005).

122. Francavilla, C. *et al.* Functional proteomics defines the molecular switch underlying FGF receptor trafficking and cellular outputs. *Mol. Cell* **51,** 707–22 (2013).

123. Kim, K.-H., Lee, T. R. & Cho, E.-G. SH3BP4, a novel pigmentation gene, is inversely regulated by miR-125b and MITF. *Exp. Mol. Med.* **49,** e367 (2017).

124. Kiss, A. L. & Botos, E. Endocytosis via caveolae: alternative pathway with distinct cellular compartments to avoid lysosomal degradation? *J. Cell. Mol. Med.* **13,** 1228–37 (2009).

125. Nabi, I. R. & Le, P. U. Caveolae/raft-dependent endocytosis. *J. Cell Biol.* **161,** 673–7 (2003).

126. Lundmark, R. *et al.* The GTPase-Activating Protein GRAF1 Regulates the CLIC/GEEC Endocytic Pathway. *Curr. Biol.* **18,** 1802–1808 (2008).

127. Doherty, G. J. & Lundmark, R. GRAF1-dependent endocytosis. *Biochem. Soc. Trans.* **37,** 1061–5 (2009).

128. Glebov, O. O., Bright, N. A. & Nichols, B. J. Flotillin-1 defines a clathrin-independent endocytic pathway in mammalian cells. *Nat. Cell Biol.* **8,** 46–54 (2006).

129. CD Souza-Schorey, G Li, MI Colombo, P. S. A regulatory Role for Arf6 in Receptor-mediated Endocytosis.

130. Sigismund, S. *et al.* Clathrin-Mediated Internalization Is Essential for Sustained EGFR Signaling but Dispensable for Degradation. *Dev. Cell* **15,** 209–219 (2008).

131. McMahon, H. T. & Boucrot, E. Molecular mechanism and physiological functions of clathrin-mediated endocytosis. *Nat. Rev. Mol. Cell Biol.* **12,** 517–533 (2011).

132. Doherty, G. J. & Mcmahon, H. T. Mechanisms of Endocytosis. (2009). doi:10.1146/annurev.biochem.78.081307.110540

133. Edeling, M. A., Smith, C. & Owen, D. Life of a clathrin coat: insights from clathrin and AP structures. *Nat. Rev. Mol. Cell Biol.* **7,** 32–44 (2006).

134. Ford, M. G. J. *et al.* Curvature of clathrin-coated pits driven by epsin. *Nature* **419,** 361–366 (2002).

135. Yamabhai, M. *et al.* Intersectin, a novel adaptor protein with two Eps15 homology and five Src homology 3 domains. *J. Biol. Chem.* **273,** 31401–7 (1998).

136. Henne, W. M. *et al.* FCHo proteins are nucleators of clathrin-mediated endocytosis. *Science* **328,** 1281–4 (2010).

137. Maib, H., Smythe, E. & Ayscough, K. Forty years on: clathrin-coated pits continue to fascinate. *Mol. Biol. Cell* **28,** 843–847 (2017).

138. Kirchhausen, T., Owen, D. & Harrison, S. C. Molecular Structure, Function, and Dynamics of Clathrin-Mediated Membrane Traffic. *Cold Spring Harb. Perspect. Biol.* **6,** a016725–a016725 (2014).

139. McMahon, H. T. & Boucrot, E. Molecular mechanism and physiological functions of clathrin-mediated endocytosis. *Nat. Rev. Mol. Cell Biol.* **12,** 517–533 (2011).

140. Bridge, J. A. *et al. Short Communication Fusion of the ALK Gene to the Clathrin Heavy Chain Gene, CLTC, in Inflammatory Myofibroblastic Tumor*. *The American Journal of Pathology* **159,** (2001).

141. Keen, J. H., Willingham, M. C. & Pastan, I. H. Clathrin-coated vesicles: Isolation, dissociation and factor-dependent reassociation of clathrin baskets. *Cell* **16,** 303–312 (1979).

142. Robinson, M. S. Forty Years of Clathrin-coated Vesicles. *Traffic* **16,** 1210–1238 (2015).

143. van Dam, E. M. & Stoorvogel, W. Dynamin-dependent Transferrin Receptor Recycling by Endosome-derived Clathrin-coated Vesicles. *Mol. Biol. Cell* **13,** 169–182 (2002).

144. Ramachandran, R. & Schmid, S. L. The dynamin superfamily. *Curr. Biol.* **28,** R411–R416 (2018).

145. Faelber, K. *et al.* Structural insights into dynamin-mediated membrane fission. *Structure* **20,**

1621–8 (2012).

146. Sousa, L. P. *et al.* Suppression of EGFR endocytosis by dynamin depletion reveals that EGFR signaling occurs primarily at the plasma membrane. *Proc. Natl. Acad. Sci. U. S. A.* **109,** 4419–24 (2012).

147. Schlunck, G. Modulation of Rac Localization and Function by Dynamin. *Mol. Biol. Cell* **15,** 256–267 (2003).

148. Sousa, L. P. *et al.* Suppression of EGFR endocytosis by dynamin depletion reveals that EGFR signaling occurs primarily at the plasma membrane. *Proc. Natl. Acad. Sci. U. S. A.* **109,** 4419–24 (2012).

149. Zhang, Y. *et al.* Dynamin2 GTPase contributes to invadopodia formation in invasive bladder cancer cells. *Biochem. Biophys. Res. Commun.* **480,** 409–414 (2016).

150. Meng, J. Distinct functions of dynamin isoforms in tumorigenesis and their potential as therapeutic targets in cancer. *Oncotarget* **8,** 41701–41716 (2017).

151. Sever, S. & Schiffer, M. Actin dynamics at focal adhesions: a common endpoint and putative therapeutic target for proteinuric kidney diseases. *Kidney Int.* **93,** 1298–1307 (2018).

152. Grassart, A. *et al.* Actin and dynamin2 dynamics and interplay during clathrin-mediated endocytosis. *J. Cell Biol.* **205,** 721–35 (2014).

153. Mosesson, Y., Mills, G. B. & Yarden, Y. Derailed endocytosis: an emerging feature of cancer. *Nat. Rev. Cancer* **8,** 835–50 (2008).

154. Disanza, A., Frittoli, E., Palamidessi, A. & Scita, G. Endocytosis and spatial restriction of cell signaling. *Mol. Oncol.* **3,** 280–296 (2009).

155. Barbieri, E., Di Fiore, P. P. & Sigismund, S. Endocytic control of signaling at the plasma membrane. *Curr. Opin. Cell Biol.* **39,** 21–27 (2016).

156. Miaczynska, M., Pelkmans, L. & Zerial, M. Not just a sink: Endosomes in control of signal transduction. *Curr. Opin. Cell Biol.* **16,** 400–406 (2004).

157. Aguet, F., Antonescu, C. N., Mettlen, M., Schmid, S. L. & Danuser, G. Advances in Analysis of Low Signal-to-Noise Images Link Dynamin and AP2 to the Functions of an Endocytic Checkpoint. *Dev. Cell* **26,** 279–291 (2013).

158. Wang, Y., Pennock, S., Chen, X. & Wang, Z. Endosomal signaling of epidermal growth factor receptor stimulates signal transduction pathways leading to cell survival. *Mol. Cell. Biol.* **22,**

7279–90 (2002).

159. Neckers, L. M. Regulation of Transferrin Receptor Expression and Control of Cell Growth. *Pathobiology* **59,** 11–18 (1991).

160. Andrews, N., Levy, J. E., Jin, O., Fujiwara, Y. & Kuo, F. Transferrin receptor is necessary for development of erythrocytes and the nervous system. *Nat. Genet.* **21,** 396–399 (1999).

161. Cheng, Y. *et al.* Structure of the Human Transferrin Receptor-Transferrin Complex Albert Einstein College of Medicine. *Cell* **116,** 565–576 (2004).

162. Daniels, T. R., Delgado, T., Rodriguez, J. A., Helguera, G. & Penichet, M. L. The transferrin receptor part I: Biology and targeting with cytotoxic antibodies for the treatment of cancer. *Clin. Immunol.* **121,** 144–158 (2006).

163. Habashy, H. O. *et al.* Transferrin receptor (CD71) is a marker of poor prognosis in breast cancer and can predict response to tamoxifen. *Breast Cancer Res. Treat.* **119,** 283–293 (2010).

164. Habeshaw, J. A., Lister, T. A., Stansfeld, A. G. & Greaves, M. F. CORRELATION OF TRANSFERRIN RECEPTOR EXPRESSION WITH HISTOLOGICAL CLASS AND OUTCOME IN NON-HODGKIN LYMPHOMA. *Lancet* **321,** 498–501 (1983).

165. Sutherland, R. *et al.* Ubiquitous cell-surface glycoprotein on tumor cells is proliferation-associated receptor for transferrin. *Proc. Natl. Acad. Sci. U. S. A.* **78,** 4515–9 (1981).

166. Chan, K. T. *et al.* Overexpression of transferrin receptor CD71 and its tumorigenic properties in esophageal squamous cell carcinoma. *Oncol. Rep.* **31,** 1296–304 (2014).

167. Ryschich, E. *et al.* Transferrin receptor is a marker of malignant phenotype in human pancreatic cancer and in neuroendocrine carcinoma of the pancreas. *Eur. J. Cancer* **40,** 1418–1422 (2004).

168. Xue, X. & Shah, Y. Intestinal Iron Homeostasis and Colon Tumorigenesis. *Nutrients* **5,** 2333–2351 (2013).

169. Okazaki, F. *et al.* Circadian Clock in a Mouse Colon Tumor Regulates Intracellular Iron Levels to Promote Tumor Progression *. doi:10.1074/jbc.M115.713412

170. Habashy, H. O. *et al.* Transferrin receptor (CD71) is a marker of poor prognosis in breast cancer and can predict response to tamoxifen. *Breast Cancer Res. Treat.* **119,** 283–293 (2010).

171. Mayle, K. M., Le, A. M. & Kamei, D. T. The intracellular trafficking pathway of transferrin ☆. *BBA - Gen. Subj.* **1820,** 264–281 (2012).

172. Steere, A. N., Byrne, S. L., Chasteen, N. D. & Mason, A. B. Kinetics of iron release from transferrin bound to the transferrin receptor at endosomal pH ☆. *BBA - Gen. Subj.* **1820,** 326–333 (2012).

173. Tortorella, S. & Karagiannis, T. C. Transferrin receptor-mediated endocytosis: A useful target for cancer therapy. *J. Membr. Biol.* **247,** 291–307 (2014).

174. Fonseca-Nunes, A., Jakszyn, P. & Agudo, A. Iron and Cancer Risk--A Systematic Review and Meta-analysis of the Epidemiological Evidence. *Cancer Epidemiol. Biomarkers Prev.* **23,** 12–31 (2014).

175. Ruder, E. H. *et al.* Dietary iron, iron homeostatic gene polymorphisms and the risk of advanced colorectal adenoma and cancer. *Carcinogenesis* **35,** 1276–1283 (2014).

176. Yeoman, L. C., Wan, C. W. & Zorbas, M. A. Transferrin and insulin enhance human colon tumor cell growth by differentiation class specific mechanisms. *Oncol.Res.* **8,** 273–279 (1996).

177. Prutki, M. *et al.* Altered iron metabolism, transferrin receptor 1 and ferritin in patients with colon cancer. *Cancer Lett.* **238,** 188–196 (2006).

178. Brookes, M. J. *et al.* Modulation of iron transport proteins in human colorectal carcinogenesis. *Gut* **55,** 1449–1460 (2006).

179. Tortorella, S. & Karagiannis, T. C. The Significance of Transferrin Receptors in Oncology: the Development of Functional Nano-based Drug Delivery Systems. *Curr. Drug Deliv.* **11,** 427–43 (2014).

180. Wells, A. *Molecules in focus: EGF receptor*.

181. Schlessinger, J. Ligand-Induced, Receptor-Mediated Dimerization and Activation of EGF Receptor. *Cell* **110,** 669–672 (2002).

182. Anthony R. French, Douglas K. Tadaki, S. K. N. and D. A. L. intracellular Trafficking of Epidermal Growth Factor Family Ligands Is Directly Influenced by the pH Sensitivity of the Receptor/Ligand Interaction.

183. Inger Helene Madshus, and E. S. Internalization and intracellular sorting of the EGF receptor: a model for understanding the mechanisms of receptor trafficking. doi:10.1242/jcs.050260

184. Haglund, K. *et al.* Multiple monoubiquitination of RTKs is sufficient for their endocytosis and degradation. *Nat. Cell Biol.* **5,** 461–466 (2003).

185. Baldys, A. & Raymond, J. R. Critical Role of ESCRT Machinery in EGFR Recycling. *Biochemistry*

48, 9321–9323 (2009).

186. Schmid L. Sandra, Christophe Lamaze, A. V. V. Control of EGF receptor signaling by clathrin-mediated endocytosis.

187. Wang, B. *et al.* EGFR regulates iron homeostasis to promote cancer growth through redistribution of transferrin receptor 1. *Cancer Lett.* **381,** 331–340 (2016).

188. Radhakrishnan, H. *et al.* MACC1-the first decade of a key metastasis molecule from gene discovery to clinical translation. *Cancer Metastasis Rev.* **37,** 805–820 (2018).

189. Wolf, J. *et al.* Role of EBAG9 protein in coat protein complex I-dependent glycoprotein maturation and secretion processes in tumor cells. *FASEB J.* **24,** 4000–4019 (2010).

190. Rappsilber, J., Mann, M. & Ishihama, Y. Protocol for micro-purification, enrichment, pre-fractionation and storage of peptides for proteomics using StageTips. *Nat. Protoc.* **2,** 1896–906 (2007).

191. Huang, D. W., Sherman, B. T. & Lempicki, R. A. Systematic and integrative analysis of large gene lists using DAVID bioinformatics resources. *Nat. Protoc.* **4,** 44–57 (2009).

192. Mellman, I. Endocytosis and molecular sorting. *Annu. Rev. Cell Dev. Biol.* **12,** 575–625 (1996).

193. Robinson, M. S. Forty Years of Clathrin-coated Vesicles. *Traffic* **16,** 1210–1238 (2015).

194. Huang, F., Khvorova, A., Marshall, W. & Sorkin, A. *Analysis of clathrin-mediated endocytosis of EGF receptor by RNA interference Downloaded from*. **5,** (JBC Papers in Press. Published on, 2004).

195. Chung, B. *et al.* Aberrant trafficking of NSCLC-associated EGFR mutants through the endocytic recycling pathway promotes interaction with Src@. *BMC Cell Biol.* **10,** 84 (2009).

196. Tartakoff, A. M. *Perturbation of Vesicular Traffic with the Carboxylic Ionophore Monensin*. *Cell* **32,**

197. Gui, A. *et al.* Impaired degradation followed by enhanced recycling of epidermal growth factor receptor caused by hypo-phosphorylation of tyrosine 1045 in RBE cells. doi:10.1186/1471-2407-12-179

198. Tosoni, D. *et al.* TTP specifically regulates the internalization of the transferrin receptor. *Cell* **123,** 875–888 (2005).

199. Zhang, C., Li, A., Zhang, X. & Xiao, H. A novel TIP30 protein complex regulates EGF receptor

signaling and endocytic degradation. *J. Biol. Chem.* **286,** 9373–81 (2011).

200. Fan, Y., Li, F. & Chen, D. Scavenger receptor-recognized and enzyme-responsive nanoprobe for fluorescent labeling of lysosomes in live cells. *Biomaterials* **35,** 7870–7880 (2014).

201. Kapellos, T. S. *et al.* A novel real time imaging platform to quantify macrophage phagocytosis. *Biochem. Pharmacol.* **116,** 107–119 (2016).

202. Topper, M. B., Tonra, J. R., Pytowski, B. & Eastman, S. W. Differentiation between the EGFR antibodies necitumumab, cetuximab, and panitumumab: Antibody internalization and EGFR degradation. *J. Clin. Oncol.* **29,** e13022–e13022 (2011).

203. Madshus, Inger Helene; Stang, E. Internalization and intracellular sorting of the EGF receptor: a model for understanding the mechanisms of receptor trafficking. doi:10.1242/jcs.050260

204. Anthony R. French, Douglas K. Tadaki, S. K. N. and D. A. L. Intracellular Trafficking of Epidermal Growth Factor Family Ligands Is Directly Influenced by the pH Sensitivity of the Receptor/Ligand Interaction.

205. Roepstorff, K. *et al.* Differential effects of EGFR ligands on endocytic sorting of the receptor. *Traffic* **10,** 1115–27 (2009).

206. Nishimura, Y., Takiguchi, S., Ito, S. & Itoh, K. K. EGF-stimulated AKT activation is mediated by EGFR recycling via an early endocytic pathway in a gefitinib-resistant human lung cancer cell line. *Int. J. Oncol.* **46,** 1721–9 (2015).

207. Bray, F. *et al.* Global cancer statistics 2018: GLOBOCAN estimates of incidence and mortality worldwide for 36 cancers in 185 countries. *CA. Cancer J. Clin.* **68,** 394–424 (2018).

208. Mettlen, M., Pucadyil, T., Ramachandran, R. & Schmid, S. L. Dissecting dynamin's role in clathrin-mediated endocytosis. *Biochem. Soc. Trans.* **37,** 1022–6 (2009).

209. Bitoun, M. *et al.* Dynamin 2 mutations associated with human diseases impair clathrin-mediated receptor endocytosis. *Hum. Mutat.* **30,** 1419–1427 (2009).

210. Ramachandran, R. & Schmid, S. L. The dynamin superfamily. *Curr. Biol.* **28,** R411–R416 (2018).

211. White, S., Miller, K., Hopkins, C. & Trowbridge, I. S. Monoclonal antibodies against defined epitopes of the human transferrin receptor cytoplasmic tail. *Biochim. Biophys. Acta - Mol. Cell Res.* **1136,** 28–34 (1992).

212. Schonteich, E. *et al.* The Rip11/Rab11-FIP5 and kinesin II complex regulates endocytic protein recycling. *J. Cell Sci.* **121,** 3824–33 (2008).

213. Le, N. T. V & Richardson, D. R. The role of iron in cell cycle progression and the proliferation of neoplastic cells.

214. Okazaki, F. *et al.* Circadian Clock in a Mouse Colon Tumor Regulates Intracellular Iron Levels to Promote Tumor Progression *. doi:10.1074/jbc.M115.713412

215. Stein, U. & Schlag, P. Clinical, Biological, and Molecular Aspects of Metastasis in Colorectal Cancer. in *Targeted Therapies in Cancer SE - 7* (red Dietel, M.) **176,** 61–80 (Springer Berlin Heidelberg, 2007).

216. Pantopoulos, K., Porwal, S. K., Tartakoff, A. & Devireddy, L. Mechanisms of Mammalian Iron Homeostasis. doi:10.1021/bi300752r

217. Hu, X., Fu, X., Wen, S., Zou, X. & Liu, Y. [Prognostic value of MACC1 and c-met expressions in non-small cell lung cancer]. *Zhongguo Fei Ai Za Zhi* **15,** 399–403 (2012).

218. Shirahata, A. *et al.* MACC 1 as a marker for vascular invasive hepatocellular carcinoma. *Anticancer Res.* **31,** 777–80 (2011).

219. Chen, S. *et al.* The role of metastasis-associated in colon cancer 1 (MACC1) in endometrial carcinoma tumorigenesis and progression. *Mol. Carcinog.* **56,** 1361–1371 (2017).

220. Hu, H. *et al.* Metastasis-Associated in Colon Cancer 1 Is a Novel Survival-Related Biomarker for Human Patients with Renal Pelvis Carcinoma. *PLoS One* **9,** e100161 (2014).

221. Kim, G.-E., Lee, J. S., Park, M. H. & Yoon, J. H. Metastasis associated in colon cancer 1 predicts poor outcomes in patients with breast cancer. *Anal. Quant. Cytopathol. Histopathol.* **37,** 96–104 (2015).

222. Wang, L. *et al.* Metastasis-associated in colon cancer-1 upregulation predicts a poor prognosis of gastric cancer, and promotes tumor cell proliferation and invasion. *Int. J. Cancer* **133,** 1419–1430 (2013).

223. Daniels, T. R., Delgado, T., Helguera, G. & Penichet, M. L. The transferrin receptor part II: targeted delivery of therapeutic agents into cancer cells. *Clin. Immunol.* **121,** 159–76 (2006).

224. El Hout, M., Dos Santos, L., Hamaï, A. & Mehrpour, M. A promising new approach to cancer therapy: Targeting iron metabolism in cancer stem cells. *Semin. Cancer Biol.* (2018). doi:10.1016/j.semcancer.2018.07.009

225. Sigismund, S. *et al.* Endocytosis and Signaling: Cell Logistics Shape the Eukaryotic Cell Plan. *Physiol. Rev.* **92,** 273–366 (2012).

226. Qing-Hai Ye, A. *et al.* GOLM1 Modulates EGFR/RTK Cell-Surface Recycling to Drive Hepatocellular Carcinoma Metastasis. *Cancer Cell* **30,** 444–458 (2016).

227. Nishimura, T. & Kaibuchi, K. Numb Controls Integrin Endocytosis for Directional Cell Migration with aPKC and PAR-3. doi:10.1016/j.devcel.2007.05.003

228. Parachoniak, C. A., Luo, Y., Abella, J. V., Keen, J. H. & Park, M. Article GGA3 Functions as a Switch to Promote Met Receptor Recycling, Essential for Sustained ERK and Cell Migration. *Dev. Cell* **20,** 751–763 (2011).

229. Schmid L. Sandra, Christophe Lamaze, A. V. V. Control of EGF receptor signaling by clathrin-mediated endocytosis.

230. Damke, H., Binns, D. D., Ueda, H., Schmid, S. L. & Baba, T. Dynamin GTPase Domain Mutants Block Endocytic Vesicle Formation at Morphologically Distinct Stages. *Mol. Biol. Cell* **12,** 2578–2589 (2001).

231. Cerveny, K. L. & Jensen, R. E. The WD-repeats of Net2p Interact with Dnm1p and Fis1p to Regulate Division of Mitochondria. *Mol. Biol. Cell* **14,** 4126–4139 (2003).

232. Sesaki, H., Southard, S. M., Yaffe, M. P. & Jensen, R. E. Mgm1p, a Dynamin-related GTPase, Is Essential for Fusion of the Mitochondrial Outer Membrane. *Mol. Biol. Cell* **14,** 2342–2356 (2003).

233. van Dam, E. M. & Stoorvogel, W. Dynamin-dependent Transferrin Receptor Recycling by Endosome-derived Clathrin-coated Vesicles. *Mol. Biol. Cell* **13,** 169–182 (2002).

234. Zhang, R. *et al.* Effects of metastasis-associated in colon cancer 1 inhibition by small hairpin RNA on ovarian carcinoma OVCAR-3 cells. *J. Exp. Clin. Cancer Res.* **30,** 83 (2011).

235. Hua, F.-F. *et al.* MiRNA-338-3p regulates cervical cancer cells proliferation by targeting MACC1 through MAPK signaling pathway. *Eur. Rev. Med. Pharmacol. Sci.* **21,** 5342–5352 (2017).

236. Zhang, K. *et al.* MACC1 is involved in the regulation of proliferation, colony formation, invasion ability, cell cycle distribution, apoptosis and tumorigenicity by altering Akt signaling pathway in human osteosarcoma. *Tumor Biol.* **35,** 2537–2548 (2014).

237. Muendlein, A. *et al.* Significant survival impact of MACC1 polymorphisms in HER2 positive breast cancer patients. *Eur. J. Cancer* **50,** 2134–2141 (2014).

238. Ji, D. *et al.* MACC1 expression correlates with PFKFB2 and survival in hepatocellular carcinoma. *Asian Pac. J. Cancer Prev.* **15,** 999–1003 (2014).

239. Joffre, C. *et al.* A direct role for Met endocytosis in tumorigenesis. *Nat. Cell Biol.* **13,** 827–837 (2011).

240. de Castro-Carpeño, J. *et al.* EGFR and colon cancer: a clinical view. *Clin. Transl. Oncol.* **10,** 6–13 (2008).

241. Mellman, I. & Yarden, Y. Endocytosis and Cancer. *Endocytosis* **5,** 1–24 (2014).

242. Caldieri, G., Malabarba, M. G., Di Fiore, P. P. & Sigismund, S. EGFR Trafficking in Physiology and Cancer. in 235–272 (2018). doi:10.1007/978-3-319-96704-2_9

243. Lemmon, M. A. & Schlessinger, J. Cell Signaling by Receptor Tyrosine Kinases. *Cell* **141,** 1117–1134 (2010).

244. Hubbard, S. R. EGF Receptor Activation: Push Comes to Shove. *Cell* **125,** 1029–1031 (2006).

245. Boardman, L. A. Overexpression of MACC1 leads to downstream activation of HGF/MET and potentiates metastasis and recurrence of colorectal cancer. *Genome Med.* **1,** 36 (2009).

246. Knoll, S. *et al.* E2F1 induces miR-224/452 expression to drive EMT through TXNIP downregulation. *EMBO Rep.* **15,** 1315–1329 (2014).

247. Yao, Y., Dou, C., Lu, Z., Zheng, X. & Liu, Q. MACC1 suppresses cell apoptosis in hepatocellular carcinoma by targeting the HGF/c-MET/AKT pathway. *Cell. Physiol. Biochem.* **35,** 983–996 (2015).

248. Zhen, T. *et al.* MACC1 promotes carcinogenesis of colorectal cancer via β-catenin signaling pathway. *Oncotarget* **5,** 3756–69 (2014).

249. Wang, G. *et al.* MACC1: A potential molecule associated with pancreatic cancer metastasis and chemoresistance. *Oncol. Lett.* **4,** 783–791 (2012).

250. Mellman, I. & Yarden, Y. Endocytosis and cancer. *Cold Spring Harb. Perspect. Biol.* **5,** a016949 (2013).

251. LI, H.-F. *et al.* Downregulation of MACC1 inhibits invasion, migration and proliferation, attenuates cisplatin resistance and induces apoptosis in tongue squamous cell carcinoma. *Oncol. Rep.* **33,** 561–660 (2015).

252. Sueta, A. *et al. Differential role of MACC1 expression and its regulation of the HGF/c-Met pathway between breast and colorectal cancer*. *International Journal of Oncology* **46,** (University of Crete, Faculty of Medicine, Laboratory of Clinical Virology, 2015).

Abbreviations

AP-2α	α Adaptor-related Protein complex-2 subunit alpha
APC	Adenomatous Polyposis Coli
apo-Tf	apo-Transferrin
ATM	serine-protein kinase ATM
BAR	Bin/amphiphysin/Rvs
bHLH	basic Helix Loop Helix
Cbl	E3 ubiquitin ligase CBL
CCP	Clathrin Coated Pit
CCV	Clathrin Coated Vesicle
CDK4/6/D	Cyclin-Dependent Kinase 4/6/D
CIN	Chromosomal Instability
CHC	Clathrin Heavy Chain
CLC	Clathrin Light Chain
CLTC	clathrin heavy chain 1
CME	Clathrin-Mediated Endocytosis
CRC	Colorectal Cancer
CTD	clathrin terminal domain
DAVID	Database for Annotation, Visualization, and Integrated Discovery
DCC	Deleted in CRC
DD	Death Domain
DNM2	Dynamin 2
DPF	α-adaptor complex protein binding motif
ECM	Extra Cellular Matrix
EEA1	Early Endosome Antigen 1
EGF	Epidermal Growth Factor
EGFR or ErbB-1	EGF Receptor
EMT	Epithelial Mesenchymal Transition
ERC	Endocytic Recycling Compartment
ESCRT	Endosomal Sorting Complexes Required for Transport

FAP	Familial Adenomatous Polyposis
FCHO1,2	F-BAR domain-containing Fer/Cip4 homology domain-only proteins 1 and 2
FGFR	Fibroblast Growth Factor Receptor
GAB1	GRB2 associated binding protein 1
GADD45A	Growth Arrest and DNA Damage Inducible Alpha
GAK	G-associated kinase
GRB2	Growth Factor Receptor Bound Protein 2
GSK3β	Glycogen Synthase Kinase 3 beta
GTPase	Guanosine Triphosphate hydrolase
HNPCC	Hereditary Non-polyposis Colorectal Cancer
h-Tf	holo-Transferrin
KRAS	GTPase Hras (RAS)
LAMP-1	Lysosome-Associated Membrane glycoProtein 1
LDLR	Low Density Lipoprotein Receptor
LOH	Loss Of Heterozygosity
MACC1	Metastasis Associated in Colon Cancer 1
MAPK	Mitogen-Activated Protein Kinase
MAPK2K	MAP kinase kinase
MAP3K	MAP kinase kinase kinase
MDM2	E3 ubiquitin-protein ligase Mdm2
MET	Hepatocyte Growth Factor Receptor
MYH	MutY Homologue gene
MLH1/2	Mismatch Repair Protein 1 and 2
MMP9/2	Matrix MetalloProteinase-9/2
MS	Mass Spectrometry
MVB	Multi Vesicular Bodies
NCE	Non-Clathrin Endocytosis
NLSC	Non-Small Cell Lung Cancer
NPF	Epsin homology (EH) binding motif
PIDD	p53-induced death domain protein 1
PI3K	Phosphatidylinositol-3 kinase

PIP_2	Phosphatidylinositol 4,5-bisphosphate
PM	Plasma Membrane
PTEN	Phosphatase and Tensin homolog (PTEN)
PRD	Proline-Rich Domain
p21	Cyclin-Dependent Kinase inhibitor 1
p53	Cellular tumor antigen p53
RAB11	Ras-related protein 11A
RE	Recycling Endosomes
Rip11/Fip5	Rab11-family-interacting protein 5
Rho	Ras homologue
ROS	Reactive Oxygen Species
RTK	Tyrosine-Kinase Receptor
SH3	Src Homology 3 domain
SNAIL	Zinc finger protein Snai1
SMAD	Small Mother Against Decapentaplegic protein
SOS	Guanine Nucleotide Exchange Factor
SRC	Proto-oncogene tyrosine kinase
TCF/LEF	T-cell factor/lymphoid enhancer-binding factor
TfR	Transferrin Receptor
TGFα	Transforming Growth Factor α
TTP	Transferrin Trafficking Protein
TWIST	Twist-related Protein 1 (bHLH)
p53	Tumor Protein p53
UICC	Union for International Cancer Control
UPA	uncoordinated-5, p53-induced death domain protein 1 and ankyrins domain
VEGFR	Vascular Endothelial Growth Factor Receptor
Wnt	Int1 and Wingless
ZEB	Zinc finger E-box-Binding homeobox 1
ZO-1	Zona Occludens 1

Acknowledgements

I would like to warmly thank my research supervisor, Prof. Dr. Ulrike Stein, for giving me the opportunity to work in her group and the opportunity to develop this thesis with the freedom that only Science can provide. Sincere thanks to Dr. Dahlmann for the interest throughout the course of the investigation and in the manuscript.

A special and sincere “grazie” goes to Prof. Dr. Wolfgang Walther for his scientific questions and valuable discussions in every lab meeting. Above all, the daily and warmly “buongiorno” along the years which have been lighting up my days and made me feel at home when homesick.

My most heart felt acknoledgment to our collaborator Dr. Armin Rehm for the smart, puctual, and precise scientific discussions and for his inspiring considerations and encouragments along the years. His valuable mentorship led me to feel a very lucky and appreciated student and most importantly I learned the importance of improving my findings and validate them. Learning with him was constanly challenging but infinitely rewarding personally and scientifically. Thank you, Armin. A special thanks to Dr. Florian Scholz of Armin’s team for letting me learn any secret of FACS, leading to fruitful and wonderful results.

My deepest gratitude to Dr. Anje Sportbert and the entire ALM team of MDC. Thank you for the technical, scientific, and personal support for the development of this thesis and for teaching me every secret of confocal microscopy leading me to love this field more than anything else.

I would like to acknowledge Helmholtz-Gemeinschaft Deutscher Forschungszentren and MDC Graduate school for the financial support and all the administrative assistance during my doctoral study period. The MDC school was the most awesome and fantastic training experience I’ve ever had in my life; coaching and making me a better scientist and woman. I would like to express my gratitude to Dr. Michaela Herzig and to Annette Schledz for their professional, technical, and moral support throughout my entire PhD.

Earnest gratitude to Dr. Harikrishnan Radhakrishnan for the continuous scientific discussions, for carefully considering and discussing my experiments my thesis and for always patiently listening to me. A special metion to Dr. Lemos and Dr. Juneja wonderful women, which have been inspiring me along the years. Many thanks to Dr. Tanja Maritzen, Dr. Tanja Lopez Hernandez, Dr. Domenico Azarnia Tehran for their high quality/superlative scientific discussions, antibodies, and compounds sharing and the discussion and correction of this thesis.

I would also like to express my gratitude to my loving and patient boyfriend Fabrizio for being there always in the good but mostly in the bad bad days, keeping me stably and firmly on earth when I got lost, reminding me what’s really important in life. My deepest gratitude goes to all my friends: Denjo, Miguel, Francesca, Lorena, Cristina&Pat, Teo&Carlo, Silvia&Silvia, Vero&Juan, Tom&Eve, for being there always and specially in the last four months of my Ph.D, but also for all the olympionic clubbing weekends we had before and while writing

and after this thesis, which headed me safely and metally sanely to the end. Without you guys unstoppably feeding me, laughing with me, carefully taking care of me closely and from far but constantly every single day as a family, I would have never survived it. Part of my beautiful life are also Antonio, Alessandra, Camilla, Rocio, Marta, Kamila&Andrea and the half of MDC I know, for the restless beer hours and the awesome memories.

Special thanks to my past colleagues especially to Müge & Nazli for making me laugh always of Science and to everyone else who made the work environment extremely friendly and cooperative and always supported me in various ways. Above all thanks to the technicians of the lab: Claudia Roeefzaad, Gudrun Koch, Pia Hermann, Inga Krüger, and Patrizia Kamps for their valuable technical and moral support.

Last but most importantly. Words are never enough to thank my Mamma and Papà to whom I dedicate my thesis, for their unstoppable support and their unconditional love.